INVESTIGATION AND DESIGN OF SHORT-RANGE FREE-SPACE OPTICAL COMMUNICATION SYSTEM FOR FLIGHT PLATFORMS

HENG KIANG HUAT, LESTER

School of Electrical & Electronic Engineering

A thesis submitted to the Nanyang Technological University
in partial fulfillment of the requirement for the degree of
Master of Engineering

2010

Acknowledgments

I like to take this opportunity to express my sincere thanks to everyone who has supported and helped me during the past 2 years.

I thank Dr Goh Cher Hiang for his support towards financing my degree and Miss Goh Lily for her administrative assistance rendered during the duration of the course. Without the support and assistance from them, DSO National Laboratories (DSO)/Satellite Engineering Centre (SEC) and Defence Science & Technology Agency (DSTA), my research would not have proceeded smoothly.

I am especially grateful to Prof. Zhong Wende, my supervisor, for his invaluable guidance. This thesis would not have been possible without his effort and time spent on discussing my research work with me. His suggestions and insights allowed me to make progress on my research work.

I also thank my family, who has always been my greatest source of encouragement and strength.

Abstract

Free-space optical communications (FSOC), also known as free-space optics (FSO), offers the potential of having high data rate communications on the wireless domain. FSOC is largely similar to fiber-optics communications except for the difference in their transmission medians. Instead of the fiber-optics cable, FSOC transmits through atmosphere or vacuum, depending on where it is applied. FSOC takes advantage of the laser beam's small divergence to generate high energy density within the beam footprint. The narrow beam spread, coupled with receiver's small field-of-view (FOV), offers immunity to interference, interception and jamming. It also allows the employment of smaller and less power consuming optical devices. However, pointing of the beam and receiver's aperture are required for the line-of-sight (LOS) alignment for both transmit and receive terminals before FSOC can commerce.

The flight platforms of interest here are satellites or unmanned aerial vehicles (UAVs) flying within a cluster, adopting formation flying and separated spatially between hundreds of meters to numerous kilometers apart. The distance between each flight platforms can vary along the course of their flights depending on their mission requirements. Due to their potential applications, there is increasing interest and research in satellites and UAVs in a cluster and FSOC has been examined to be a suitable communications channel between the platforms within the cluster. However, automatic pointing systems have to be incorporated with the platforms in order to make dynamic adjustments to maintain the LOS during

flight.

As the distance between the communicating flight platforms varies during their missions, the problems associated with using a single fixed beam divergence for varying short-range FSOC are discussed. To overcome the problems, a beam divergence changing mechanism is proposed in this thesis with four different methods to implement it and it enables FSOC between the flight platforms over the range of varying distances.

Transmitting and receiving FSOC channels are typically housed together, creating a compact FSOC transceiver. Thus, the pointing system is required to have sufficient motor power and material strength to support the entire FSOC transceiver. For a flight platform to perform multipoint communications, more FSOC transceivers are required to be installed on it due to the point-to-point limitation of the FSOC transceivers. However, there is always a payload limit on any flight platform and this will set a constraint to the number of FSOC transceivers that can be employed on a flight platform. With weight, size and power constraints, the mission capability and flight duration of the flight platforms can be affected as well as restricting the network design. As such, a new multipoint FSOC system design is proposed in this thesis to allow multipoint communications on flight platforms. It can replace the use of multiple transceivers with weight, size and power advantages, and can potentially be employed within the weight, size and power constraints faced on flight platforms that require multipoint communications, aiding in the network design.

Also, when optical components cannot be further enhanced to support communications at longer distance, by reducing the data rate as distance increases, inter-satellite FSOC can be maintained despite the lower received power at longer distance. Instead of using two sets of photoreceivers for dual data rate switching, two schemes that use only one photoreceiver are proposed in this thesis to extend the communications distance.

Table of Contents

List of Figures

List of Tables

List of Acronyms

Abbreviations	Full Expressions
AFRL/SN	United States Air Force Research Laboratory Sensors Directorate
APD	Avalanche photodiode
BER	Bit error rate
BPF	Band pass filter
CCD	Charge coupled device
CMOS	Complementary metal-oxide-semiconductor
CPC	Compound parabolic concentrator
CW	Continuous wave
DGPS	Differential Global Positioning System
DPSK	Differential phase shift keying
EDFA	Erbium-doped fiber amplifier
ESA	European Space Agency
FOR	Field-of-regard
FOV	Field-of-view
FSO	Free-space optics
FSOC	Free-space optical communications
GEO	Geostationary orbit
GOPEX	Galileo Optical Experiment
GPS	Global Positioning System
Gbps	Gigabits per second
HV model	Hufnagel-Valley model
INS	Inertial Navigational System

JAXA	Japan Aerospace Exploration Agency
JPL	Jet Propulsion Lab
kbps	Kilobits per second
LED	Light emitting diodes
LEO	Low earth orbit
LOS	Line-of-sight
LPF	Low pass filter
MEMS	Micro-electromechanical system
NRZ	Non-return-to-zero
OCD	Optical communications demonstrator
OEO	Optical-electrical-optical
OICETS	Optical Inter-orbit Communications Engineering Test Satellite
OOK	On-off keying
PAT	Pointing, acquisition and tracking
PD	Photodetector
PIN	P-type-intrinsic-n-type
QAPD	Quadrant avalanche photodiode
RF	Radio frequency
RZ	Return-to-zero
SILEX	Semiconductor Laser Inter-Satellite Link Experiment
UAV	Unmanned aerial vehicle
WDM	Wavelength division multiplexing

Chapter 1. Introduction

1.1 Background and Motivation

Free-space optical communications (FSOC), also known as free-space optics (FSO), has attracted a lot of research interests in the last two decades as it presents itself as a variable wireless alternative to radio frequency (RF) communications due to numerous advantages over the latter [1-5]. The differences between FSOC and RF are due to the huge difference in wavelengths; wavelengths at optical frequencies are much shorter compared to RF. Since the frequency at optical spectrum is very high (hundreds of THz), it can support much higher data rates than RF communications. Wavelength division multiplexing (WDM) technique can be employed to increase the aggregated transmission capacity by several orders of magnitude [6]. With a coherent and highly directional laser beam, a small beam footprint can be achieved with high energy density as the beam spread is very small due to the short wavelength, even after traversing a long distance. As such, the transmit gain is higher and less power can be used with smaller receiving antenna in the form of an aperture. This feature also offers lesser interference with more security due to the difficulty in intercepting the beam or jamming the receiver with a small field-of-view (FOV) [2,5,7]. However, the narrow beam requires line-of-sight (LOS) to the receiver, thus pointing system is required to provide LOS alignment.

The communication principle behind FSOC is similar to that of fiber-optics communications with the difference being the transmission medium [1]. For fiber-

optics communications, the transmission medium is the optical fiber, which is made to have low attenuation. For FSOC, the transmission medium can be atmosphere or vacuum, depending on whether it is applied within or outside earth. Under atmospheric conditions, with weather conditions being random and uncontrollable, FSOC performance will vary accordingly. FSOC system can possibly communicate with any other compatible FSOC systems within its LOS. Given good LOS alignment with little disturbances, FSOC has the ability to transfer data at high data rates in the range of gigabits per second (Gbps). It is free from frequency regulation, thus saving itself the cost of licensing fee and has been explored for fixed point-to-point terrestrial applications such as setting up communication links between buildings and connecting locations without fiber-optics infrastructure to the fiber-optics ring backbone, bridging the 'last mile' of connectivity [1]. In addition, FSOC systems can also be easily installed or removed compared to fiber-optics systems [1,8].

Given the advantages and successful demonstration of FSOC in land applications, there is a growing interest to implement FSOC on flight platforms [9-10]. Compared to RF systems, FSOC systems requires lesser power and are more compact in size and weight, therefore they are rising as a very attractive alternative for payload-limited flight platforms [2-6,11]. However, as FSOC depends on a direct LOS link between the transmitter and receiver, it is a challenge to establish and maintain the narrow LOS between two flight platforms [12]. FSOC system requires reliable pointing ability from additional pointing system amid the flight maneuvers of the flight platforms to maintain the FSOC link. Apart from LOS alignment, when FSOC is applied within the atmosphere, its

performance can be degraded due to random and uncontrollable adverse atmospheric conditions along the transmission path, affecting its reliability to provide high transmission availability [13-14].

One of the two types of flight platforms within the author's area of interest is small satellites within a cluster, where these micro-satellites or nano-satellites fly in a formation to fulfill functions as a larger satellite. There has been an increasing demand for high-speed spaceborne communication systems and FSOC in spaceborne platforms such as satellites or spacecrafts has been actively researched by space agencies such as NASA's Jet Propulsion Lab (JPL), European Space Agency (ESA) and Japan Aerospace Exploration Agency (JAXA) [3,15-19]. JPL had conducted Galileo Optical Experiment (GOPEX), a deep space communications experiment, successfully sending small amount of optical data to deep space Galileo spacecraft over 6 million km in 1992 and ESA demonstrated inter-satellite FSOC through the Semiconductor Laser Inter-Satellite Link Experiment (SILEX) using low earth orbit (LEO) satellite SPOT-4 and geostationary orbit (GEO) satellite ARTEMIS in 2001 [15-17]. JAXA had also successfully established inter-satellite FSOC between ARTEMIS and their developed Optical Inter-orbit Communications Engineering Test Satellite (OICETS) in 2005 [18]. These researches were based on exploring usage of FSOC as a substitution to RF to enhance the data rate sent back to earth by deep space spacecrafts over outer space distances and to provide high data rate communication between two satellites spaced large distance apart. The compact FSOC system with lower power requirement serves well to meet the weight and power conversation principles for satellite design to reduce the launch cost, which

is an increasing function of the mass and volume of a satellite [3]. The development of LEO small satellite clusters, which consists of a number of collocated and interlinked small satellites flying in formation, places even more emphasis on the compactness and weight of FSOC system for communications between them [20-24].

The other type of flight platforms within the author's interest is mini unmanned aerial vehicles (UAVs) within a cluster. Compared to satellites, UAVs are relatively newer but there is also an increasing importance in the role of UAV for military applications, especially in the area of surveillance, due to the zero risk of human casualty [25-26]. Without this risk, UAVs can perform mission in radiation environment such as nuclear clouds or in dangerous situations such as flying in enemy territories. Research in this area leads to new methodology such as using multiple UAVs in cooperative mode to survey a larger area within shorter duration and increasing robustness by sharing surveyed information between the UAVs [26-27]. For missions into hostile enemy territories, there is always the risk of UAVs being shot down, thus the information sharing element is crucial to mitigate the risk of losing important information housed within each individual UAV [26-27]. Communication links in UAVs are presently based on RF and with better imaging sensors, the high data rate required for communication links to transfer more information results in the evaluation of employing FSOC to meet the increasing demand. The properties of FSOC suit the stealth nature of the UAVs as the narrow optical beam along the LOS between UAVs provides immunity to detection, interference, interception or jamming. An investigation of UAV-to-ground FSOC was previously studied by JPL at data rate of 2.5Gbps and

aircraft-to-aircraft FSOC was studied by United States Air Force Research Laboratory Sensors Directorate (AFRL/SN) [28-31].

Although the two types of flight platforms are fundamentally different, when they are applied within a cluster and equipped with FSOC, similar FSOC problems among them emerge such as inaccuracy in acquiring positioning information, short and varying separation distance between platforms, and the need for multipoint communications etc. The micro-satellites or mini-UAVs also require the FSOC system to conserve on power, weight and size due to their payload limits. These similar problems allow this research project to be focused on investigating FSOC for flight platforms instead of a specific platform, addressing the common problems faced by them. Unlike long distance space applications or fixed point-to-point FSOC links, varying short-range separation distance between flight platforms in cluster presents new FSOC challenges to be investigated. The LOS requirement restrict FSOC link to only point-to-point, limiting communications within the cluster network. As such, enabling method to implement multipoint FSOC is a highly desirable area to be explored. Last but not least, apart from increasing optical parameters such as higher transmit power, bigger receive aperture etc, method such as lowering the data rate as the separation distance between two communication platforms is explored to extend the transmission distance. The reduction in data rate can be performed when optical components cannot be further enhanced to extend the distance, thus instead of designing two sets of FSOC components for each data rate, the data rate reduction should be performed using only one set of FSOC components.

1.2 Objectives

The aims of this research project are to investigate the application of FSOC on flight platforms, which are satellites and UAVs, within a cluster. Due to the clustering, there are problems such as varying separation distance between the platforms and point-to-point limitation of FSOC systems. The objectives are:

a) To study the effect of varying separation distance on the FSOC channel between two platforms in a cluster and to propose techniques to overcome that effect, so as to enable FSOC availability across the range of varying separation distance.

b) To study the point-to-point limitation of typical FSOC transceiver package design and its impact on the FSOC network between all the flight platforms in a cluster, and to propose a feasible solution to enable multipoint FSOC for the payload-limited flight platforms within the cluster.

c) To extend FSOC range by making modifications to the electrical domain instead of the optical domain. Flight platforms' payload capacities are limited and this puts a restriction on upgrading the optical components such as bigger receive aperture or higher transmit power. Assuming that the optical components are taxed to their limits, modification to the electrical domain is explored to further extend the transmission distance.

1.3 Major Contribution of the Thesis

The main contributions of the thesis are listed as follows:

a) A study on the impact of varying separation distance between flight platforms on the FSOC channel is carried out. The uncertainty in acquiring the position of the platforms due to the accuracy limitations of the on-board positioning systems creates an uncertainty area whose angular size varies with the separation distance. Free-space signal loss also varies along with the separation distance. As such, a typical fixed beam divergence FSOC system cannot accommodate the variation in separation distance. A beam divergence changing mechanism is proposed in this thesis to solve the problem. Our study shows that the proposed beam divergence changing mechanism, which reduces the beam divergence for larger separation distance, can improve the transmission distance. Four different methods are presented to implement the proposed beam divergence changing mechanism and their performances are evaluated.

b) A multipoint FSOC system design is proposed in this thesis to replace the typical FSOC transceiver package design to enable multipoint FSOC between the flight platforms in the cluster. The problems with using conventional FSOC transceiver designs for multipoint FSOC on the platforms are discussed and shown to be impractical in implementing multipoint communications. The proposed multipoint FSOC system design

allows multiple concurrent communications with other platforms with power, size and weight advantages compared to the typical way of using multiple FSOC transceivers to form a multipoint system, each for a point-to-point link.

c) Two dual data rate schemes are proposed in this thesis to further extend the communications range between two flight platforms by changing the data rate using a single photoreceiver. The proposed dual data rate schemes, which operate by switching to lower data rate as the distance increases, can be implemented through the addition of electrical components without increasing any optical components. Our study shows that the proposed schemes can increase the communication range significantly.

1.4 Organization of the Thesis

The rest of the thesis is organized as follows:

a) Chapter 2 gives a literature review of the basic design of a FSOC system, the design considerations for FSOC link, the pointing, acquisition and tracking (PAT) process, FSOC for flight platforms within a cluster and multipoint FSOC system designs.

b) Chapter 3 discusses about the impracticality of using a fixed beam

divergence for the flight platforms in a cluster when the separation distance between the platforms varies greatly. A beam divergence changing mechanism is proposed in this thesis and described with four methods of implementation to enable FSOC across a range of separation distances between the flight platforms.

c) In Chapter 4, a new multipoint FSOC system design is proposed, which allows a flight platform to have multiple concurrent communications with other flight platforms. The proposed design overcomes the problems faced when multiple FSOC transceivers are employed on the platforms to provide multiple point-to-point links. The proposed multipoint FSOC system design has power, weight and size advantages over the use of FSOC transceivers for multipoint communications and assist in network implementation in the cluster.

d) In Chapter 5, two new dual data rate schemes are proposed. The newly proposed schemes allow the reduction in communications data rate between two communicating satellites as the separation distance between them increases. The dual data rate schemes assumed that the optical components cannot be improved any further due to flight platform's payload constraints, and explored the changing of data rate through enhancements in the electrical domain using only one photoreceiver. Although the data transfer duration is longer, it allows communications to continue at a longer distance within acceptable error rate performances.

e) Chapter 6 concludes this thesis and briefly discusses future work.

Chapter 2. Review on Free-Space Optical Communications on Flight Platforms

In this chapter, the typical design of a FSOC system will be discussed first, followed by the design considerations of a FSOC link. We then review the PAT process and existing work on FSOC for flight platforms in a cluster. Lastly, we review on existing work on multipoint FSOC systems.

2.1 Typical Design of a FSOC System

In this section, the design of a typical FSOC system is discussed to provide background understanding on how the FSOC system works and what the typical components required for FSOC system are.

2.1.1 Logical Subsystems of FSOC System

The typical FSOC system is divided into two major logical subsystems; PAT subsystem and communication subsystem [32]. It is to be noted that these are logical partitions and not physical partitions as the components may share common optics hardware.

The PAT subsystem is responsible for establishing and maintaining the LOS. Its pointing system usually comprises a low bandwidth coarse pointing mechanism holding the aperture to provide rough pointing of the aperture over large angles and a high bandwidth fine pointing mechanism (with bandwidth at few kHz) to direct the beam over very small angles [3]. The pointing mechanisms are also used to reduce various disturbances, including platform jitters, so that a stable link can be established before actual data communication begins [12,33-34]. The subsystem has the ability to gather information on the relative direction of the far platform by using a laser beacon from the far platform to identify the incoming beacon direction through the use of a position sensing detector. Depending on the link distance, a point-ahead mechanism may be required, which is used to compensate for the time that is needed for the light to travel over the crosslink range [3].

The communication subsystem consists of various optical communication components such as laser source, modulator, detector etc and it is responsible for the communication process such as modulating, demodulating, encoding and decoding the optical signal and electrical signal for the transfer of data information [32]. Digital data is modulated onto the optical beam from the transmitter and coupled to the aperture for transmission over free-space. At the receiving aperture, the light is collected and directed to the receiver to be converted to electrical signal and the data is recovered by electronic decision module.

2.1.2 Block Diagram of FSOC System

Figure 2-1 shows the connectivity of the physical components in a generic FSOC system [3]. Note that the solid line connections are electrical signals while the breaking line connections are the optical signals.

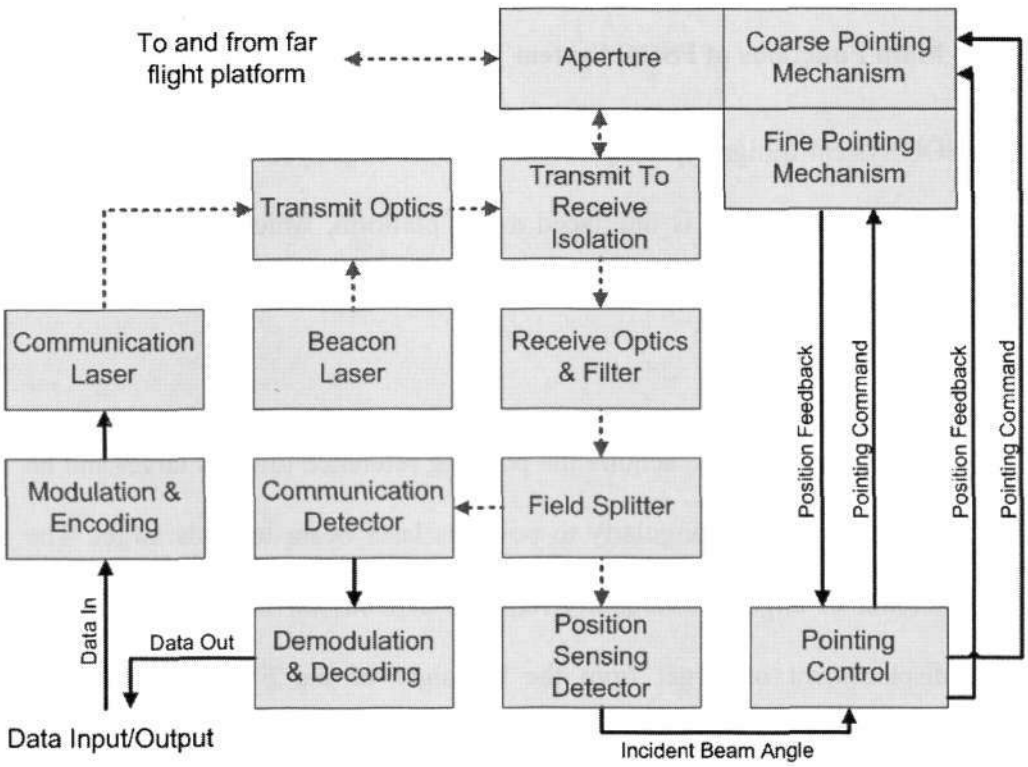

Figure 2-1: FSOC System Block Diagram

Digital data is encoded and modulated onto a communications laser source, which will emit a modulated beam signal [35]. The transmit optics will relay the beam from the transmitter to the aperture and send the beam towards the far platform. A beacon beam will also be sent to provide fine alignment for the far platform. On the other hand, laser beam from far platform will be collected by the aperture and relayed by optics to the communications detector, which will convert optical signal into electrical signal and subsequently converted to digital data after demodulation and decoding [35]. Beacon beam from far platform will be relayed

to the position sensing detector, which will produce directional information on far platform. The pointing of the FSOC system is performed by the pointing system, which consists of coarse and fine pointing mechanisms.

2.1.3 Main Functions of FSOC System

The FSOC system design typically evaluated to be employed on flight platforms is of transceiver design. It is interfaced to the platform, which will provide the power, ephemeris and support structure. The main functions of the FSOC transceiver are to [15]:

a) Possess the ability to acquire the pointing reference towards target and be able to steer itself angularly to point its laser beam towards target. The amount of angular steerability required depends on the relative angular displacement of target from the boresight of the FSOC transceiver's default resting position.

b) Perform data modulation and demodulation on optical carrier to input or extract information.

c) Transmit the modulated optical signal to target with appropriate beam power and gain under application scenario to enable communications.

d) Receive modulated optical signal from target with appropriate receive gain under application scenario to enable communications.

Discussions on design of FSOC systems can be found in [3,6,11,15,29,32,36-43].

2.2 FSOC System Design Considerations

2.2.1 Selection of Wavelength

Figure 2-2 shows the atmospheric attenuation from 700nm to 1600nm, generated by MODTRAN under clear weather conditions [13,44].

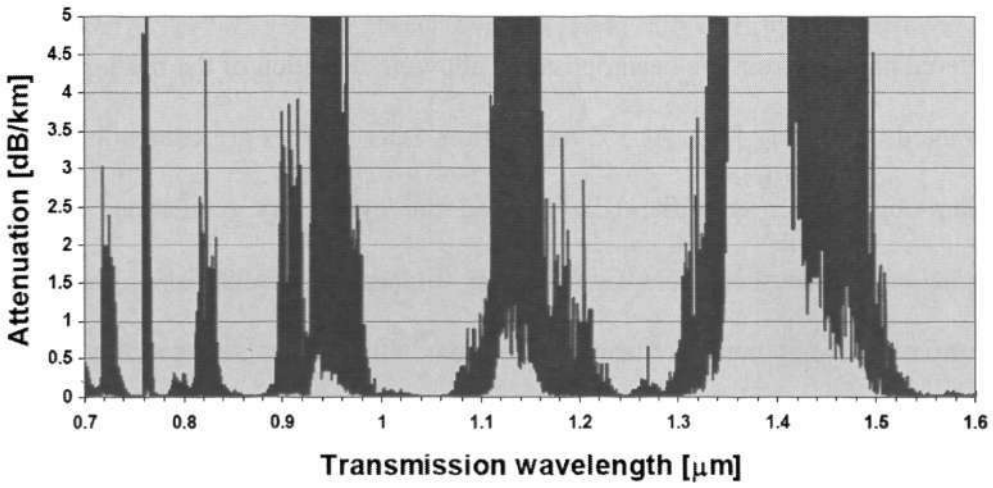

Figure 2-2: Atmospheric attenuation from 700nm to 1600nm [13]

Within the 700nm to 10,000nm wavelength spectrum, there are several atmospheric transmission windows [4,45]. The high attenuation in regions outside the transmission windows is due to molecular absorption of photons by the gases in the atmosphere. For FSOC applications, the primary wavelengths of interest are in the region of 850nm and 1550nm as these wavelengths are within the high transmission, low attenuation windows, as can be observed from Figure 2-2, and they are also extensively used in fiber-optics communications [1]. Because of the similarity between fiber-optics communications and FSOC, FSOC system can employ the components used in fiber-optics communications [1]. As such, costs for FSOC system components can be lowered since they can be purchased off-the-

shelf in the commercial market, leveraging on the development of components at these wavelengths by the fiber-optics communications industry [46].

At the 850nm region, inexpensive and reliable components are available. However, at this wavelength, it is possible for night vision equipments to pick up scattered photons from the beam, possibly allowing detection of the beam path by unwanted third party [13]. At 1550nm region, laser sources are compatible with erbium-doped fiber amplifier (EDFA) and the eye safety regulations set by International Electrotechnical Commission (Standard IEC60825-1) allows the transmission of 1550nm laser beam to be around 50-65 times stronger than that at 850nm region, due to the high attenuation of laser beam in the human eye at 1550nm [9,13,47-48]. Due to the spectrum distribution of background (solar, sky etc) irradiance, communications at 1550nm is less affected by background noise compared to at 850nm [47,49]. Furthermore, the 1550nm region is the wavelength region that the fiber-optics communications industry is heavily based on, therefore component developments are occurring in this region [46,48]. This will result in emergence of components with better performance and lower cost, reducing the price of the overall FSOC system. As a result, 1550nm is the frequent wavelength choice for FSOC systems and is the wavelength chosen for evaluation in this thesis.

2.2.2 Detection Schemes

For FSOC, there are mainly two detection schemes: coherent detection and direct detection [3,15,38]. In the coherent detection receiver, a strong optical local oscillator is added to the received optical signal, resulting in linear amplification, and the output is sent to a photodetector. For direct detection receiver, the optical signal is converted to electric signal by directly operating on the intensity of the signal.

In practice, direct detection receiver is preferred to the coherent detection receiver since a stable local oscillator is required for the coherent detection receiver [50,51]. Although coherent detection offers theoretical 7db to 10dB of signal margin over direct direction, the theoretical advantage is degraded by practical implementations such as mechanical or thermal instabilities [38]. On the other hand, direct detection is easier to implement and offers lower risk. Furthermore, under atmospheric effects, the coherence of the laser beam wavefront will be distorted, affecting the performance of coherent detection. As a result, direction detection with on-off keying (OOK) as the modulation format is widely employed for FSOC and is used for evaluations in this thesis.

2.2.3 Positioning Sensing Detector

In the past, a quadrant avalanche photodiode (QAPD) was typically used to detect the angular direction of the beacon signal [12]. However, with improvement in pixel array detector technology, detectors like charge coupled device (CCD) or

complementary metal-oxide-semiconductor (CMOS) can perform the directional detection with high charge transfer efficiency, high quantum efficiency, fast frame update rate in several kHz and better resolution in micro-radians [31,34,52]. Centroiding algorithm can be used to achieve resolution higher than the pixel resolution and with the use of windowed algorithm, the frame rate can be increased to provide even higher bandwidth to track the far platform in the presence of platform jitters.

2.2.4 Pointing System

The pointing system is usually comprised of coarse and fine pointing mechanisms. Gimbals are commonly used for coarse pointing, allowing the LOS to be moved over a large angular range over two axes with pointing resolution in milli-radians [36]. For even smaller adjustments, a fine pointing mechanism, such as beam steerer, is required [36]. The main function of the fine pointing mechanism is to move over a small angle quickly, allowing fine adjustment in micro-radians and providing high-bandwidth adjustments. The performance of the pointing system is largely dependent on:

a) Pointing resolution: The smallest adjustment the coarse and fine pointing mechanisms can make. The fine pointing resolution is usually several times smaller than the size of the beam divergence so that better alignment of beam centre towards target can be made. A gimbal typically has resolution in the scale of milli-radians while the fine pointing mechanism can provide higher resolution in micro-radians.

b) Pointing bandwidth: The rate at which the pointing mechanisms can make adjustments. The bandwidth has to be higher than the platform jitter spectrum in order to suppress the effects of the jitter.

c) Platform Jitter (vibration): The undesired fluctuations in pointing due to environment or structural interactions degrade the pointing accuracy [12,33-34]. The jitter problem is not well defined since the magnitude and effect of this jitter varies from platform to platform and poses great difficulty in establishing its effect.

Ideally, the pointing system should be able to provide an adjustment range slightly greater than the hemispherical field-of-regard (FOR) with approximately ±190° of azimuth rotation and +10 to -90° of elevation rotation [29,31].

2.2.5 Gaussian Beam Propagation

Due to the nature of laser resonant cavity, the beams typically produced from lasers are approximately of Gaussian distribution, which corresponds to the TEM_{00} mode [13]. Similar to other FSOC research, the beam propagation for evaluation in this thesis is assumed to be of Gaussian distribution too. The beam irradiance distribution is as followed [53]:

$$I(r,z) = \frac{2}{\pi\left[w(z)\right]^2} e^{-2r^2/\left[w(z)\right]^2} \tag{2.1}$$

where $I(r,z)$ is the irradiance distribution, r is the cross-sectional distance away from the beam centre, $w(z)$ is the radius of $1/e^2$ beam power irradiance at z and z is the propagated distance from the point where the wavefront is flat. The beam diameter is defined as the diameter at which the beam irradiance falls to $1/e^2$ (13.5%) of its peak at on-axis of the beam. Figure 2-3 shows the illustration of Gaussian beam $1/e^2$ diameter.

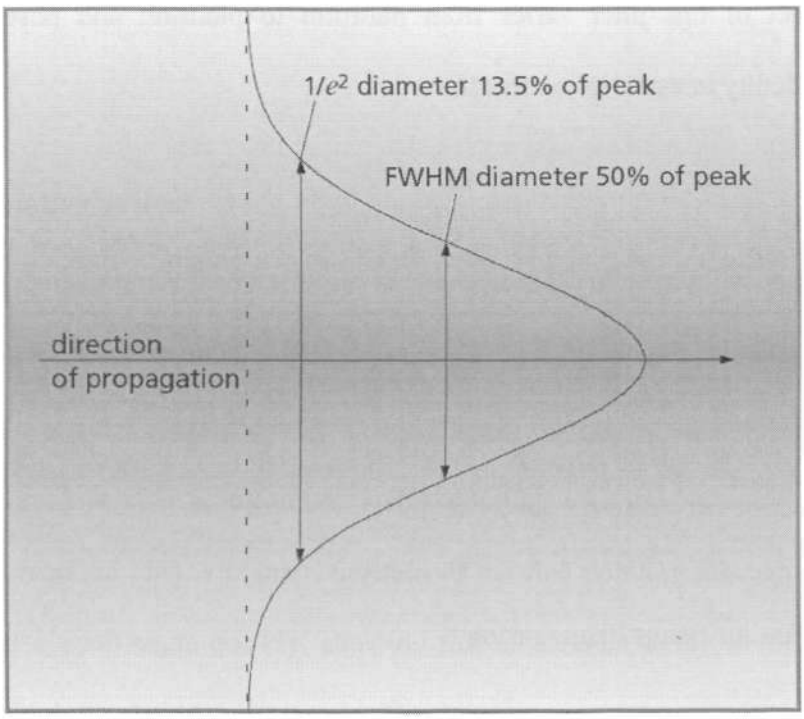

Figure 2-3: Diameter of Gaussian Beam [54]

Due to diffraction effects to spread light waves transversely, a perfectly collimated beam cannot be maintained as it propagates [54]. For a Gaussian beam with flat wavefront, it will acquire wavefront curvature during propagation according to [53]:

$$R(z) = z\left[1+\left(\frac{\pi w_0^2}{\lambda z}\right)^2\right] \tag{2.2}$$

where $R(z)$ is the radius of wavefront curvature at z, λ is the beam wavelength and w_0 is the radius of the $1/e^2$ beam power irradiance at the point where the wavefront is flat. Similarly, the radius of $1/e^2$ beam power irradiance after propagation, $w(z)$, is given by [53]:

$$w(z) = w_0 \left[1 + \left(\frac{\lambda z}{\pi w_0^2} \right)^2 \right]^{1/2} \tag{2.3}$$

As z increases to large value, $w(z)$ approaches $\frac{\lambda z}{\pi w_0^2}$ and the half angle beam divergence is $\frac{\lambda}{\pi w_0}$ [53]. Thus the full angle beam divergence, θ_{div}, can be approximated by:

$$\begin{aligned} \theta_{div} &= 2 \times \frac{\lambda}{\pi w_0} \\ &= \frac{2\lambda}{\pi \frac{d_0}{2}} \\ &= \frac{4\lambda}{\pi d_0} \end{aligned} \tag{2.4}$$

where d_0 is the diameter of the $1/e^2$ beam power irradiance at the point where the wavefront is flat and is equal to $2 w_0$.

2.3 Pointing, Acquisition and Tracking (PAT) Process

2.3.1 PAT Phases

The PAT process of establishing and maintaining the LOS can be divided

separately into pointing, acquisition and tracking phases [55]. The entire process is crucial prior to the commencement of FSOC due to the narrow transmit beam divergence and the narrow FOV of the receiving aperture [37,52]. Inaccurate beam pointing can result in pointing losses and degrade the performance of FSOC, therefore these losses must be kept to a minimum through the PAT process. Moreover, it is desirable to achieve short duration from the start of pointing phase to the tracking phase so that FSOC can commence quickly when required [56]. The factors to consider for PAT, duration of PAT and probabilities for successful PAT are discussed in [57-58].

Before FSOC can begin between two flight platforms, the flight platforms are required to establish the LOS towards each other. Knowledge of self and far platform's location and orientation is required and the degree of accuracy in this knowledge will depend on the positioning system on board the platforms and several other factors [59-60]. The exchange of the platform location information is required and can be possibly transferred through a control channel or through ground station relay [60]. Thus for each flight platform, there is a lack in ability to determine its exact instantaneous position and this results in a spherical error region and its size depends on the confidence value of error probability [3]. When this region is being viewed from the far flight platform, it becomes a 2D circular region known as the uncertainty area around the measured position coordinates and the actual position can be anywhere within this uncertainty area, from the centre to the edge of the circular area. Thus in the pointing phase, the two platforms have to calculate the pointing vector based on the measured position coordinates and steer their aperture towards the far platform's uncertainty area.

Thus, the pointing phase provides the coarse alignment between the platforms.

Once coarse alignment between the two flight platforms is completed, the acquisition phase can commerce. Both platforms will send a beacon signal towards each other and upon capturing the beacon signal, more accurate directional knowledge of far platform is gathered through the usage of a positioning sensing detector and thus fine alignment can be performed [3,31,52,55]. The use of the beacon signal is to reduce the initial uncertainty knowledge to a level that is compatible for fine alignment and allow the closed-loop correction of the pointing angle to achieve a more precise alignment that FSOC requires. When this precise alignment is achieved, both platforms are considered to have acquired each other and the tracking phase starts immediately to maintain this alignment within a tight tolerance range with higher frequency that allows uninterrupted communications. FSOC can begin while both platforms will continue to track each other. As laser beam is very narrow in the region of milli to micro-radians, accurate pointing is critical since pointing errors may result in intolerable signal loss and cause FSOC link to drop.

The PAT process occurs in the presence of vibration disturbances, generated internally and externally and overcoming these disturbances is a big challenge [37,61]. Jitter generated from gimbal is an internal disturbance while external disturbances can be due to other platform mechanisms, platform jitter during flight and other payload active systems [3,58]. The FSOC system must be able to accommodate such disturbances and if not, disturbance suppression methods, such

as jitter compensation control loop or vibration isolation, are to be employed to bring them under the system's tolerance level [33]. There may be a need to point-ahead the laser beam ahead of the position of the far platform, if the FSOC link distance is large, to compensate for the time of travel for the beam over the link distance, so that the beam will fall upon the far platform after traveling this distance. A step-by-step description of PAT can be found in [42].

2.3.2 Uncertainty Area of Flight Platforms

The uncertainty area of flight platforms affects the FSOC link evaluation in this thesis and its size is largely dependent on these factors [62]:

a) Positioning accuracy: Accuracy of on-board navigation positioning system, which is typically the Global Positioning System (GPS) [45]. Table 2-1 shows the overall horizontal position errors of GPS and Differential GPS (DGPS), the error sources and their negative contributions to the overall errors for GPS receivers on earth [63]. The accuracy is expected to be better for LEO satellites due to the absence of several error causes listed in Table 2-1.

Table 2-1: Position Errors in GPS [63]

Error cause	Error without DGPS (m)	Error with DGPS (m)
Ephemeris data	2.1	0.1
Satellite clocks	2.1	0.1
Effect of the ionosphere	4.0	0.2

Effect of the troposphere	0.7	0.2
Multipath reception	1.4	1.4
Effect of the receiver	0.5	0.5
Total RMS value	5.3	1.5
Total RMS value (filtered, slight averaged)	5.0	1.3

According to commercial products, GPS receiver designed for aircraft reports position error of 7.62m (spherical error probable) while spaceborne GPS receiver for satellite reports position error of 10m for 95% of the time [64-66].

b) Positioning update rate: The rate at which the on-board navigation positioning system receives successive update of the position coordinates. Lower positioning update rate will result in larger position error as the platform would have traveled away from the last reported position coordinates provided by the last update. The amount of distance travelled from last reported coordinates depends on the platform's velocity and the time duration since the last update. Table 2-2 shows an example of the positioning error associated with the platform's velocity and the positioning update rate [56]. Due to low update rates of GPS receivers, GPS-Inertial Navigational System (INS) will be used to provide higher update rates with readings taken from the INS between successive GPS readings [31,56]. In addition, position prediction based on common

filtering techniques such as Kalman filters or g-h filter can be used to predict the trajectory of the platforms [60,67-68].

Table 2-2: Position errors related to platform's velocity and positioning update rate [56]

Platform's velocity (km/h)	Positioning update rate (Hz)	Maximum Position Error (m)
10	1	2.7
10	5	0.6
10	100	0.03
50	1	13.9
50	5	2.8
50	100	0.14
900	1	250
900	5	50
900	100	2.5

c) Positioning transmission delay: The transmission delay is the duration it takes for the positioning information to get from one flight platform to the other. Significant transmission delay will result in larger position error of the far platform.

d) Internal calculation delay: Aperture pointing angle is calculated based on the received positioning information of the far platform and its own position. The longer this calculation takes, the more inaccurate the pointing angle will be as the far platform travels further away from positioning information during the calculation period. The calculation

speed depends on the on-board processor capability and is required to be as fast as possible.

2.3.3 Acquisition Methods

There are generally two methods to acquire the LOS towards each other and they are dependable on the sizes of the beam divergence and the uncertainty area [39,69]. While the uncertainty area is determined by accuracy of positioning system, the size of the beacon beam divergence is determined by the amount of beam intensity required at the far platform. For beam divergence that are smaller than the angular size of the uncertainty area, to ensure that the beacon beam is incident onto the far aperture, the entire uncertainty area is required to be covered by moving the beam in systematic scanning patterns within the uncertainty area, such as spiral scan, raster scan etc [3,39,57-58,70]. The far platform will have its FOV sized to the uncertainty area of the transmitting platform and wait for detection of the beacon signal. The moment the beacon beam is incident on far aperture, the beam will be relayed through optics from the aperture to a position sensing detector to determine the beam's incident angle. The far platform will in turn adjust its aperture back towards that direction and return with another beacon beam. Through this method, both platforms will rely on the beacon beams from each other for acquisition. The closed-loop correction of the pointing direction requires additional beacon beam at the transmitter as reference signal and a position sensing detector at the receiver end for the detection of beam incident angle. The ratio of the beam divergence to the uncertainty area and the search pattern affects the duration of scanning the uncertainty area. The smaller the beam

divergence is, the longer it will take to acquire the far platform.

However, if there is sufficient power to transmit a broad beacon beam divergence, the other method is to employ a beam divergence that sufficiently covers the angular size of the uncertainty area such that the moment the beam is transmitted, the far aperture will instantaneously receive the beam [2-3,39]. This method provides instantaneous detection of the beacon signal by the far platform, thus cutting down on the acquisition process duration. However, this instantaneous process is incurred at the expense of lower beam intensity due to large beam divergence and is limited by distance between the platforms.

2.4 FSOC for Flight Platforms in a Cluster

The current limitations to FSOC for satellite, applicable to UAVs as well, are transmit power, data rate and receiver sensitivity, beam divergence angle and PAT accuracies [71]. FSOC can use the optical devices produced by the fiber-optics communications industry, thus the current limitations to transmit power, data rate and receiver sensitivity from the transmitters and receivers can be improved with advances in fiber-optics communications.

The beam divergence is an important factor for FSOC as it affects the transmit gain and PAT. The beam divergence, θ_{div}, is related to beam's transmit gain, G_{tx}, according to [3]:

$$G_{tx} = \frac{16}{\theta_{div}^2} \tag{2.5}$$

Thus, a wide beam divergence will produce low transmit gain, leading to lower power received by the receiver. On the other hand, narrow beam divergence produces high transmit gain but it requires a big aperture to produce micro-radians beams, according to [3]:

$$\theta_{div} = \frac{4\lambda}{\pi D_{tx}} \tag{2.6}$$

where D_{tx} is the transmit aperture diameter, assuming the entire aperture is used for the beam collimation. A 1μrad 1550nm beam will require an aperture of 1.97m diameter, which is impossibly large for flight platforms. A narrow beam also requires more stringent PAT to keep the narrow beam fixed on the receiver. Thus PAT is also a limiting factor to FSOC and its requirements is affected by the beam divergence and FOV. To support a large aperture, which is required to provide a narrow beam, and to have high pointing resolution will require a powerful pointing system.

Leeb *et al.* suggested that FSOC between flight platforms can occur with reduced PAT requirements, and if the flight platform formation within the cluster is fixed, there is no need for PAT [22]. Using a wide beam and wide FOV of several degrees, the flight platforms will have fixed transmit and receive direction towards far platforms, as shown in Figure 2-4. However, the cluster can only support FSOC distance of 1km and low data rate of 100 kilobits per second (kbps).

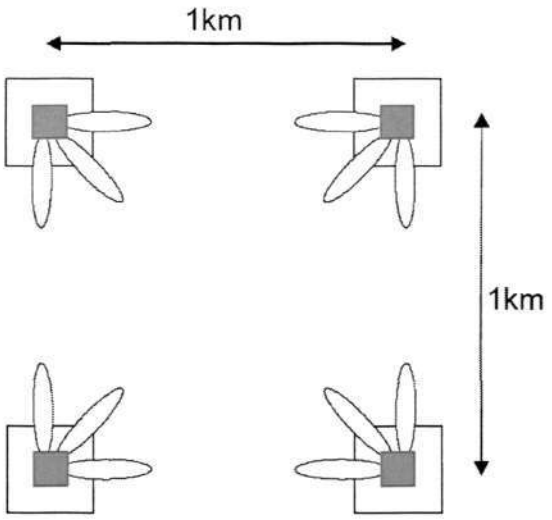

Figure 2-4: Fixed flight platform formation with fixed transmit and receive direction [22]

In the event where PAT is required, miniature gimbaled mirrors implemented using micro-electromechanical systems (MEMS) are explored to steer the transmit beam [22]. Another method is to electromechanically pivot the output end of a fiber that carries the transmit beam, with the fiber acting as the output aperture itself, as shown in Figure 2-5. Figure 2-6 shows that a single receiver can be designed to receive beams from different directions, which is through the use of separate apertures to couple light from a certain direction to the same receiver. Galvanometer actuators or miniature dc motors or stepping motors can also be used as gimbal actuators that can provide low but sufficient pointing resolution [22].

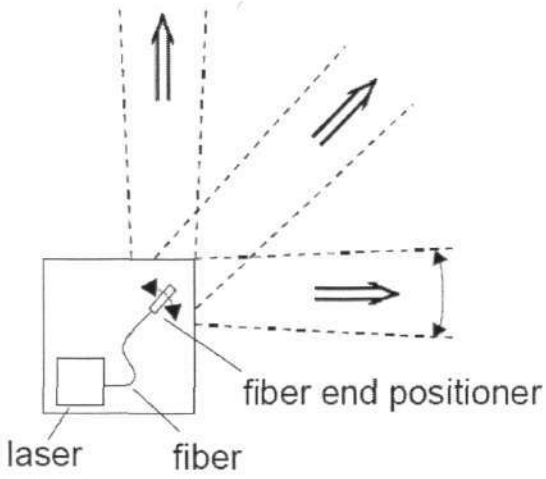

Figure 2-5: Fiber transmitter [22]

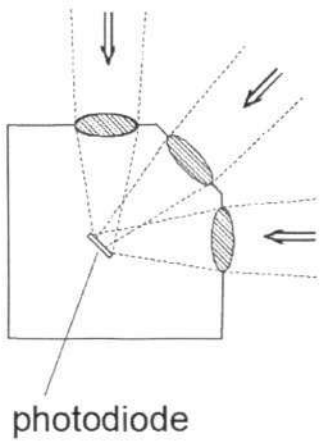

Figure 2-6: Multiple-direction receiver [22]

Similarly, Mendez *et al.* also proposed using broad beams to avoid or minimize the PAT cost and complexity [21]. These ideas focus on reducing PAT requirements and result in very limited short distance communications of less than 1km with low data rate of less than 0.25Gbps. To be able to handle larger FSOC distance up to several kilometers with higher data rate in several Gbps, it can be deduced that PAT functionality has to be incorporated so that the beam divergence can be reduced from degrees to milli-radians. It is also readily

observed that the beam divergence is an important factor in FSOC design as it affects directly the PAT requirement and communications link.

The received power for FSOC is given by [15,72]:

$$P_{rx} = (P_{tx})(G_{tx})(L_{tx})(L_{atm})(L_R)(L_p)(G_{rx})(L_{rx}) \tag{2.7}$$

where P_{rx} is the receive signal power at the input to the detector, P_{tx} is the transmit signal level, L_{tx} is the transmit optics efficiency, L_{atm} is the loss due to atmospheric effects, L_R is the free-space range loss at transmission distance R, L_p is the pointing loss, G_{rx} is the receive gain and L_{rx} is the receive optics efficiency. For inter-satellite FSOC, there will be no atmospheric losses since the transmission medium is vacuum. Sufficient received power is required to transmit as few bit errors as possible and the commonly accepted bit error rate (BER) used in analysis of FSOC link is 10^{-9}.

Free-space range loss, L_R, is a result of the diverging wavefront of the optical energy as the beam travels through the link distance from the transmitter to the receiver. Its equation is given as [3]:

$$L_R = \left(\frac{\lambda}{4\pi R}\right)^2 \tag{2.8}$$

The receive gain, G_{rx}, is a result of the effective collecting aperture of the receiver. It is calculated from the aperture size and the wavelength of the incident optical energy, given as [3,72]:

$$G_{rx} = \left(\frac{\pi D_{rx}}{\lambda} \right)^2 \tag{2.9}$$

where D_{rx} is the receive aperture diameter. For each optic element along the optical path, there is a multiplicative loss factor on its optical surface that will affect the overall transmit power. Each optical component can absorb, reflect or scatter some portion of the light, causing in the reduction of the optical transmittance. L_{tx} and L_{rx} are used to denote those losses.

Apart from the link parameters, the FSOC link design is always driven by the conservation of weight, power and size of the FSOC system and its supporting pointing system [3]. More weight means that more fuel is required for the flight platforms to fly. For satellites, it will result in shorter lifespan since satellites' fuel is limited while for UAV, they will have shorter mission duration since fuel is depleting faster. Higher power requirement exerts pressure on the flight platform's power generation system and bigger size will require a bigger flight platform in order to be structurally supportable to carry the FSOC system. Thus there is high amount of trade off between improving FSOC performance and conserving weight, power and size of the FSOC system for flight platforms. As a result, the improvements that can be made to FSOC system to increase communications performance are limited.

In this thesis, the author examines that the varying short-range separation distance between the flight platforms poses a problem to the FSOC for the flight platforms and proposes using a beam divergence changing mechanism to overcome it. The

author also proposes two dual data rate schemes to enable the extension of transmission distance using a single photoreceiver when the optical channel cannot be further enhanced to increase transmission distance.

2.5 Multipoint FSOC

Research into FSOC has been largely based on the intrinsic characteristic of point-to-point communications due to the narrow laser beamwidth. Although typical FSOC transceiver design is sufficient for point-to-point communications between two nodes, for networking applications, multipoint or omnidirectional capability is usually required to communicate with multiple nodes. In a cluster network, three basic topologies are considered and they are mesh, star and ring, as shown below in Figure 2-7 [22,27].

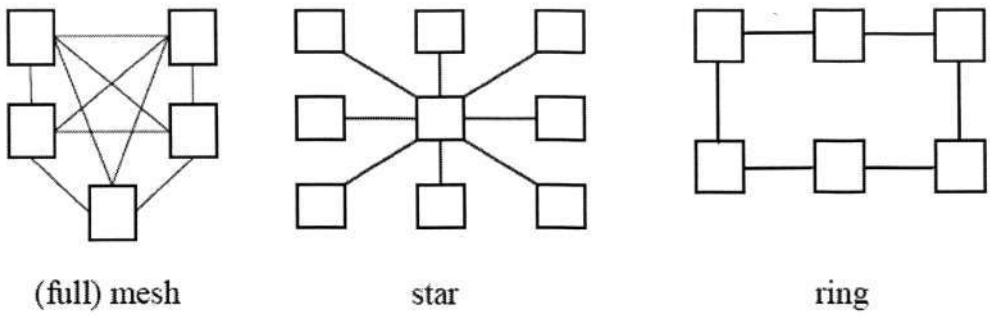

Figure 2-7: Basic Network Topologies [22]

Each topology has an effect on the network data rate, communications delay, routing and network complexity. In a fully mesh network, there is high reliability since communications can be routed in case of any direct link failure. However, with N number of flight platforms, the number of FSOC links is $\left[N(N-1)\right]/2$,

thus the network complexity increases rapidly with the number of platforms. As such, mesh topology is only suitable for clusters with small number of platforms.

In star topology, all the platforms communicate only with a central platform, which acts as hub to direct communications traffic between the individual platforms. The star topology simplifies the network but the trade-offs are having to build a complex central platform and if the central platform fails, the entire cluster lost communication means.

Lastly, for ring topology, each platform is connected to two neighboring platforms so that they form a loop within the network. From source to destination, the data will be passed through many relay platforms and the data bandwidth available for that link will be reduced linearly with the number of platforms. Partial security against communications failure, such as loss of LOS, is provided by the ring topology since data can be passed through the other direction.

However, there is little work on enabling multipoint FSOC, and the star topology is usually preferred. A point-to-multipoint FSOC terrestrial network for metropolitan area was proposed by Panak *et al.* based on connecting individual users within a cell to the network optical router on a cell tower through the use of individual transceiver for each user [73]. Meant for short communication distances, 250 actively aligned transceivers of small form factor were used for each optical router. The solution was to employ many point-to-point FSOC

transceiver units, with a pointing system each, to implement a point-to-multipoint optical router. The same concept was proposed by Leitgeb *et al.* to implement a star architecture to link buildings to an optical multipoint unit [10]. However, this method is not possible for flight platforms due to capacity limitations, especially when there are many multipoint FSOC links.

Customized beam diverging optics placed after transmitters to create very wide beam divergences and usage of several such transmitters to create full spherical coverage were proposed by Trisno *et al.* [74]. The use of wide beam divergences removed the need for pointing capability. A prototype transceiver that could provide hemisphere coverage is shown in Figure 2-8. It had four transmitters with diverging beams and four receivers with FOV of a quarter of a hemisphere each. Non-imaging optics, such as compound parabolic concentrator (CPC) which collects light rays over its entrance aperture and concentrates them over a smaller exit aperture, were considered for the beam diverging optics. However, the results from the prototype showed communications range of up to only 10m with very low data rates between 10 to 64kbps, due to the very low power received. Moreover, because of the big FOVs of the receivers, the performance of the prototype dropped when there was background noise.

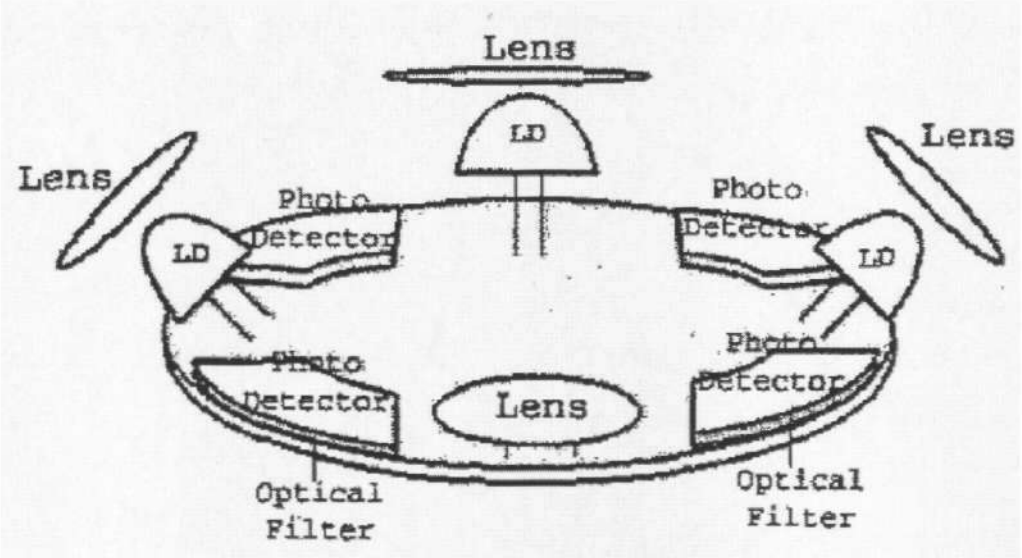

Figure 2-8: Prototype omnidirectional transceiver [74]

A spherical FSOC antenna design made of numerous hexagonal boards in "soccer-ball-shaped" arrangement was proposed by Yuksel *et al.* with each hexagonal board mounted with light emitting diodes (LED) and photodetector (PD) in array arrangement, as shown in Figure 2-9 [75-77]. They were packed densely onto the spherical node's surface such that each LED and PD pair formed a transceiver and each transceiver was fixed to cover a small angular range such that the entire lot of transceivers provided full spherical coverage. It demonstrated the ability to have FSOC between two such spherical FSOC systems with one system moving relative to another, such that LOS between them was continuously lost and re-established by switching between the transceivers. However, their analysis showed that the spherical FSOC antenna was largely limited to a few hundred meters of communications range.

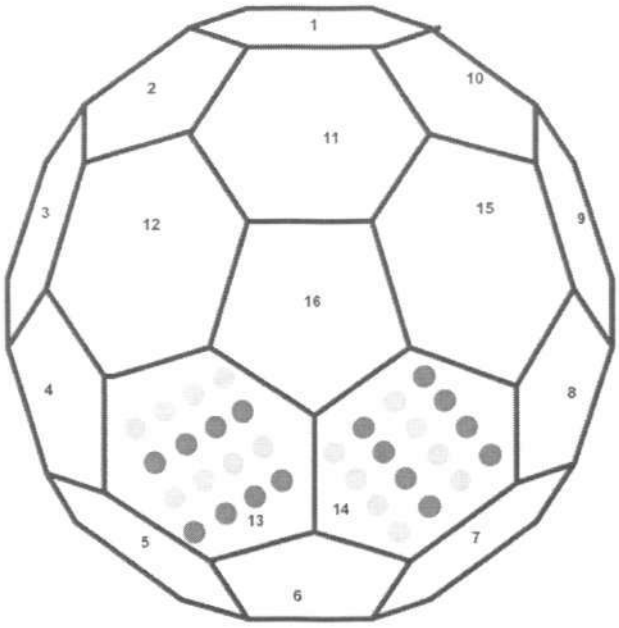

Figure 2-9: Spherical FSOC system with hexagonal boards in 'soccer-ball-shaped' arrangement [75]

Similarly, a method using transceivers densely packed in spherical configuration with the use of truncated CPC was reported by Agrawal *et al.* [78]. In all these mentioned methods, the capabilities of the designs are limited to extremely short distance and/or low data rates. They are not suitable for flight platforms since they negate the reasons and advantages for having FSOC on flight platforms in the first place. These multipoint FSOC system designs are largely driven towards indoor FSOC.

A novel scheme proposed by Song *et al.* introduced the use of a fisheye lens as aperture to facilitate acquisition between nodes [79]. It demonstrated the ability to create an ultra-wide FOV, close to hemisphere, for the acquisition receiver and proposed optical distortion-correcting algorithm to compensate the distortion introduced by the fisheye lens. With the wide FOV, the scheme enabled fast

acquisition and, with an optical filter known as Voigt anomalous dispersion optical filter, suppressed the background noise that increased with the wide FOV. Although not used for FSOC itself, the scheme showed how an ultra-wide FOV can be created and can possibly be used for multipoint FSOC receiver design.

Multipoint FSOC for communications range in kilometers continues to be largely based on the use of multiple point-to-point transceivers whereas innovative omnidirectional design methods revolve around the usage of many transmitters and receivers with large beam divergence and FOVs, leading to low transmit gain and high background noise. They fail to establish high data rate and longer communications distance capabilities as a result. Based on the literatures, there is no suitable multipoint FSOC design for flight platforms in cluster to enjoy concurrent multiple communications with high data rate with suitable specifications within the capacity limits of flight platforms. In this thesis, the author proposes a multipoint FSOC system design that is more suitable for flight platforms. The proposed design can provide high receive gain, receive beams across a wide range of angular region and has power, weight and size advantages over the use of multiple transceivers as multipoint system.

2.6 Summary

Background knowledge that is required to understand FSOC for flight platforms in a cluster was provided in this chapter for clearer understanding and is essential for evaluations within this thesis. An overview of the basic design and functions

of a typical FSOC system was described with the connectivity between various optical components shown. Some of the key optical components are laser sources, communication detector, position sensing detector, pointing mechanisms and the optics to support the beam transmission and relay. Next, several important FSOC design considerations were discussed. Due to the advantages over other wavelengths, 1550nm is the most preferred wavelength for FSOC applications and direct detection scheme with OOK as modulation format is widely used throughout the FSOC industry and research. Then, the functions and performances of the position sensing detector and pointing system were discussed. The propagation of Gaussian beam and its associated parameters such as divergence and power distribution are also described. The PAT process was also reviewed to produce background knowledge on the three PAT phases and the factors determining the uncertainty area were explained.

Existing work on FSOC for flight platforms in a cluster were reviewed with discussions on FSOC limitations. FSOC link parameters were also discussed on how they impact the link and PAT. Although FSOC system with very wide beam divergences and FOVs are suggested for the platforms within cluster to reduce reliance on PAT, they often result in low data rate and less than 1km of transmission distance. It was observed that PAT is required to provide better FSOC performances in terms of higher data rate and longer distance. Innovative and practical approaches that are suitable for flight platforms are required to improve the FSOC link.

Lastly, past researches on multipoint FSOC system were reviewed. Among mesh, star and ring basic network topologies, the star architecture is preferred for FSOC for the flight platforms in cluster and multipoint FSOC system is required to implement that architecture. Due to the difficulty in designing a multipoint FSOC system, multipoint systems proposed by others were usually based on using multiple transceivers with a pointing system each for every point-to-point link. Therefore, they are not feasible for flight platforms due to payload limits. Although some compact and creative multipoint designs were also proposed, their concepts were largely based on using many transmitter and receivers with very wide beam divergences and FOVs respectively with adjacent or overlapping coverage to provide the omnidirectional ability. However, these innovative designs failed to produce high data rate with transmission distance in kilometers. As such, a multipoint FSOC system that is suitable for flight platforms, support high data rate and long transmission distance will be highly desirable.

Chapter 3. Beam Divergence Changing Mechanism

3.1 Introduction

Over the years, there is rising interest in satellite cluster as the advantages of using several smaller satellites within a cluster to meet larger mission goals lead to cost effectiveness [21]. Replacing a single and larger satellite, satellite cluster requires the individual satellites to cooperate and perform applications such as synthetic aperture radar, remote sensing and data collection etc, missions that are not possible with a single satellite. Similarly, UAV cluster explores the use of multiple smaller UAVs by arranging themselves in optimal formation to maximize their surveillance capability [26].

When these flight platforms are within a cluster, they provide robustness against a single point of failure, which may occur with a single satellite or UAV mission. A failure of one platform within the cluster will not cripple the entire cluster and the mission can be possibly continued with reconfiguration of cluster formation. The robustness is also enhanced by the sharing of data within the cluster such that important data are not missing with the loss of a certain platform. For the cooperation and data sharing to occur within the cluster, communications are required and FSOC has been found to be suitable for such clusters with its high data rate, low power consumption, small size and weight [21].

Most research on FSOC focus on fixed point-to-point communications or very long distance communications and typically uses a fixed beam divergence. For these satellites and UAVs in a cluster, they face a common problem for FSOC. Depending on their mission requirements, they are required to adopt certain cluster formation. The changes in formations mean that each flight platform will have varying separation distances with its neighboring platforms, ranging around 1km to over 10km. The amount of change in the separation distance is on the same order as the distance itself and our study shows that it is not practical to use a fixed beam divergence for this situation.

The varying short-range distance between any two flight platforms poses a unique challenge to the PAT beacon signal link and FSOC links. In this chapter, the author proposes a beam divergence changing mechanism to solve the problem and present four different methods to implement it. It is shown how the beam divergence changing mechanism can overcome the problem caused by the varying short-range separation distance. In addition, for inter-UAV FSOC, the improvement in FSOC transmission distance is evaluated under different adverse weather conditions.

3.2 Effects of Varying Distance for Inter-satellite FSOC

It is assumed that the separation distance between the satellites will be between 1.5km to 10km, depending on the cluster formation. Given the general accuracy of typical spaceborne GPS receiver of ±10m for 95% (2-sigma) of the time, the

accuracy for 99.7% (3-sigma) of the time will be ±15m [65]. Therefore, the diameter of the uncertainty area for a satellite is assumed to be 30m. Discussion was held with staff from NTU's Satellite Engineering Centre and they agreed on the 30m uncertainty area diameter assumption. It is to be noted that the accuracy of GPS receiver is beyond the scope of this thesis. To ensure that the transmit beam can be received by the far satellite, which can be anywhere within the uncertainty area, the beam has to illuminate the entire certainty area with a beam footprint that is equal or larger than the uncertainty area after travelling through the varying communication distance.

With GPS coordinates of both satellites, the coarse pointing vector can be derived [80]. When viewed from a satellite towards the far satellite's uncertainty area, the 30m diameter circular area has different angular sizes at different distances. At 1.5km separation, the angular size is 20mrad but it is reduced to 3mrad when the separation distance increases to 10km. In Figure 3-1, it can be observed that the angular size created by uncertainty area at 10km is significantly smaller than the one at 1.5 km.

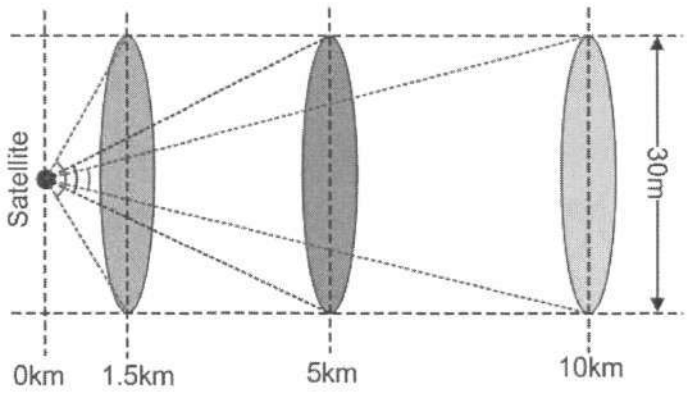

Figure 3-1: Illustration of varying angular size of uncertainty area

Figure 3-2 shows the angular size of 30m diameter of uncertainty area at the various distances between 1.5km and 10km.

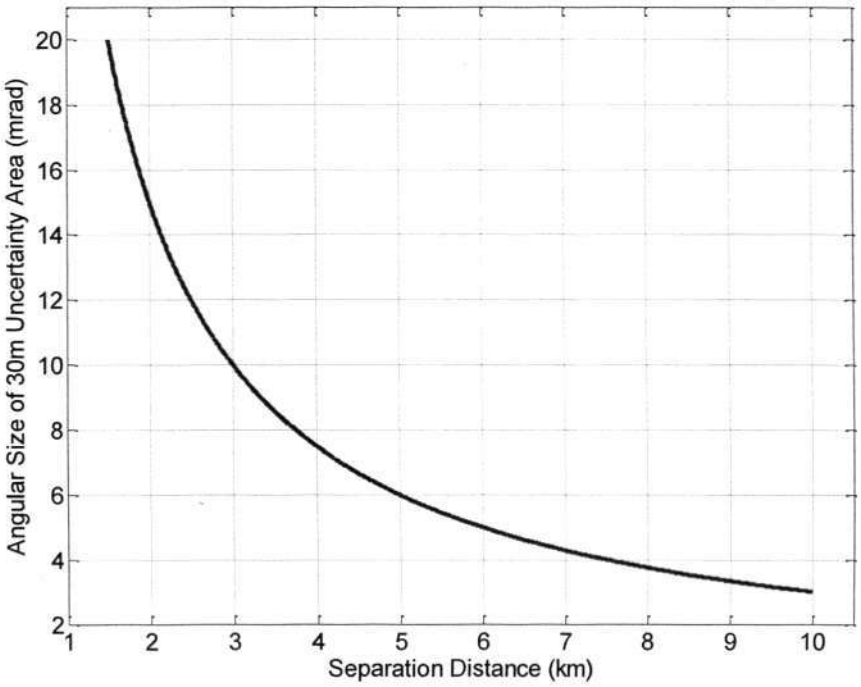

Figure 3-2: Angular size of 30m uncertainty area at different separation distances

With a wide range of angular size from 3mrad to 20mrad, the use of a single beacon beam divergence is not practical to cover the entire uncertainty area across the range of separation distances. For example, assume that a beacon beam with a fixed divergence of 20mrad is to be used. At 1.5km distance, the beam will cover the entire uncertainty area adequately. However, when the same divergence is applied at 10km distance, the beam will form a circular footprint of 200m diameter. Thus only 2.25% of the beam coverage will fall within the 30m uncertainty area. The remaining 97.75% of the beam footprint is outside the required region and will not be utilized.

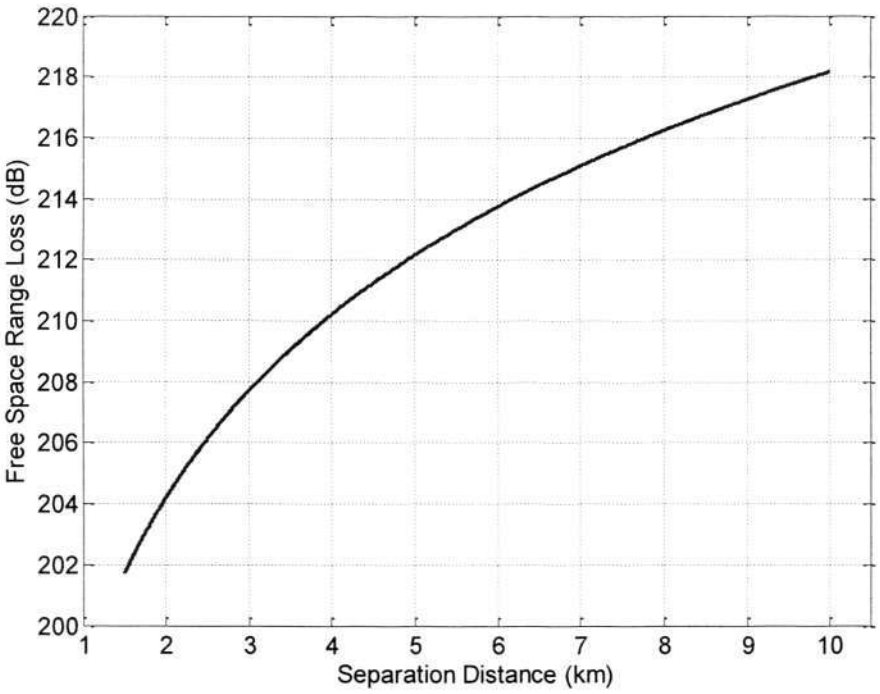

Figure 3-3: Range loss at different separation distances based on 1550nm wavelength

Figure 3-3 shows the free-space range loss in dB at the distances between 1.5km and 10km. It is plotted using Matlab based on transmission wavelength of 1550nm using Equation (2.8). The free-space range loss is due to the diverging wavefront of the optical energy as the beam travels through the space from the transmitter to the receiver, resulting in lower optical power at the receiver. The effect of range loss further reinforces the impracticality of using a fixed beam divergence since the range loss increases by around 16.5dB when separation distance increases from 1.5km to 10km. At 10km distance, more gain is required to meet the link budget but a fixed beam divergence will not produce the additional gain.

3.3 Link Budget Analysis for Inter-satellite FSOC

The link budget analysis is presented here in Table 3-1. The analysis is based on a 30mW semiconductor laser diode transmitter and CCD detector with detector sensitivity of 1nW (-60dBm), based on typical value found in [81].

Table 3-1: Link budget table

Parameter	Value	dB	Comments
Transmission power	30mW	14.77 (dBm)	Nil
Transmit optics efficiency	50%	-3.0	Assumption
Transmit pointing loss	50%	-3.0	Assumption
Range loss	6.76×10^{-21} to 1.52×10^{-22}	-201.70 to -218.18	1.5km to 10km
Receive optics efficiency	50%	-3.0	Assumption
Required signal power	1nW	-60.0 (dBm)	Assume 1nW for CCD detector
System Margin	10.0	10.0	Nil
Required total gain for PAT	3.91×10^{14} to 1.75×10^{16}	145.93 to 162.43	Required transmit & receive gain

Some losses are assumed to be 50% and the link margin is currently set to a high 10.0dB to compensate for any additional losses. Unlike UAVs, satellites are not given access to any maintenance work after being launched to space. Therefore degradations for optics efficiency and optical components' performances have to be catered for long term planning. The link budget analysis determines the required total transmit and receive gain. A 10cm aperture is chosen for this

evaluation, giving a receive gain of up to 106.14dB. Eliminating the receive gain from the total gain required, the transmit gain is required to be between 39.79dB and 56.29dB for the distance between 1.5km and 10km, as shown in Figure 3-4.

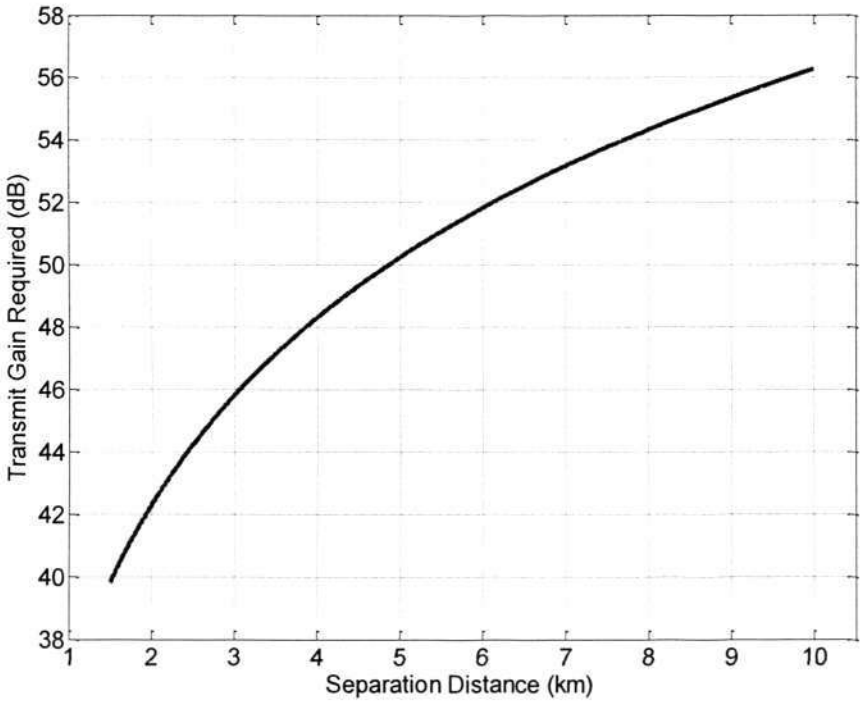

Figure 3-4: Transmit gain required at various separation distances

The divergence of a beam has an inverse relationship with its transmit gain; the gain will decrease for bigger beam divergence. The gain associated with the range of beam divergence between 3mrad to 20mrad is examined and shown in Figure 3-5.

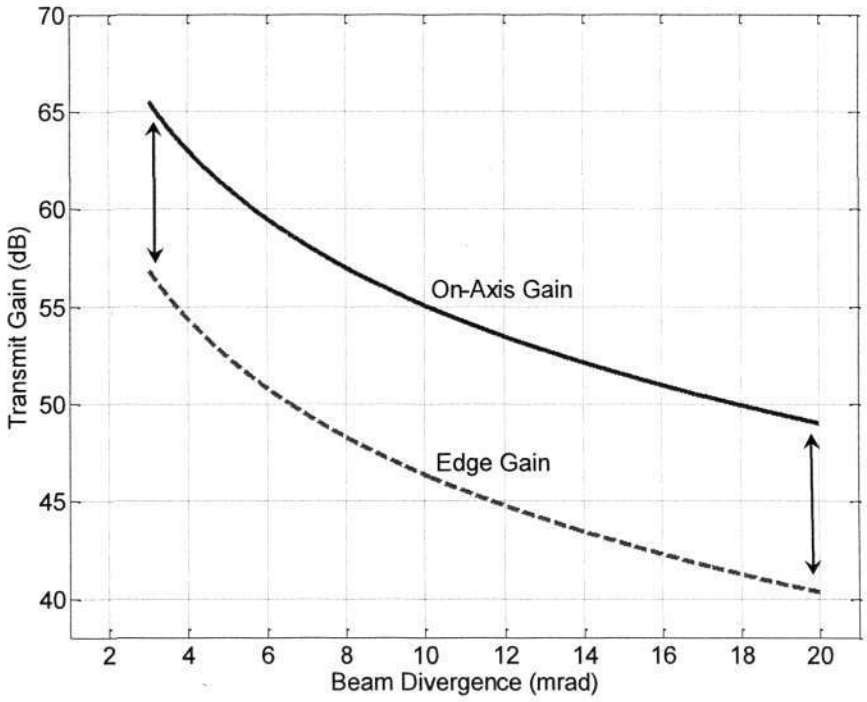

Figure 3-5: Transmit gain produced at various beam divergences

Figure 3-5 is plotted using Matlab based on Equations (2.1) and (2.5). At each beam divergence, there is a range of gain produced rather than a single value. The dotted line in Figure 3-5 shows the gain at the edge of the beam. This is because of the Gaussian distributed beam profile. Instead of a huge range of beam divergence selection, only a few divergence sizes will be employed to provide sufficient transmit gain. The entire 3mrad to 20mrad uncertainty area range is divided into different regions, each operating with a certain beam divergence. The beam divergence to be used for a certain region shall be examined and it can be created through the use of optics, to be discussed in Section 3.4. Combining Figure 3-2 and Figure 3-4, a single plot is produced that shows the amount of gain required against the angular coverage of the uncertainty area, which also represents the uncertainty area at various distances. The plot is shown in Figure 3-6.

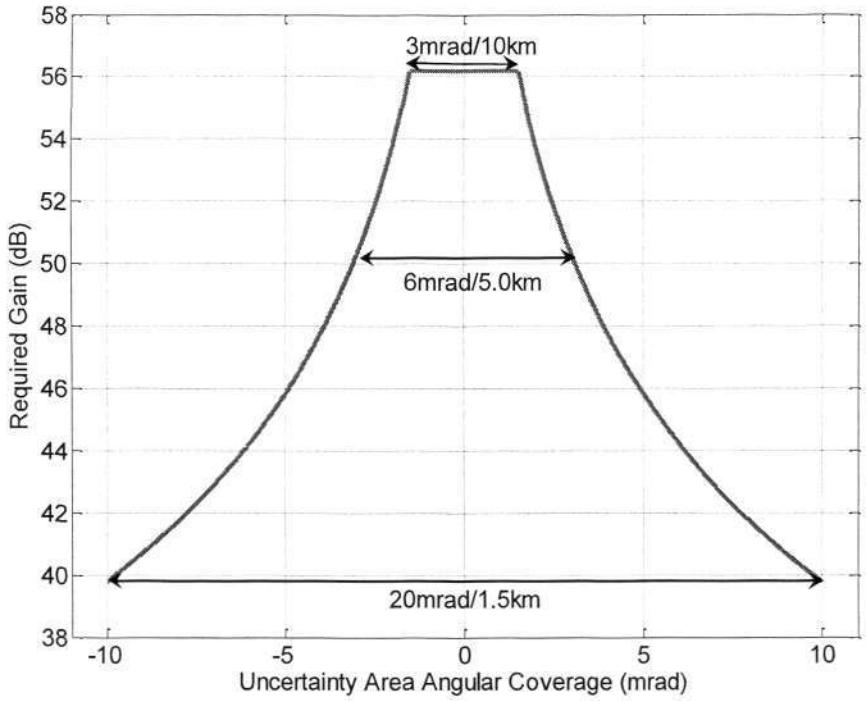

Figure 3-6: Required gain at various angular uncertainty area sizes

The transmit gain required over separation distance and the angular coverage over separation distance are combined in Figure 3-6 using Matlab to show the transmit gain required over the angular coverage, removing the common separation distance variable. It can be observed that a 20mrad uncertainty area requires around 39.8dB gain and a 3mrad uncertainty area requires around 56.3dB gain. Figure 3-6 is plotted to allow easy comparison of beam gain profile against the required gain.

Since at 1.5 km distance, 20mrad beam is required for 30m diameter uncertainty area, thus the first divergence size to be used is 20mrad. In the 20mrad beam, due to the variation of the beam gain profile within the divergence, the gain at certain offset angle from the on-axis gain can sufficiently meet the required transmit gain for uncertainty areas at various distances, as shown in Figure 3-7.

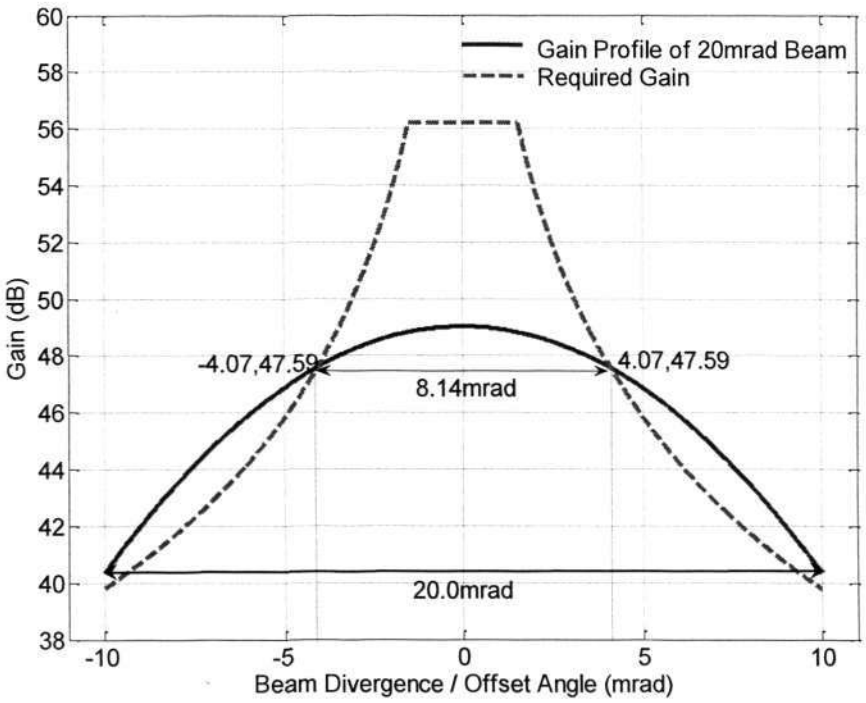

Figure 3-7: Range of required gain satisfied by a 20mrad beam

In Figure 3-7, the gain profile of a 20mrad beam, presented by the solid line, is shown with increasing offset angle from its on-axis (zero offset), from 49.03dB on-axis gain to 40.35dB edge gain at the edge of the beam footprint, 10mrad angle offset from the on-axis. The dotted line shows the required gain. Within the beam profile, it can be seen that the 20mrad beam has produced range of transmit gain across its beam profile higher than the required gain from 10mrad up to 4.07mrad angle offset, which is also 20mrad at 1.5km to 8.14mrad uncertainty area at approximately 3.69km distance. Beyond this distance, the 20mrad beam is unable to produce sufficient transmit gain for the increasingly angularly smaller and further uncertainty areas. As a result, the 20mrad beam can be employed to illuminate the entire uncertainty area from 20mrad down to 8.14mrad for range from 1.5km to 3.69km.

A 10mrad beam, instead of an 8.14mrad beam, is selected next to provide overlapping of coverage between the 20mrad and 10mrad beams. Using the same method, Figure 3-8 shows the gain profile of a 10mrad beam and the required gain at various uncertainty area sizes at various separation distances. It can be observed that the 10mrad beam divergence produces sufficient transmit gain up to 2.04mrad angle offset, which is 4.08mrad uncertainty area at 7.35km distance. Thus the 10mrad beam can be utilized to illuminate entire uncertainty area from 20mrad to 4.08mrad for range from 3km to 7.35km.

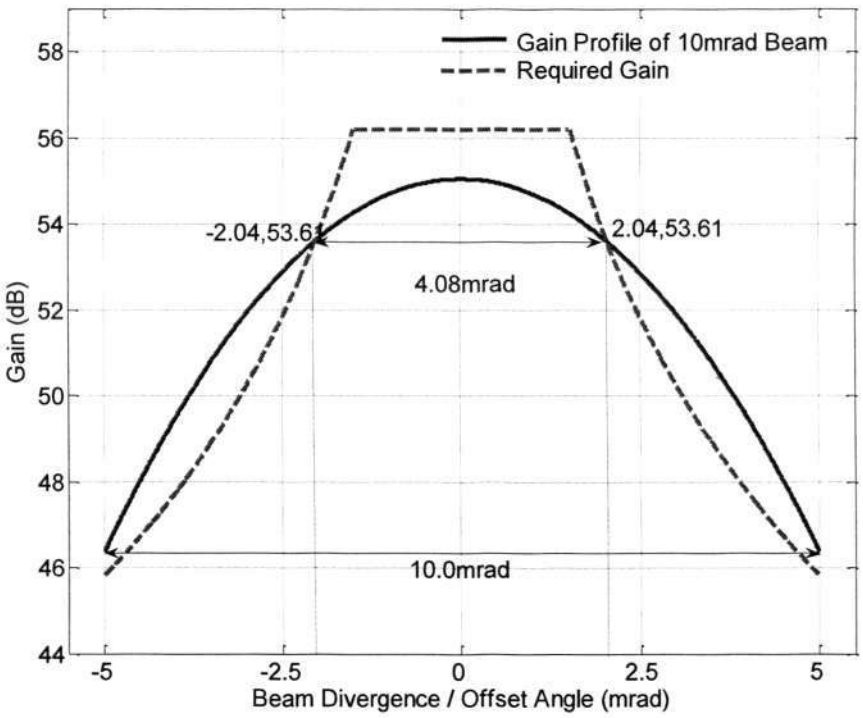

Figure 3-8: Range of required gain satisfied by a 10mrad beam

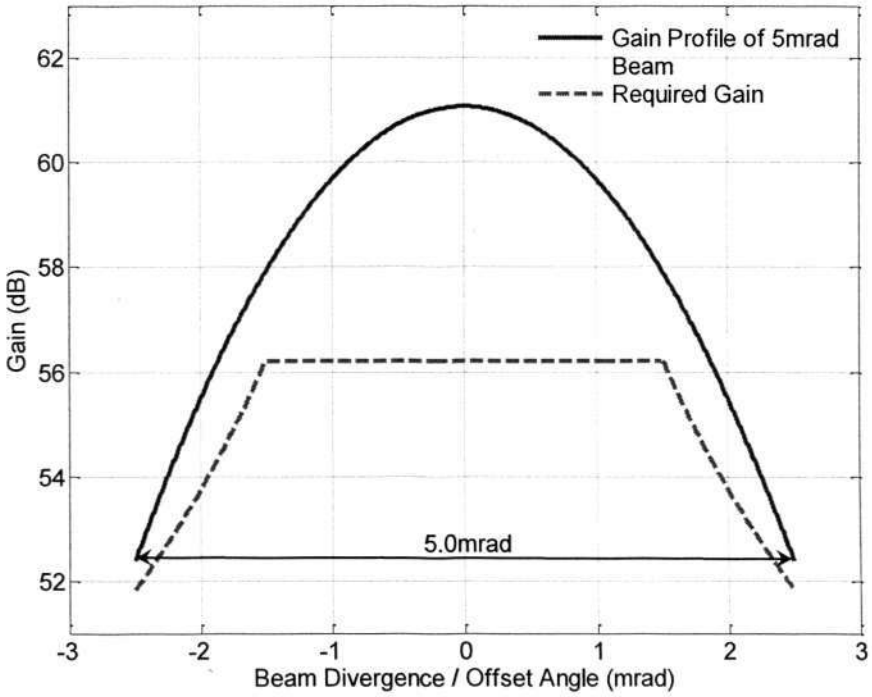

Figure 3-9: Range of required gain satisfied by 5mrad beam

A 5mrad beam is selected to provide overlapping of coverage between the 10mrad and 5mrad beams. In Figure 3-9, it is shown that a 5mrad beam can provide sufficient gain to illuminate the uncertainty area from 5mrad down to 3mrad for range of 6km to 10km. Thus the regions in which the 5mrad, 10mrad and 20mrad beams will be employed are designated and shown in Table 3-2.

Table 3-2: Beam divergence selection

30m Angular Uncertainty Area (mrad)	Distance (km)	Beam Divergence (mrad)
20 to 9.5	1.5 to 3.16	20.0
9.5 to 4.6	3.16 to 6.52	10.0
4.6 to 3	6.52 to 10.0	5.0

Although the discussion so far is limited to the beacon beam for inter-satellite PAT beacon link, the same situation discussed above with regards to the problems that arises from varying separation distance with a fixed beam divergence will apply to the communications beam too. The same type of evaluation method discussed can be applied to the inter-satellite FSOC link to determine the range of beam divergences required for the communication beams.

3.4 Methods to implement Beam Divergence Changing Mechanism

While the required beam divergences are known, a beam divergence changing mechanism is required to implement the change in the beam divergences. Four methods are hereby proposed by the author to implement the beam divergence changing mechanism, as shown in Figure 3-10.

For all the methods, the aim is to produce different collimated beam diameters, d, which are inversely related to the beam divergences, described by Equation (2.6). Thus having a certain collimated beam diameter is equivalent to having a certain beam divergence. The relationship between beam divergence and beam's transmit gain is described by Equation (2.5); for every halving of beam divergence, the beam's transmit gain increases by 6dB. The first method is to select one out of N movable lenses into the transmit optics path to create a desired output collimated beam diameter. Since the selection of each lens corresponds to selecting a beam divergence, a total of N beam divergences can be selected from this method. This

method requires precise positioning of the lenses to prevent optics misalignment since each lens has its own focal length, *f*, and focal point and misalignment will lead to poor collimation of the beam.

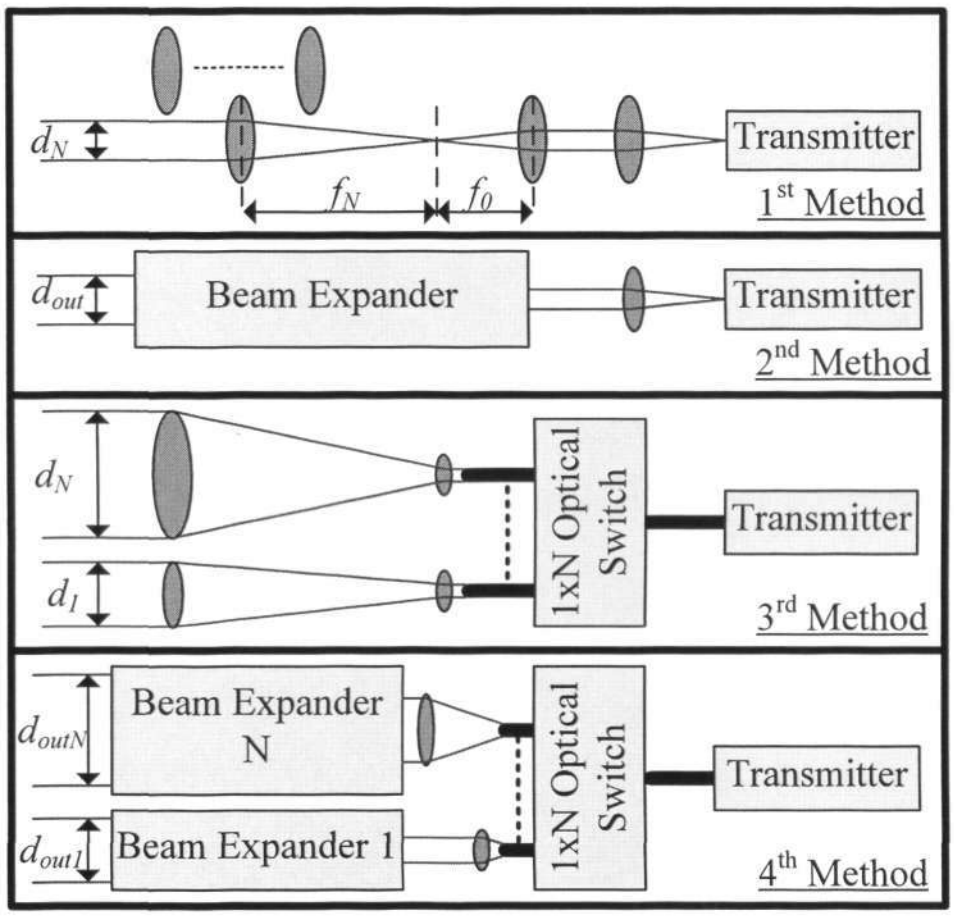

Figure 3-10: Beam divergence changing methods

The second method is to incorporate a motorized beam expander into the transmit path. A beam expander is an optical component that is designed to increase the diameter of a collimated beam. By including the beam expander into the transmit path after the beam emitting source, the output beam diameter can be increased or decreased within the expansion ratio range of the beam expander [82]. This inversely changes the beam divergence accordingly. The output beam diameter of a motorized beam expander typically has a variable expansion ratio from 1 to 4;

thus the output collimated beam diameter can be increased by up to 4 times the input beam diameter. Therefore the divergence of the beam at the input of the beam expander can be reduced by up to 4 times upon exiting the beam expander. During operations, only the internal optics within the beam expander shift and the beam expander as a whole does not move. This feature allows the motorized beam expander to be fixed-mounted in the transmit path, and optical misalignment is not a concern. However, the limited range of the expansion ratio may not be sufficient if the range of required beam divergence is larger than the range supportable by the beam expander.

The third method is to include an optical switch into the transmit path. A fiber-based laser source output is connected to the input of a 1 × N optical switch, and the N output ports of the switch will be followed by N number of lens groups, with each lens group corresponding to a certain beam divergence. By controlling the optical switch, the input optical beam can be switched to any of the N number of output ports. After exiting from the fiber output of the optical switch, the optical beam will enter into the free-space and be manipulated by the fixed-mounted lens groups to achieve the desired beam divergence accordingly.

The fourth method is a combination of the second and third methods. An optical switch is incorporated after the laser source fiber output to switch the optical beam between multiple beam expanders. This is to further increase the beam diameter expansion ratio, which is limited for a single beam expander but multiplied when using more beam expanders. As an example, consider two

motorized beam expanders combined with a 1×2 optical switch. Initially, the optical switch can be set to direct the optical beam to beam expander 1 to increase the output beam diameter by 4 times. Correspondingly, the beam divergence is reduced by 4 times. For an even larger beam diameter beyond the expansion limit of beam expander 1, the optical switch will select the output port connected to beam expander 2 and direct the optical beam toward it. By using lens to set the beam diameter from this output port into beam expander 2 equivalent to the maximum beam diameter output from beam expander 1, beam expander 2 can further expand the beam diameter by 4 times. Thus the usage of two beam expanders allows an expansion ratio up to 16 times, reducing the beam divergence with the same ratio. However, it should be noted that different models of beam expanders with different input and output apertures have to be used since the input and output beam diameters for the two beam expanders are different. By having the beam expanders in parallel arrangement through the use of optical switch, the beam divergence changing mechanism will be more compact with smaller overall loss created by losses such as insertion loss, alignment loss etc. With the beam expanders in parallel arrangement, individual loss will only be limited to a particular beam path from a particular switch's output port and will not affect the beam path of other output ports. In a cascaded arrangement of beam expanders, the single beam path that travels through all the beam expanders will be affected as long as there is some loss introduced at some point along the cascaded beam expanders' arrangement. If each beam expander introduced a certain amount of loss, the overall loss in the single beam path will be compounded and be higher, leading to undesirable performance.

This proposed beam divergence changing mechanism can be potentially used to produce any desired beam divergences with methods to switch between the beam divergences during FSOC operations. Since the amount of beam divergence is largely dependent on the choice of the size of optics aperture used and is limited by the aperture size, it is impossible to accommodate increasingly large optics within the payload limited platforms. If large aperture of up to 10cm diameter is used, small beam divergence up to microradians can be produced. However, such small beam divergence is not necessary for short-range FSOC.

This proposed beam divergence changing mechanism is suitable for short-range FSOC for both satellites and UAVs because the beam divergences required are in the milli-radians range. In the four methods proposed by the author for the beam divergence changing mechanism, the optical components are of small sizes, expected to be less than 1cm for the lenses. Thus, the additional of the beam divergence changing mechanism will not add tremendously to the FSOC system's size and weight but can produce significant improvements to FSOC transmission distance.

3.5 Effects of Varying Distance for Inter-UAV FSOC

For inter-UAV FSOC, depending on the UAVs' flight path and altitude, the LOS may be blocked due to impenetrable objects such as thick clouds, mountains, buildings and birds or due to flight maneuver dynamics. These temporary outages are expected to be on the scale of tenth of a second to a few seconds. Taking the

temporary outages and dynamic relative position changes into consideration, the method of employing a wide communications beam divergence that sufficiently covers the angular size of the uncertainty area is preferred such that the moment the communications beam is transmitted, the far UAV's aperture will instantaneously receive the communications beam. This method of establishing the LOS is preferred to allow speedy recovery of communications, especially during mission critical phase. This method is possible because the separation distances between the UAVs are not large and UAVs are not as power constrained as satellites, thus higher transmit power can be sent by using higher power laser with broad beam divergence. Thus the LOS is established without the need to reduce the uncertainty knowledge through a beacon beam and communication can commerce through closed-loop pointing correction based only on position coordinates of both flight platforms.

In this section, the optical link design for inter-UAV FSOC is evaluated in the presence of atmospheric effects based on the communications method mentioned above. A typical differential GPS provides ±5m accuracy at 1Hz with the INS providing coordinate updates at 50Hz, thus the maximum positioning error of each UAV is ±5.83m. Due to the delay in positioning information exchange and processing (assumed 50ms), the maximum error of the partner UAV increases to ±7.92m. When the two UAVs are flying in opposite directions, the error becomes ±13.75, resulting in a maximum uncertainty area of 27.5m diameter with the GPS/INS coordinates at the centre of the uncertainty area.

Figure 3-11 shows the angular size of 27.5m uncertainty area diameter as a function of the distance, as well as the required gain to meet the link budget without atmospheric effects. These values define the minimum requirements of the transmit beam at various distances under no atmospheric effects, thus the transmit beam's beam divergence and the gain have to be equal or larger than the angular size and required gain respectively. With consideration of weather conditions, the required gain will increase further for the same distance.

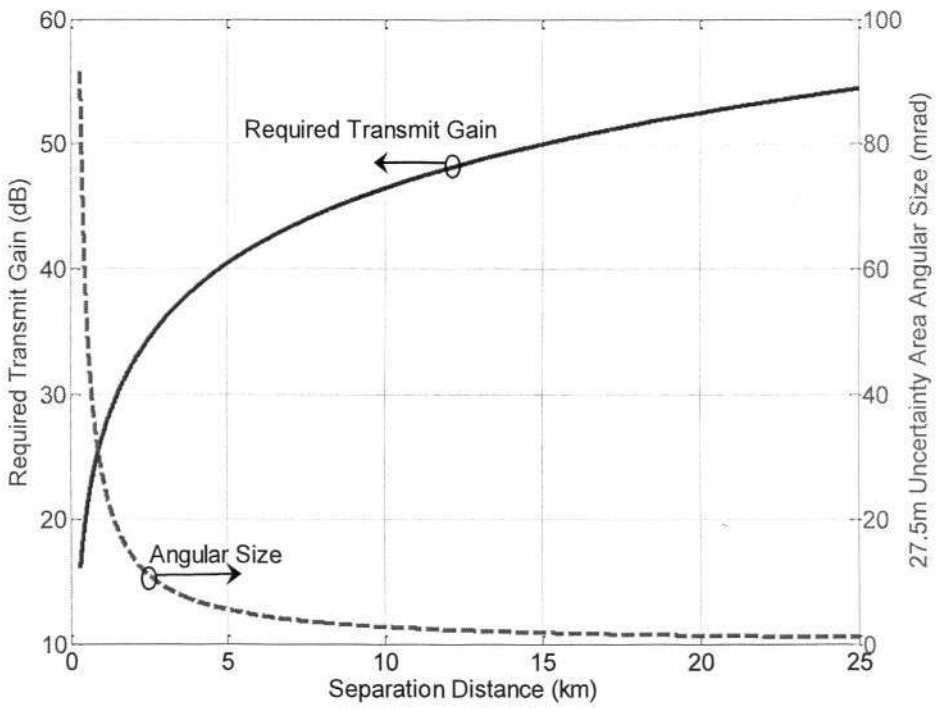

Figure 3-11: Angular size of 27.5m uncertainty area diameter and required gain

The possible transmission distance under different weather conditions for the three FSOC beam divergence configurations, denoted as System A, B and C in Figure 3-12, will be examined. Among the four methods shown in Figure 3-10, only the third and fourth methods are evaluated in Systems A and B respectively. The first and second methods in Figure 3-10 are not explicitly shown because the

first method can produce similar beam divergences as the third method despite the differences in implementation, and the second method is also largely similar to the fourth method except that it has a smaller expansion ratio. In System A, five different levels of beam divergences can be selected by the optical switch and the beam divergences considered are 96mrad, 48mrad, 24mrad, 12mrad and 6mrad. These values are selected based on their transmit gains and beam coverage to cover the entire uncertainty area.

For System B, two beam expanders with an expansion ratio varying from 1 to 4 are used. With the assumption of step adjustment of 0.5 in the expansion ratio from each of the beam expanders, a total of thirteen different beam divergences can be selected. Beam expander 1 allows selection of 96mrad, 84mrad, 72mrad, 60mrad, 48mrad, 36mrad and 24mrad beams, while beam expander 2 allows selection of 24mrad, 21mrad, 18mrad, 15mrad, 12mrad, 9mrad and 6mrad beams.

For System C, the beam divergence is fixed at 96mrad, which is sufficient for its beam footprint to cover the uncertainty area for the distances greater than or equal to 300m. It is included for comparison to demonstrate the transmission distance improvement through using beam divergence changing mechanism in Systems A and B.

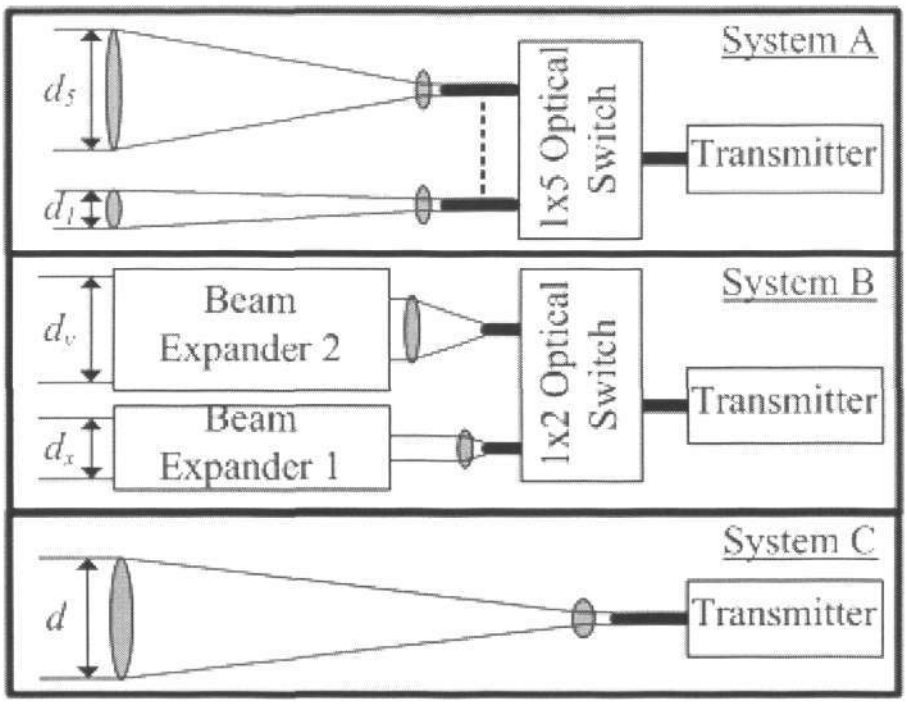

Figure 3-12: System A, B and C configuration

Figure 3-13 shows the transmit gain profile of various beams with the beam divergences of 96mrad, 84mrad, 72mrad, 60mrad, 48mrad, 36mrad, 24mrad, 21mrad, 18mrad, 15mrad, 12mrad, 9mrad and 6mrad. Figure 3-13 is plotted using Matlab based on Equations (2.1) and (2.5). As the beam divergence gets smaller, the transmit gain increases since the beam energy is concentrated in a smaller area.

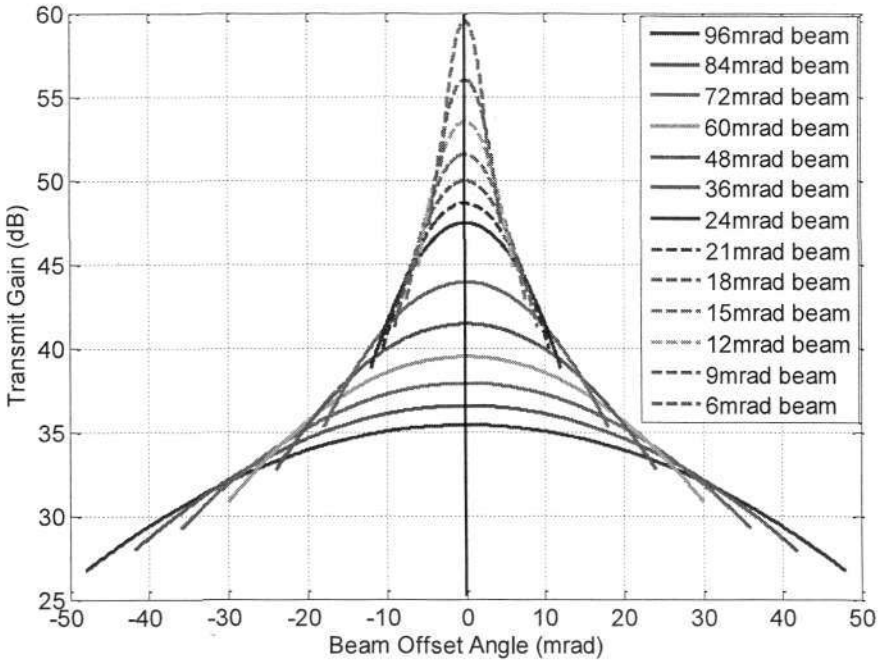

Figure 3-13: Transmit gain profile of various beams

The transmit gain profiles are of Gaussian distribution with the maximum intensity at the beam centre to e^{-2} (13.5%) of the beam intensity at the edge of the beam. Since the beam centre is pointed to the given GPS/INS coordinates and the transmit gain decreases with increasing offset angle from the beam centre, if the UAV is not at the GPS/INS coordinates, it will experience smaller transmit gain. This is regarded as pointing loss. As the UAV can be anywhere in the uncertainty area, the primary aim is to ensure there is sufficient transmit gain at the edge of the uncertainty area. To achieve that, beams are selected according to its ability to produce higher amount of the transmit gain at the edge of the uncertainty area. For example, in Figure 3-13, when the uncertainty area is bigger than 84mrad, the 96mrad beam is selected since 84mrad beam fails to cover the uncertainty area. When the distance increases and the angular size of the uncertainty area decreases to 84mrad, the 84mrad beam will not be selected since the 96mrad beam continues to produce higher transmit gain than the 84mrad beam at the edge of the

uncertainty area, as can be seen in Figure 3-13. The 84mrad beam will only be selected when the distance increases further until the angular size of the uncertainty area decreases to 63.4mrad, which is at the 31.7mrad offset angle from the beam center in Figure 3-13. At this point, the transmit gain of 84mrad beam exceeds that of 96mrad beam.

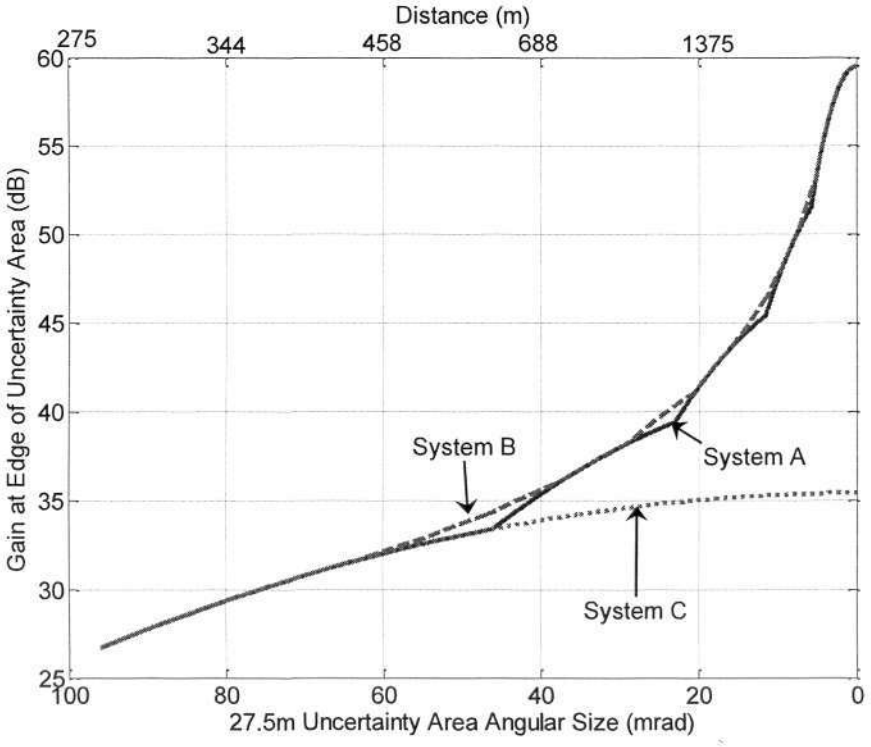

Figure 3-14: Transmit gain at edge of uncertainty area

Figure 3-14 shows the transmit gain of Systems A, B and C at the edge of the uncertainty area at varying distances between the UAVs. For example, at the uncertainty area of 80mrad, which is equivalent to the 27.5m uncertainty area at around 344m distance, the transmit gain at the edge of the uncertainty area is around 29.4dB. It can be observed that System B is able to provide higher transmit gains at some regions than System A. This is because System B has more selectable beam divergences than System A. System C produces the least gain at the edge of the uncertainty area due to its fixed beam divergence. In Table 3-3, the

beam divergence operating regions are shown for both systems A and B and will be used for subsequent evaluations.

Table 3-3: Region of beam divergence selections

Beam Divergence (mrad)	Beam divergence region of operation (m)		
	System A	System B	System C
96	300 to 596	300 to 434	300 onwards
84		434 to 501	
72		501 to 593	
60		593 to 728	
48	596 to 1192	728 to 942	
36		942 to 1341	
24	1192 to 2384	1341 to 1735	
21		1735 to 2004	
18		2004 to 2373	
15		2373 to 2911	
12	2384 to 4768	2911 to 3768	
9		3768 to 5365	
6	4768 onwards	5365 onwards	

3.6 System performance of beam divergence changing mechanism for inter-UAV FSOC under different weather conditions

In this section, we shall evaluate the three FSOC systems described earlier under varying weather conditions to evaluate and compare their transmission distance performance. In the atmosphere, inter-UAV FSOC mainly suffers from atmospheric attenuation, rain attenuation and scintillation [13]. A description of atmospheric physics can be found in [83].

Evaluations are performed using Matlab to find out the transmission distance of the systems. Table 3-4 shows the parameters used to analyze the FSO link between two UAVs. The transmitted optical beam is of 1550nm wavelength at 800mW with various beam divergences according to the distance between the UAVs, as listed in Table 3-3. For communications data rate of 2.5Gbps, the avalanche photodiode (APD) receiver is assumed to have a typical receiver sensitivity of 200nW for OOK format through a receiving aperture of 10cm. The transmit and receive optics losses are assumed to be low at 0.2dB, since maintenance work can be performed on the FSOC systems in UAVs when the UAVs are back from missions, and there is a 3dB link margin. The UAVs are assumed to be at the altitude of 1000m with a minimum 300m distance between them. With the beam centre pointing at the centre of uncertainty area, the evaluation is performed with the assumption that the UAVs are frequently experiencing large positioning uncertainty and are at the edge of their uncertainty areas. Therefore, pointing loss has to be considered. In addition, the following atmospheric models are considered in the evaluation. In the atmosphere, inter-UAV FSO mainly suffers from atmospheric attenuation, rain attenuation and scintillation loss [13].

Table 3-4: Link parameters

Parameters	Values
Transmit power	800mW (29.0dBm)
Transmit/Receive optics efficiency	0.95
Wavelength	1550nm
Minimum range	300m
Receive aperture	10cm
APD receiver sensitivity for 2.5Gbps OOK with BER of 10^{-9}	200nW (-37.0dBm)

System Margin	3dB
Altitude	1000m
UAV's speed	150km/h
Beam expander's expansion ratio	1x to 4x
Beam expander's step adjustment	0.5x

Beam transmission suffers attenuation as it is scattered and absorbed by atmospheric particles and molecules along the transmission channel. Atmospheric attenuation is related to weather conditions, ranging from clear weather (<1dB/km) to undesirable fog (>200dB/km in dense fog). As the transmission wavelength is chosen within the low absorption spectrum window, scattering effect dominates the attenuation [83-84]. Rayleigh scattering occurs when optical wavelength is larger than the size of the atmospheric particles, which are mainly the gaseous molecules. Rayleigh scattering's contribution to total attenuation is negligible. Mie scattering occurs when the optical wavelength is about the same as the size of the particles, which can be haze or fog particles. Last but not least, when the particle sizes increase and are much larger than the optical wavelength, geometrical (also known as non-selective) scattering occurs and the particles can be rain drops, snow, hail etc. Table 3-5 summaries the scattering type for the visible and IR wavelengths.

Table 3-5: Scattering regimes depending on particle size, β [84-85]

	Rayleigh Scattering	Mie Scattering	Geometrical or non-selective scattering
Particle Radius	$\beta << \lambda$	$\beta \approx \lambda$	$\beta >> \lambda$
Type of particles	Air molecules Haze	Haze Fog Aerosol	Fog Rain Snow Hail

The atmospheric attenuation is described by Beers-Lambert Law [84,86].

$$\tau(R) = e^{-\sigma R} \tag{3.1}$$

where $\tau(R)$ is the transmittance at transmission distance R and σ is the attenuation coefficient. While detailed scattering analysis, based on scattering particle size distribution, can be performed to find out the overall atmospheric attenuation, it is not practical since the particle distribution is not easily known. Instead, a simpler empirical model can be used to estimate atmospheric attenuation. Equation (3.2) relates visibility to the attenuation from visible to near infrared light as follows [84-86]:

$$Att_{atm}(\text{dB}) = -10\log\left[\exp\left(-\frac{3.912}{V}\left(\frac{\lambda}{550\text{nm}}\right)^{-q} R\right)\right]. \tag{3.2}$$

where Att_{atm} is the atmospheric attenuation, V is the visibility (km) and q is a parameter determined from experimental data based on the size distribution of the scattering particles and is given in the following [84,86]:

$$\begin{aligned}
q &= 1.6 && \text{for high visibility } (V > 50\text{km}) \\
&= 1.3 && \text{for average visibility } (6\text{km} < V < 50\text{km}) \\
&= 0.16V + 0.34 && \text{for haze } (1\text{km} < V < 6\text{km}) \\
&= V - 0.5 && \text{for mist } (0.5\text{km} < V < 1\text{km}) \\
&= 0 && \text{for fog } (V < 0.5\text{km})
\end{aligned} \tag{3.3}$$

Since UAVs conduct reconnaissance by taking photographs or video of ground activities, it is assumed that UAVs will not be deployed for missions under very poor visibility. Thus only FSOC in visibility of 1km to 23km will be investigated.

Another two main adverse atmospheric effects are rain and scintillation. Under increasing amount of rainfall, the loss due to rain attenuation will increase, resulting in shorter communications distance. Rain attenuation, Att_{rain}, can be estimated using rainfall rate, r (mm/hr), through [86-87]:

$$Att_{rain}(\text{dB}) = 0.001076 r^{2/3} R \tag{3.4}$$

Scintillation, caused by variation in the refractive index of air along the transmission path due to thermal changes, causes rapid and random fluctuations in the beam intensity by several dBs with a frequency spectrum from about 0.01Hz to 200Hz [13,88-89]. Atmospheric turbulence creates air pockets with varying refractive index due to differences in temperature and densities among the air pockets. Light traveling through different air pockets will have different paths, as shown in Figure 3-15, and it results in fluctuation of signal at the receiver.

Figure 3-15: Scintillation due to effects of air pocket [88]

Scintillation is the strongest when the temperature is at the highest, which is during midday [13,90]. The refractive index structure parameter, C_n^2, is used to characterize the atmospheric refractive turbulence. A commonly used model to estimate C_n^2 is the Hufnagel-Valley (HV) model [4,55,91]:

$$C_n^2(h) = 5.94\times10^{-53}\left(\frac{v}{27}\right)^2 h^{10}\exp\left(\frac{-h}{1000}\right) + 2.7\times10^{-16}\exp\left(\frac{-h}{1500}\right) + C_n^2(0)\exp\left(\frac{-h}{100}\right) \tag{3.5}$$

where v is the root-mean-square wind speed (m/s) at altitude h (m) and $C_n^2(0)$ is the refractive turbulence at ground level. For visual and sound concealment, it is assumed that the UAVs will not fly below 1000m. With $C_n^2(0)$ of 10^{-12} $m^{-2/3}$ which represents very strong atmospheric turbulence at ground level and average wind speed of 21m/s, $C_n^2(h)$ at altitude of 1000m is about 1.84 $\times 10^{-16}$ $m^{-2/3}$. Scintillation variance, σ_χ^2, can be expressed by the following [85-86]:

$$\sigma_\chi^2 = 23.17 \times \left(2\pi/\lambda\right)^{7/6} \times C_n^2 \times R^{11/6} \tag{3.6}$$

Scintillation has peak-to-peak amplitude of $4\sigma_\chi$ and loss related to scintillation is equal to $2\sigma_\chi$. Thus, scintillation loss, L_{scin}, can be estimated by [87]:

$$L_{scin}(\mathrm{dB}) = 2\left(23.17 \times \left(2\pi/\lambda\right)^{7/6} \times C_n^2(h) \times R^{11/6}\right)^{1/2} \tag{3.7}$$

The link transmission distance will be evaluated under the different weather conditions shown in Table 3-6. Varying atmospheric refractive turbulences are included under the different weather conditions to factor in scintillation attenuation.

Table 3-6: Weather conditions for evaluation

Weather Condition	Visibility / Rainfall	Atmospheric Turbulence at ground level ($m^{-2/3}$)
Clear weather	10 to 23km	10^{-12}, 10^{-13}, 10^{-14}
Haze	2 to 10km	10^{-14}, 10^{-15}, 10^{-16}
Light fog	1 to 2km	10^{-15}, 10^{-16}, 10^{-17}
Normal Rain	1 to 15mm/hr	10^{-13}, 10^{-14}, 10^{-15}
Strong Rain	15 to 60mm/hr	10^{-14}, 10^{-15}, 10^{-16}

Particularly strong rain	60 to 100mm/hr	10^{-15}, 10^{-16}, 10^{-17}

The following link budget equation is used to find the transmission distance:

$$G_{tx} + L_R + L_p + Att_{atm} + Att_{rain} + L_{scin} = P_{tx} - P_{rx-sen} - L_{tx} - L_{rx} - G_{rx} - M \quad (\text{dB}) \tag{3.8}$$

where $P_{rx\text{-}sen}$ and M are the receiver sensitivity and link margin, respectively. The terms on the left hand side of Equation (3.8) are dependable on the beam divergence, visibility, rainfall, atmospheric turbulence and transmission distance while the terms on the right are constants. By varying the beam divergence, visibility, rainfall and atmospheric turbulence, the terms on the left hand side of Equation (3.8) has to balance with those terms on the right hand side, thus allowing the transmission distances under the various conditions to be found.

Evaluations are conducted using Matlab to find out the transmission distance of the systems under the weather conditions stated in Table 3-6 and results are shown in Figure 3-16 to Figure 3-19.

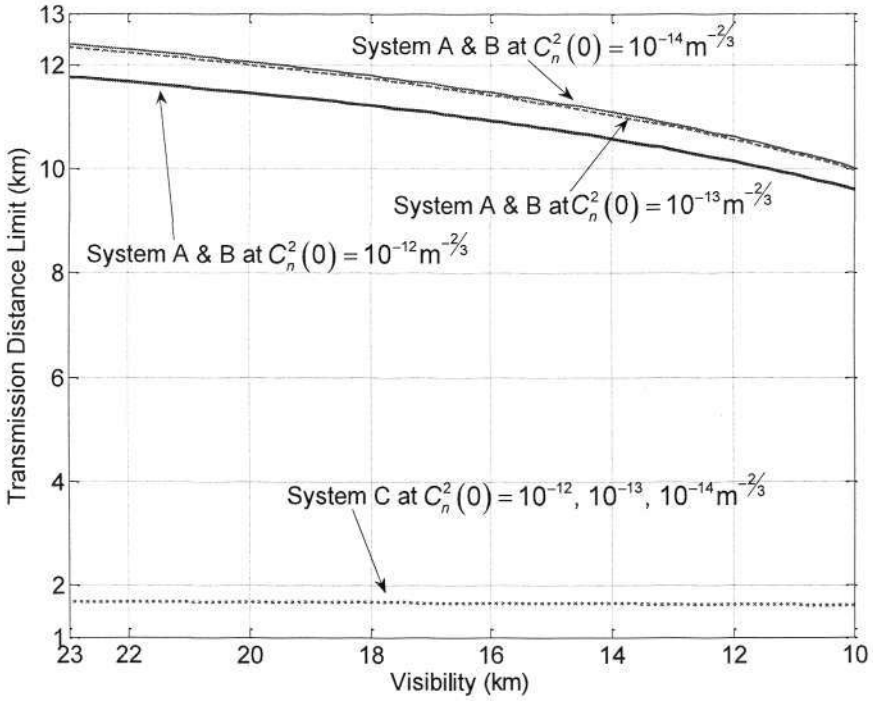

Figure 3-16: Transmission distance under clear weather conditions

Figure 3-16 and Figure 3-17 show the transmission distance limit under clear weather conditions and haze and light fog conditions respectively. Under clear weather conditions, both Systems A and B have the same transmission reach as both systems are employing the 6mrad beam at those distances. As the ground atmospheric turbulence increases, the transmission distance is reduced since scintillation loss is higher with larger atmospheric turbulence. System C, which uses 96mrad beam, has significantly much lesser transmission reach, compared with Systems A and B.

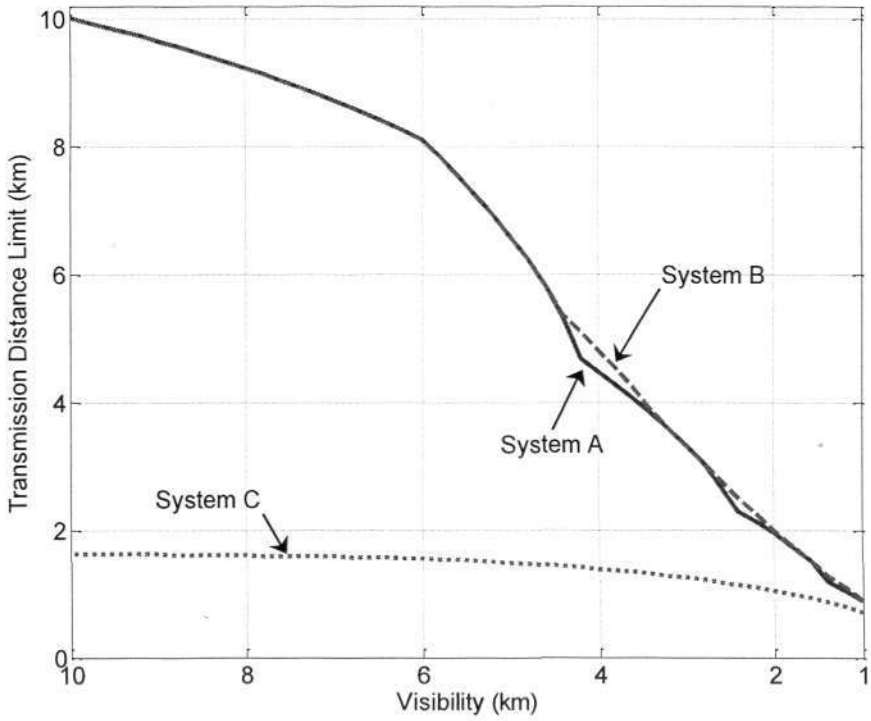

Figure 3-17: Transmission distance under haze and light fog conditions

Figure 3-17 shows that at the altitude of 1000m, the different ground atmospheric turbulences of 10^{-14} to 10^{-17} $m^{-2/3}$ produce similar scintillation losses and can be represented by a single curve each for the three systems. It can be observed that the transmission distance is greatly reduced as the visibility drops and atmospheric attenuation increases. At certain visibility regions, System B has better transmission reach than System A. This is because System B can have more beam choices to better match the uncertainty areas at those regions. The same evaluations are also conducted for rainfall attenuation, with the results shown in Figure 3-18 and Figure 3-19.

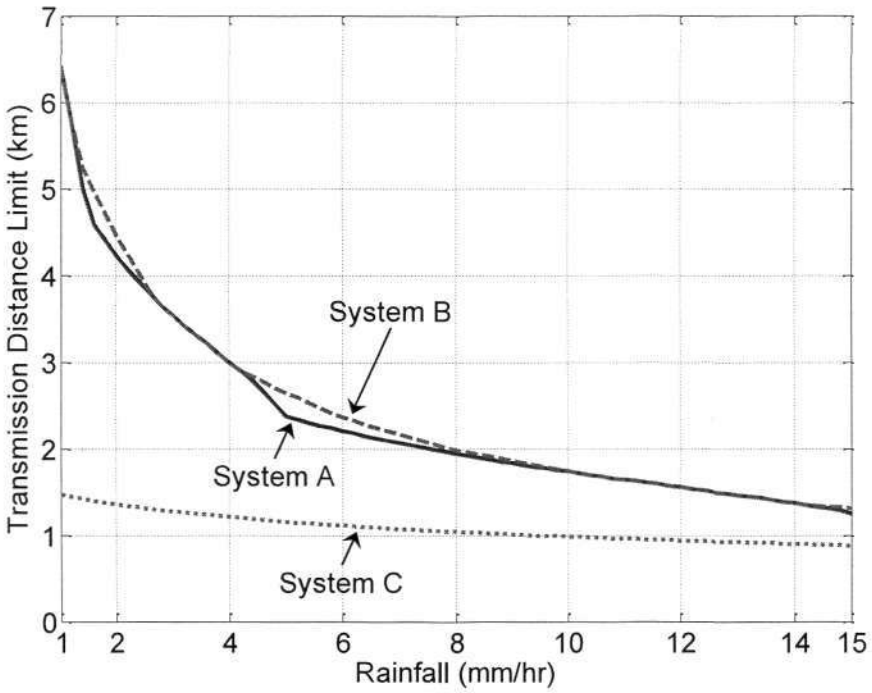

Figure 3-18: Transmission distance under normal rainfall conditions

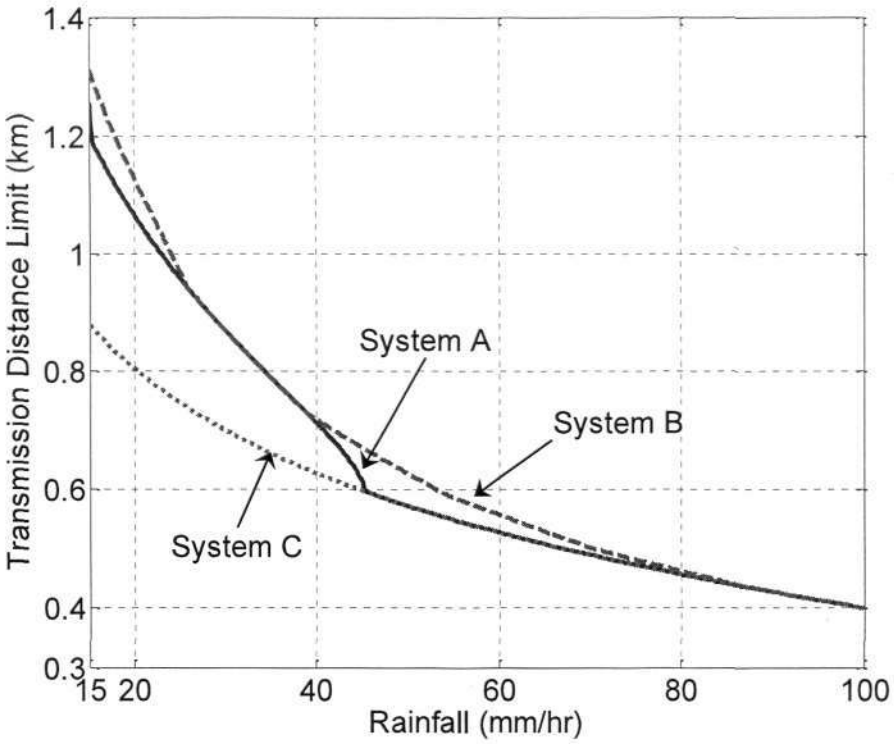

Figure 3-19: Transmission distance under strong and particularly strong rainfall conditions

Figure 3-18 and Figure 3-19 show the transmission distance performance in normal rainfall, and strong and particular strong rainfall, respectively, as stated in Table 3-6. Again, the scintillation losses are similar for varying ground atmospheric turbulences from 10^{-13} to 10^{-17} $m^{-2/3}$, so there is only a single curve each for all three systems in Figure 3-18 and Figure 3-19. In Figure 3-19, at rainfall of more than 45mm, the loss due to rainfall is higher, resulting in shorter communications distance. At that point and beyond, System A and C would have the same beam divergence of 96mrad and therefore results in the same curve after they converge. Although it can be observed again that System B performs better than System A for certain rainfall conditions, it is reasonable to say that the performance of System A is close to that of System B with System B having slightly better performance. Both systems show significant improvement in performance over System C, demonstrating the importance of using the beam divergence changing mechanism to change the beam divergences.

3.7 Summary

We have discussed and analyzed the problems associated with using a fixed beam divergence for short-range inter-satellite and inter-UAV FSOC. The varying separation distance between the flight platforms results in varying angular size of the far platform's uncertainty area and free-space range loss. With a fixed beam divergence, the beam footprint area produced can either be insufficiently or overly exceed the required uncertainty area when the distance changes. Correspondingly, the free-space range loss spans across a wide range of values according to the

distance. As such, using a fixed beam divergence is difficult to deal with the distance variation between the platforms.

To solve the problem, the author proposed to use beam divergence changing mechanism. The selection of suitable beam divergence for different regions of distances produces beam footprint that is suitable for the angular coverage of the uncertainty area at a certain distance. It also counters the effects of varying free-space range loss by producing sufficient transmit gain when required. Four methods to implement the mechanism were proposed by the author and they are driven towards producing desired collimated beam diameter. The first method is to move lenses into the transmit path, the second method is to incorporate a motorized beam expander, the third method is to switch optically between optics and the final method is to use an optical switch and beam expanders.

Analysis was made to show the value of the beam divergence required for FSOC to work for both inter-satellite and inter-UAV FSOC. In the case of inter-UAV FSOC, atmospheric effects like atmospheric attenuation, scintillation and rain were taken into account and the results showed improvement in transmission distance. Compared to a fixed beam divergence system, the results showed that inter-UAV FSOC links that switches between beam divergences are able to communicate further by a significant amount in different levels of visibility, rainfall and atmospheric turbulence, showing the importance of using the beam divergence changing mechanism for varying short-range separation distance between the flight platforms.

Chapter 4. Multipoint FSOC System

4.1 Introduction

FSOC can be employed between fixed or mobile point-to-point terminals. For fixed terminals, an initial manual pointing of the terminals will usually be sufficient. For mobile terminals, automatic pointing systems have to be incorporated with the terminals in order to make dynamic adjustments to maintain the LOS [3,15,69]. For duplex communications, the transmitting and receiving FSOC channels are typically housed together, creating a compact FSOC transceiver [10,11,15,17,32,37-38,43,59,73,92]. Thus, the pointing system is required to have sufficient motor power and material strength to support the pointing of the FSOC transceiver.

Examples of mobile terminals are flight platforms like satellites or UAVs flying within a cluster, separated spatially between hundreds of meters to a few kilometers. Due to their special potential applications, there is increasing interest and research in satellites and UAVs in a cluster and FSOC has been examined to be a suitable communications channel between the individual flight platforms within the cluster. To form a real-time or near real-time network within the cluster, at least one platform is required to have the ability to perform concurrent multiple point-to-point communications, such as individual platforms in a mesh topology or a hub platform in star topology. As a result, at least one platform is required to have more than one transceiver with its own pointing system.

However, there is always a payload capacity limit on any flight platform in terms of weight, size and power. This limit will set a constraint on the network design since the number of transceivers, with their corresponding pointing system, that can be installed on the flight platform have to be within the limit. With the weight, size and power constraints, the mission capability and duration of the flight platforms can be affected as well as restricting the network design. In this chapter, a new multipoint FSOC system design is proposed by the author to allow multipoint communications on flight platforms within a cluster. It can replace the use of multiple transceivers with weight, size and power advantages. As such, it can potentially be employed within the weight, size and power limits imposed by the flight platforms that require multipoint communications, aiding in network design. The multipoint FSOC system design, the benefits and constraints will be discussed and examined.

4.2 Problems with FSOC transceiver for Multipoint Communications on Flight Platforms

4.2.1 Point-to-Point Limitation of FSOC Transceiver

In almost all FSOC applications, a transceiver package is preferred as both the transmitter and receiver requires pointing capability to establish the LOS with the far platform's receiver and transmitter respectively. Thus, it is more economical to have both transmitter and receiver on the same gimbal (pointing system) for pointing than to have separate pointing system for both components. They share

the same optical aperture, which is used for collimating the outgoing beam and capturing the incoming beam, and alignment between the transmitting and receiving paths is also facilitated when they are housed together. For mobile and fixed long range communications or fixed short-range communications, a transceiver package is a preferred choice. Figure 4-1 shows an example of a transceiver, which is a terrestrial fixed point-to-point short-range communications product of LightPointe, a commercial FSOC company [9].

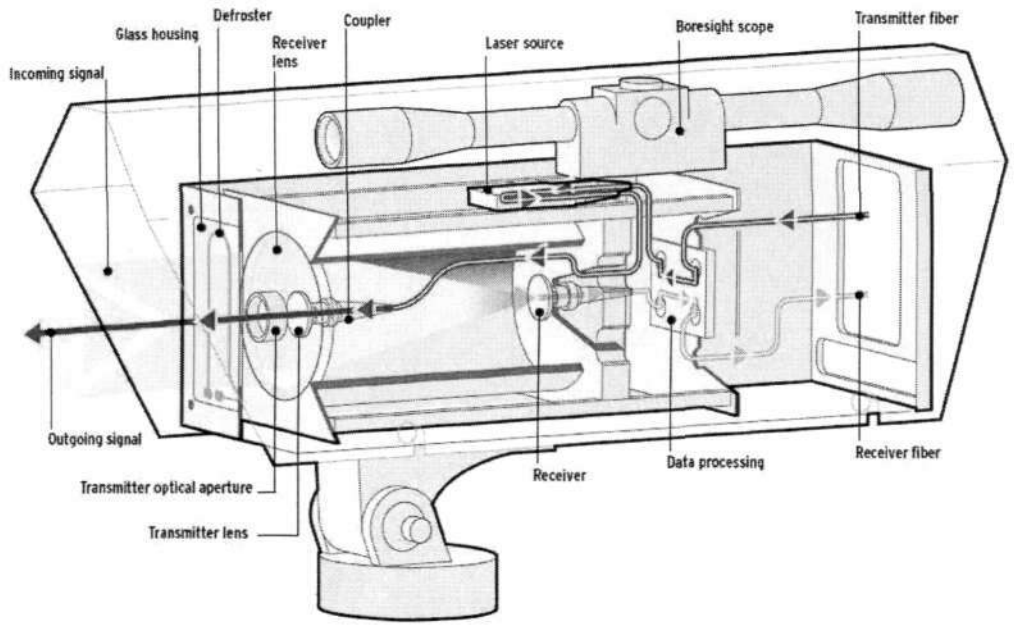

Figure 4-1: Design of LightPointe's transceiver [9]

However, almost all the FSOC transceivers, from commercial or research, are designed primarily for point-to-point communications. Multipoint communications with several other transceivers is only possible in a typical FSOC transceiver if all those far transceivers are within its FOV. This requires the far transceivers to be positioned closely to each other angularly from the perspective of the transceiver, which is not practical for flight platform network design. Although the size of the FOV of a transceiver can be dictated by the FSOC

designer, the advantage of having a large FOV is offset by the larger background noise received, which will deteriorate the communications performance. Therefore, the only practical way to implement multipoint communications through the use of transceivers is to employ more units of it, each to be used for each point-to-point channel. The number of transceivers required will increase with the number of concurrent FSOC links but the flight platform's payload capacity will limit the number of transceivers that can be installed. Thus, the use of multiple transceivers for multipoint communications on flight platforms is not suitable.

4.2.2 Weight and Power Consumption of FSOC Transceiver's Pointing System

An estimation of the weight and power consumption for transceiver and gimbal packages for different communications distance can be found in [38]. The optical communications demonstrator (OCD), developed at JPL, is a transceiver meant for flight platforms, particularly for satellites and aircrafts [15,92]. It consists of a telescope optics assembly, a gimbal and electronics to operate the terminal. The OCD terminal weighs 21kg, of which 10kg is contributed by the gimbal [94]. The gimbal also takes up more than 50% of the entire OCD's power consumption. Although the OCD is designed with intended communications range of thousands of kilometers, it is also expected for the pointing system to be a comparative load, if not bigger, with the transceiver for short-range FSOC.

The weight and power consumption of the pointing system adds on to the limited payload capacity problem when multipoint communications are required since each transceiver must be equipped with its own pointing system. The total weight, size and power requirements of a set of transceiver and its pointing system restrict the employment of multiple FSOC transceivers on smaller flight platforms such as micro-satellites, nano-satellites or mini-UAVs, which are the preferred platforms for clustering. The use of bigger flight platforms, to accommodate more FSOC transceivers, will mean higher cost, especially in the context of satellites where the launch cost escalates with the weight of the satellite load. In order to reduce the weight and power consumption of the pointing system, it is essential to reduce the pointing system's load, which is the transceiver itself and is unlikely to be scaled down without compromising communications performance.

4.3 Proposed Multipoint FSOC System Design

To address the problems highlighted above, the author hereby proposes a multipoint FSOC system design for multipoint communications, replacing the typical transceiver design. A literature review on proposed multipoint FSOC system designs by others can be found in Section 2.6 on page 31. From this point onwards until the end of the Chapter 4, only the author's proposed multipoint FSOC system design will be described and the proposed design has never been found in any literature to the best of the author's knowledge. The author proposes separating the transmitter from the receiver physically with no components being shared among them, as a result, the proposed design is entirely different from typical FSOC transceiver design.

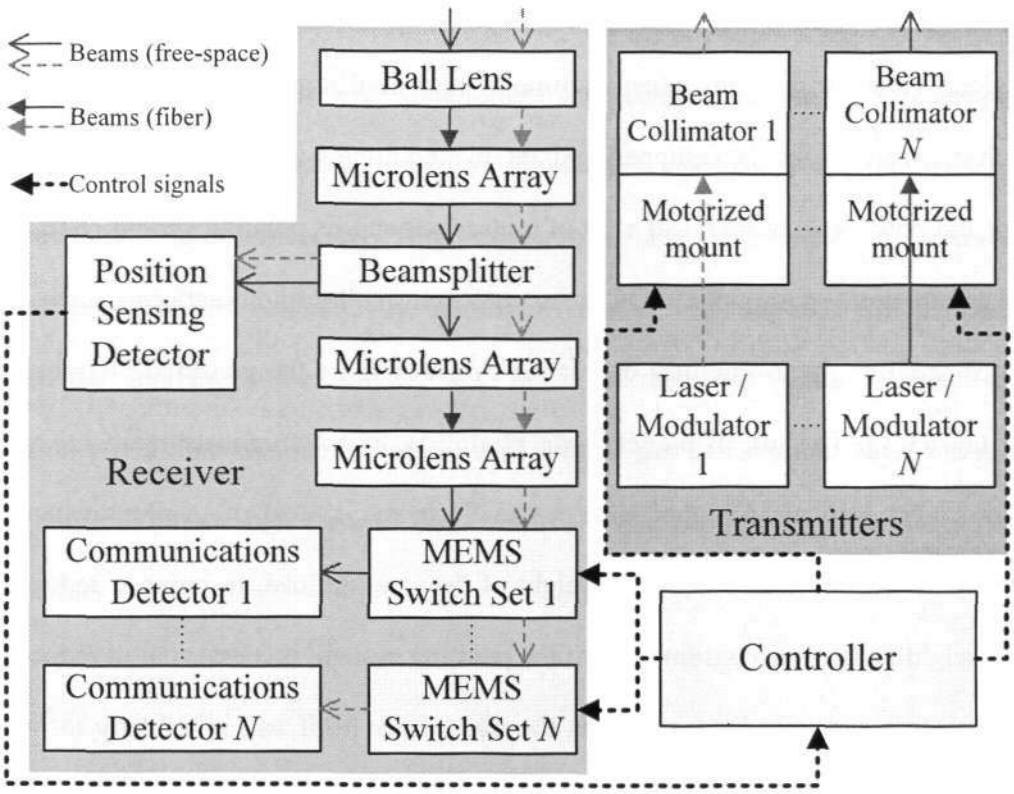

Figure 4-2: Block diagram of the proposed multipoint FSOC system design

The proposed multipoint FSOC system design is shown in Figure 4-2. The novelties of the proposed design are the use of a ball lens, which is able to receive multiple incoming beams from multiple directions, and the configuration of fibers and optical components to guide the beams to desired detectors for communications and extraction of detected beam's directional information. These features allow a single receiver to be able to receive multiple beams concurrently while being positional-fixed, therefore removing the need of a pointing system for the receiver. This proposed design also greatly reduces the weight and size of FSOC payload for multipoint communications for flight platforms since the combination of a single FSOC receiver and multiple smaller transmitters is able to replace multiple transceivers.

Incoming beams to the multipoint FSOC system will be captured by the ball lens and coupled into the optical fibers placed at the focal point of the ball lens. The beams will be subsequently guided by the fibers, exited into free-space and diverted partially to provide directional information of the captured beams through a position sensing detector. The directional information is used by the controller to control the MEMS switches to switch the guided beams to the desired optical communications detectors and to steer the pointing of the transmitters. They will be discussed in more details in the subsequent sections.

For short-range communications, the transmitters can incorporate commercially available beam collimators that can sufficiently provide the desired beam divergences, which are in the milli-radians range for short-range FSOC. This allows the reduction of the pointing systems' requirements to support the transmitters and small motorized mounts can be used instead of powerful pointing device like gimbal, reducing power, weight and size consumption. To sum up, in the proposed multipoint system design, the transmitters and receiver are separated into a single receiver for all receiving multipoint communications and multiple smaller transmitters for outgoing point-to-point communications that can be supported by small pointing devices. They will be described and discussed in detail in the next two sections.

4.4 Proposed Multipoint FSOC Receiver Design

4.4.1 Ball Lens and Fiber Coupling

This receiver design makes use of a ball lens as the receiving aperture of the proposed system, utilizing its ability to receive light from all directions. The ball lens is of sphere shape and is made of conventional optical glasses materials [95]. Due to its spherical design, incident light beams on the ball lens are focused on the opposite end of the ball lens. Its complete rotational symmetry allows it to be positioned, mounted and aligned easier than conventional lenses. A ball lens can be described by its refractive index, n, and diameter, D_{lens} [95].

A typical FSOC transceiver can only collect light from a small FOV region in the range of milli-radians but with the ball lens, there is no limit to its FOV. The ball lens can be imagined as if it consists of lenses facing every direction. However, the mounting of the ball lens onto the platform will reduce the FOV, which nevertheless will still span across a big angular region larger than a third of a sphere. Although larger and heavier compared to the normal lens used in a transceiver due to the sphere's volume, a ball lens can eliminate the need of multiple receiving apertures required in the conventional transceiver design, thus the weight and size advantages from using the ball lens increases with the increment in the number of multipoint connections. Figure 4-3 shows the path of a paraxial light beam through the ball lens and its associated parameters [95],

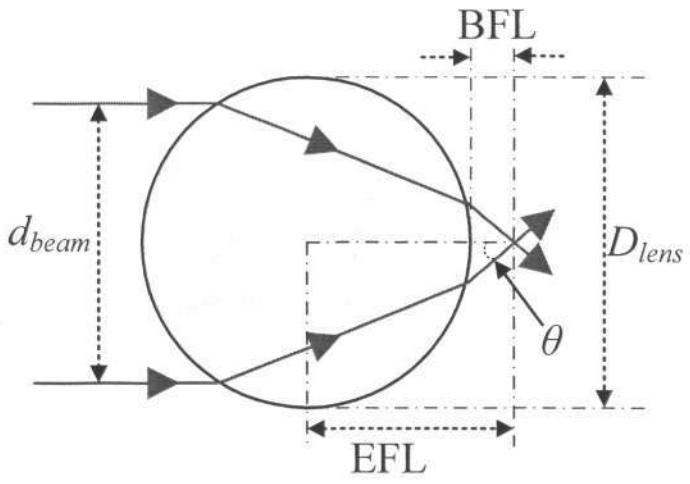

Figure 4-3: Parameters of ball lens

where EFL is the effective focal length; BFL is the back focal length; d_{beam} is the diameter of the beam which will be within the angle, θ, between the edge rays and the on-axis ray, and D_{lens} is the diameter of the ball lens. The ball lens' numerical aperture, NA_{lens}, is the sine of the angle θ. EFL is calculated by Equation (4.1) and BFL can be found by subtracting the radius of the ball lens from the EFL. NA_{lens}, n, d_{beam} and D_{lens} are related through Equation (4.2) [95]. Since the maximum value for d_{beam} to fall upon the ball lens is D_{lens}, for a ball lens with a certain n value, there is a maximum theoretical ball lens' NA. Assuming refractive index is 1.5 and d_{beam}= D_{lens}, which means that the light beam falls across the entire ball lens, the maximum theoretical ball lens' NA is 0.667.

$$\mathrm{EFL} = \frac{nD_{lens}}{4(n-1)} \tag{4.1}$$

$$d_{beam} = \frac{nD_{lens}}{2(n-1)}\mathrm{NA}_{lens} \tag{4.2}$$

Optical fibers can be placed at the focal point on the opposite side of the ball lens to couple the light incident on the ball lens into them. For the focused beam to be

coupled into the fiber with high coupling efficiency, it is required for the fiber's numerical aperture, NA_{fiber}, to be as close to the maximum ball lens' NA as possible, otherwise the light rays incident on the fiber core outside the fiber's NA will not be guided through the fiber. These fibers are positioned side by side in a hexagonal configuration such that each individual fiber has equal spacing between the neighboring 6 fibers and itself, as shown in Figure 4-4. As they are positioned on a spherical plane of BFL distance from the surface of the ball lens, each fiber is of slight angular displacement to each other, each aligning towards the centre of the ball lens. This is illustrated in Figure 4-5.

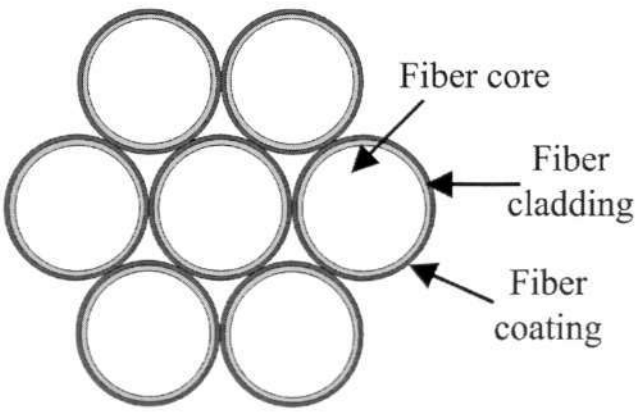

Figure 4-4: Hexagonal fiber placing

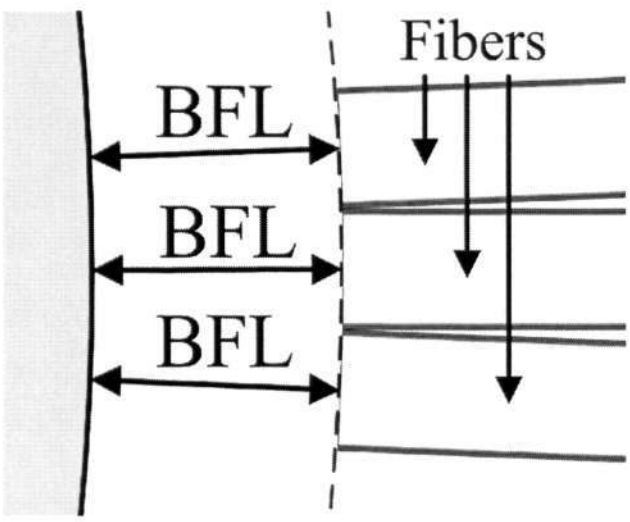

Figure 4-5: Angle displacement between fibers

Through the setup above, although the ball lens can capture light from all directions, each individual fiber will only collect the light beams coming into the ball lens from a certain small directional zone around the alignment axis of each fiber. Thus, each fiber will have an individual FOV that is different from other fibers. With a small FOV, the probability of having unwanted background light point sources within the FOV is lowered. For uniform background light, a smaller FOV means lesser background light is accepted into the fiber.

For a certain ball lens, Equation (4.2) shows that a bigger value of d_{beam} will result in higher ball lens' NA. Having larger d_{beam} is essential as the receive gain of the ball lens increases with d_{beam} and in practical situation, the incoming beam will usually fall across the entire ball lens' diameter, resulting in $d_{beam}= D_{lens}$ and maximizing the gain of the ball lens. However, this receive gain from the ball lens will be reduced as not all the light captured by the ball lens will be coupled into the fiber. Thus assuming $d_{beam}= D_{lens}$, the overall receive gain that is coupled into the fiber is related to the fiber's NA by:

$$G_{rx} = \left[\frac{\pi n D_{lens}}{2(n-1)\lambda} \mathrm{NA}_{fiber} \right]^2 \qquad (4.3)$$

For a ball lens with a certain D_{lens} and n, Equation (4.3) suggests that by increasing the fiber's NA, G_{rx} will increase. By increasing the fiber's NA to the theoretical maximum ball lens' NA, the fiber is theoretically able to be coupled with the entire light beam that falls across the ball lens' diameter. Unfortunately, Equation (4.3) is only true if all the light rays are focused onto the same point. A ball lens' ability to focus the light rays is affected by spherical aberration which in

turn is increased with higher ball lens' NA [96]. Therefore a larger d_{beam} is limited by the aberration and for a ball lens that is illuminated with light beam across its entire diameter, the result is a diffused focal point and a bigger spot beam. Thus, light rays further away from the center of the spot beam may miss the core of the fiber entirely.

Considering d_{beam} and spherical aberration, there are two requirements for higher beam coupling efficiency, the fiber's NA has to be as close as possible to the maximum ball lens' NA and the fiber core diameter has to be larger in order to capture more light rays in the spot beam. Therefore, multimode fibers with bigger NA are more suitable to be used here compared to singlemode fibers. It is also necessary for multimode fibers to have a much larger core diameter than the typical 50μm or 62.5μm diameter since the spot beam will be larger than those sizes.

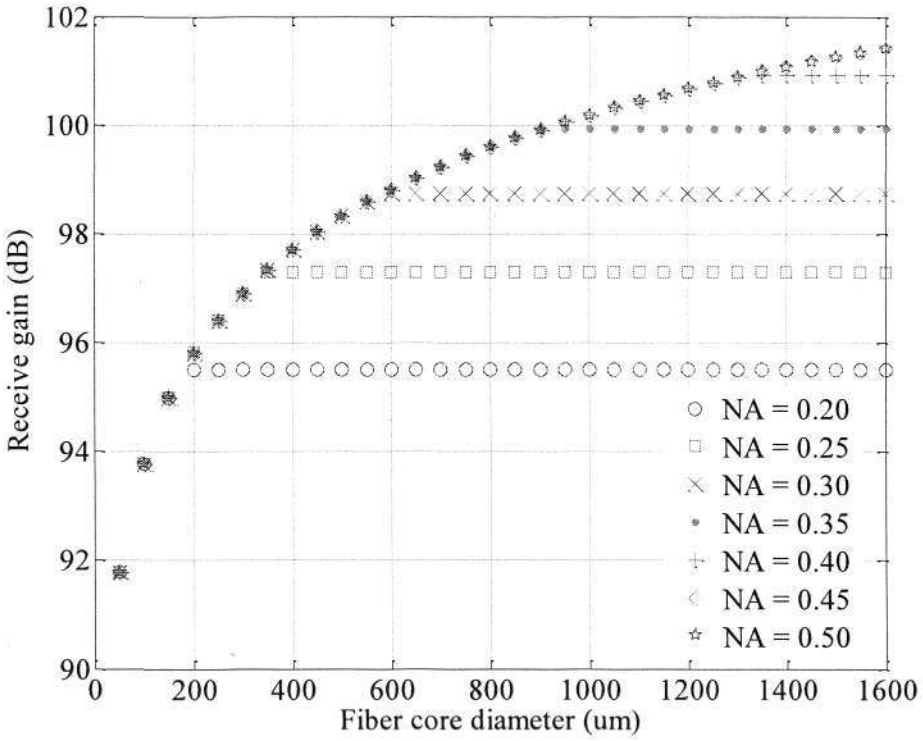

Figure 4-6: Receive gain for fibers with varying core diameters and NAs

Depending on the fiber core and cladding refractive indexes and their difference, different fiber NAs can be achieved. Figure 4-6 shows the overall receive gain, assuming that the diameter of the ball lens is 10cm with a refractive index of 1.5, against fibers of varying core diameters and NAs. The results are obtained by simulation using ZEMAX at wavelength of 1550nm and plotted in Matlab [97]. As shown in Figure 4-6, for a fiber with a certain NA, by increasing the fiber core diameter, the receive gain will only increase until a point and remain constant thereafter. Likewise for a fiber with a certain core diameter, by increasing the fiber's NA, the receive gain will also increase until a point and remain constant from that point onwards. The receive gain will only continue to increase with both bigger fiber core and higher fiber's NA.

The core diameter of commercially available multimode fibers ranges from 50μm to 1500μm with NA_{fiber} from approximately 0.2 to 0.5 [98]. Assuming a fiber with a core/cladding diameter of 1500μm/1550μm and NA_{fiber}=0.39 is used, a receive gain of 101.5dB can be obtained from Equation (4.3) with d_{beam}=5.85cm. However, ZEMAX simulation showed that only 100.7dB receive gain can be achieved after optimization at the BFL of 2.045cm with d_{beam}=5.36cm. Approximately 0.8dB difference in the theoretical and simulated receive gain is due to spherical aberration.

Figure 4-7 illustrates the path of the light rays through the ball lens due to spherical aberration. Figure 4-8 shows the bundle of light rays that is actually coupled into the fiber. The propagation of the light rays through the ball lens in Figure 4-7 and Figure 4-8 are simulated in ZEMAX using the ray tracing capability. The light rays outside the bundle in Figure 4-8 are those that fall onto other surrounding fibers. Although such fiber has high attenuation of 18dB/km, for the proposed design, the fiber length is in the range of centimeters [98]. Thus beam power loss through the fiber is negligible and pulse dispersion is also kept to very low level. The bigger fiber core also reduces losses due to positioning and alignment of the fiber since the bigger fiber core can tolerate a much larger error before significant loss appears compared to the typical singlemode or multimode fibers.

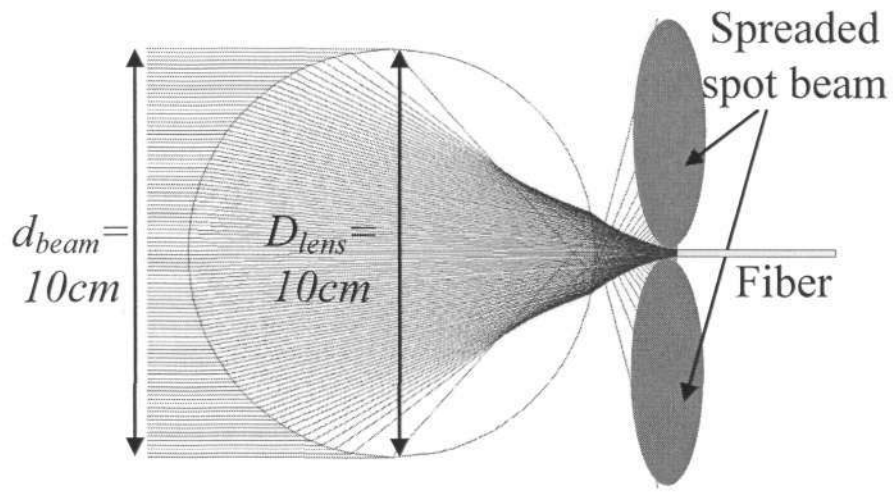

Figure 4-7: Light rays through the ball lens due to spherical aberration

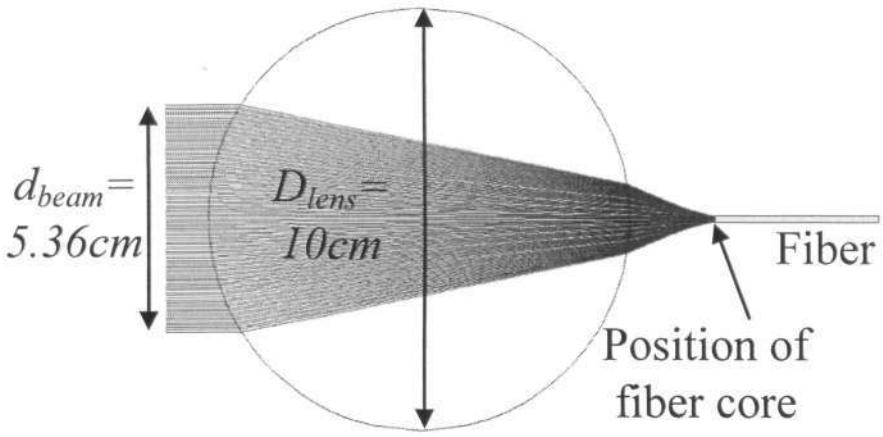

Figure 4-8: The light rays through the ball lens that is coupled into fiber

As the fibers need to be placed side by side, another factor to be considered is the fact that the center of the spot beam will not fall onto the center of a fiber for most of the time. Moreover, there are blind areas in between the fibers, including fiber cladding and coating. Figure 4-9 shows the center of the blind areas, denoted by the dots, and a hexagonal area around a fiber, which is formed by connecting the centers of the blind areas around the fiber. The hexagonal area marks out the FOV of the fiber, whose boundaries are shared with neighboring FOVs. Since there are no dead areas between adjacent FOVs, the centre of every spot beam will always fall upon at least one FOV and the fiber within that FOV will be receiving the

highest beam power compared to the neighboring fibers. However, when the centre of the spot beam falls upon the edge of the FOV, the beam will spread across two or more FOVs evenly.

The worst situation occurs when the centre of the spot beam falls onto the center of any blind areas, which is also the edge corner of three FOVs. When that happens, the spot beam will spread across three fibers and all the three fibers will receive the same amount of beam power. However, from each fiber's perspective, the receive gain is the lowest when the spot beam falls onto that position.

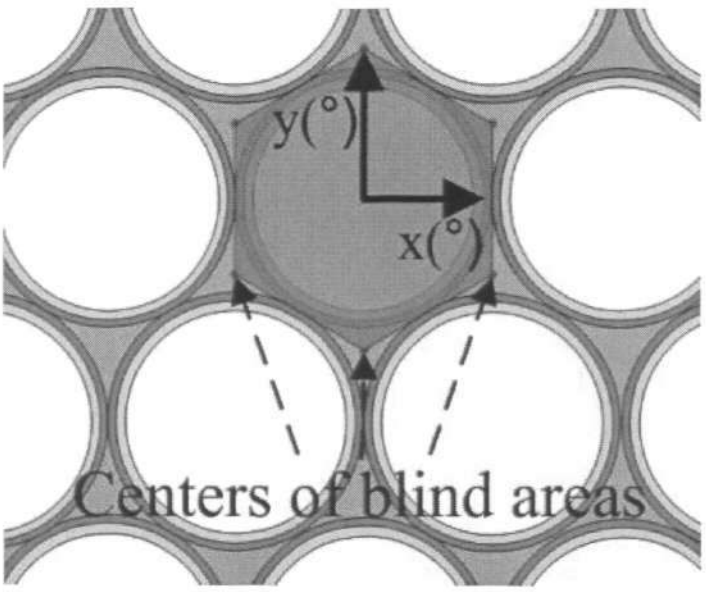

Figure 4-9: The hexagonal-shaped FOV of each fiber

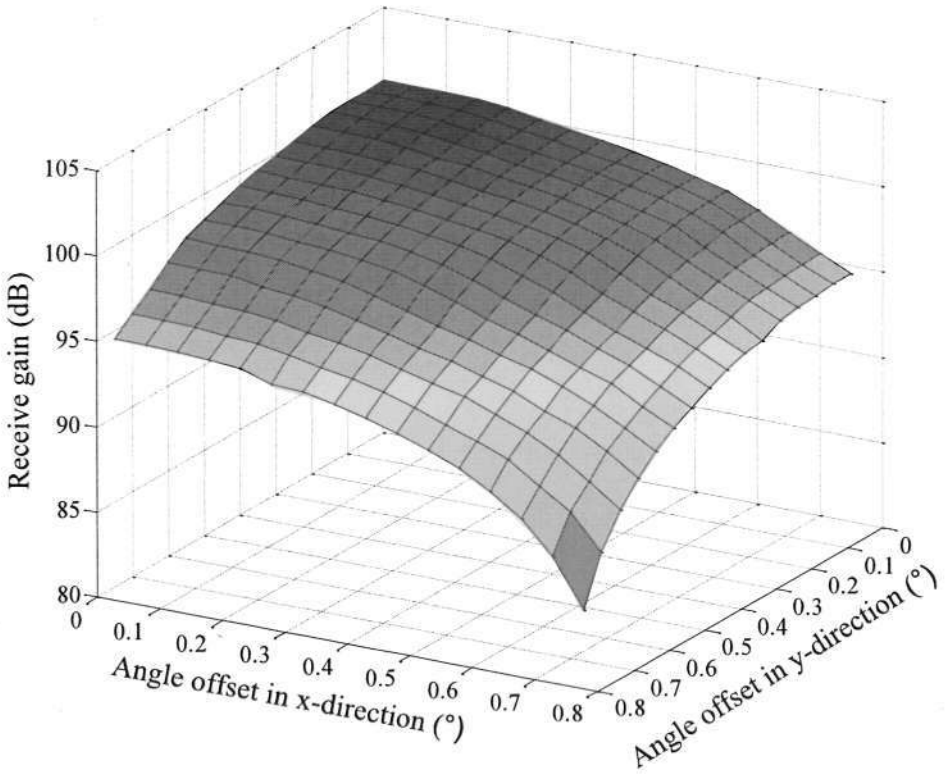

Figure 4-10: Receive gain when the spot beam lands at different areas of fiber

Assuming that the 1500μm/1550μm core/cladding fiber has a coating thickness of 100μm, Figure 4-10 shows the amount of receive gain at an angular offset in the x and y directions, indicated in Figure 4-9. The results are obtained by simulation using ZEMAX and plotted in Matlab. If the spot beam fall at the centre of the blind area, the gain will be 93.3dB each for the three adjacent fibers. Thus when the spot beam moves inwards from the edge corner of the FOV to the centre, the range of gain for the fiber with the highest beam power will be between 93.3dB and 100.7dB and correspondingly, for surrounding fibers, they will have gain ranging from 93.3dB to 71.5dB. Thus, crosstalk between fibers can be high when there are 2 closely positioned far platforms and their beams may be focused onto neighboring fibers. To mitigate crosstalk, different wavelengths with sufficient spacing may be used with narrow band pass filters (BPF) placed in front of the

detectors, which will be discussed later. It is also worth noting that flight platforms are unlikely to be flying close to each other, thus it is unlikely to have several beams coming from the same angular region.

To improve the overall receive gain from the ball lens into the fiber, it is desirable to reduce the size of the blind areas so that more beam power is captured within fiber core areas. Thus the thickness of the fiber cladding and the fiber coating can possibly be made smaller without compromising the light guiding functionality of the fiber itself.

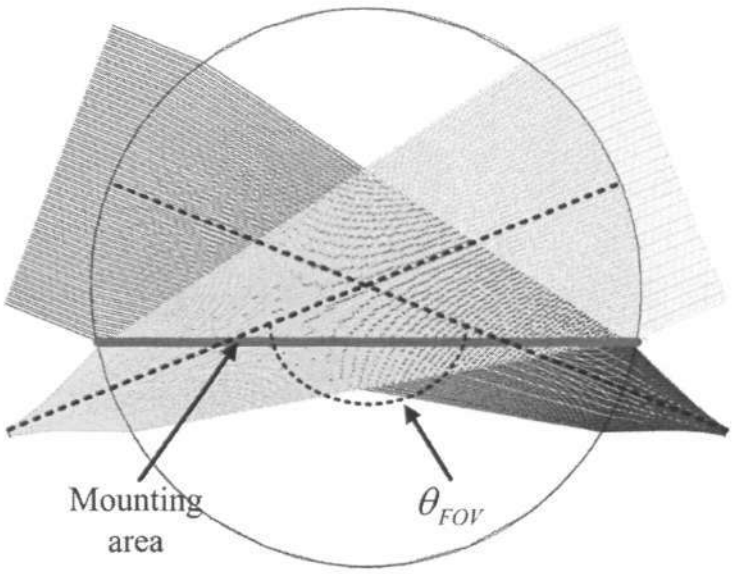

Figure 4-11: FOV of ball lens after mounting

Last but not least, from Figure 4-8, the ball lens should be mounted on the flight platform such that the light ray bundle to be coupled fully into the fiber is not obstructed by the mounting area. Figure 4-11 shows where the ball lens should be mounted on the platform surface, thus only the top portion of the ball lens is

exposed outside the flight platform. The propagation of the light rays through the ball lens in Figure 4-11 is simulated from ZEMAX. The portion of the ball lens below the mounting area, as well as the rest of the multipoint receiver components, are housed within the platform and protected from external environment. In the above example, the full FOV of the ball lens is approximately 136.6°, which is many times larger than the milli-radians FOV provided by typical FSOC transceivers.

4.4.2 Light Directional Detection through Position Sensing Detector

Figure 4-12 shows the diagram of a portion of the receiver after the ball lens. As explained above, multimode fibers with larger core diameters are placed side by side at the focal points on the opposite side of the ball lens to couple the light incident on the ball lens into the fibers. The other ends of the fibers will be connected into a microlens array with the microlenses arranged in the same hexagonal configuration as the fibers are arranged at the ball lens. However, the microlenses are of zero angular displacement with each other this time; they are placed on a flat plane. Light coupled into the fibers at the ball lens will be guided along the fibers and exited into free-space at the fibers' ends with beam spreading in a cone shape. To prevent the beam spreading, the use of the microlens array allows the light beams within the fibers to be collimated.

A beam splitter, placed after the microlens array, will split and direct a portion of the collimated beam, through focusing optics, into a pixel array position sensing

detector such as CCD or CMOS detector while allowing transmittance to the rest of the beam into another microlens array that will couple the free-space beams into fibers arranged in hexagonal shape again. The beamsplitter, with the splitting surface aligned 45° to the incoming beam direction, will maintain the beam positions after splitting so that beam directional information will not be lost.

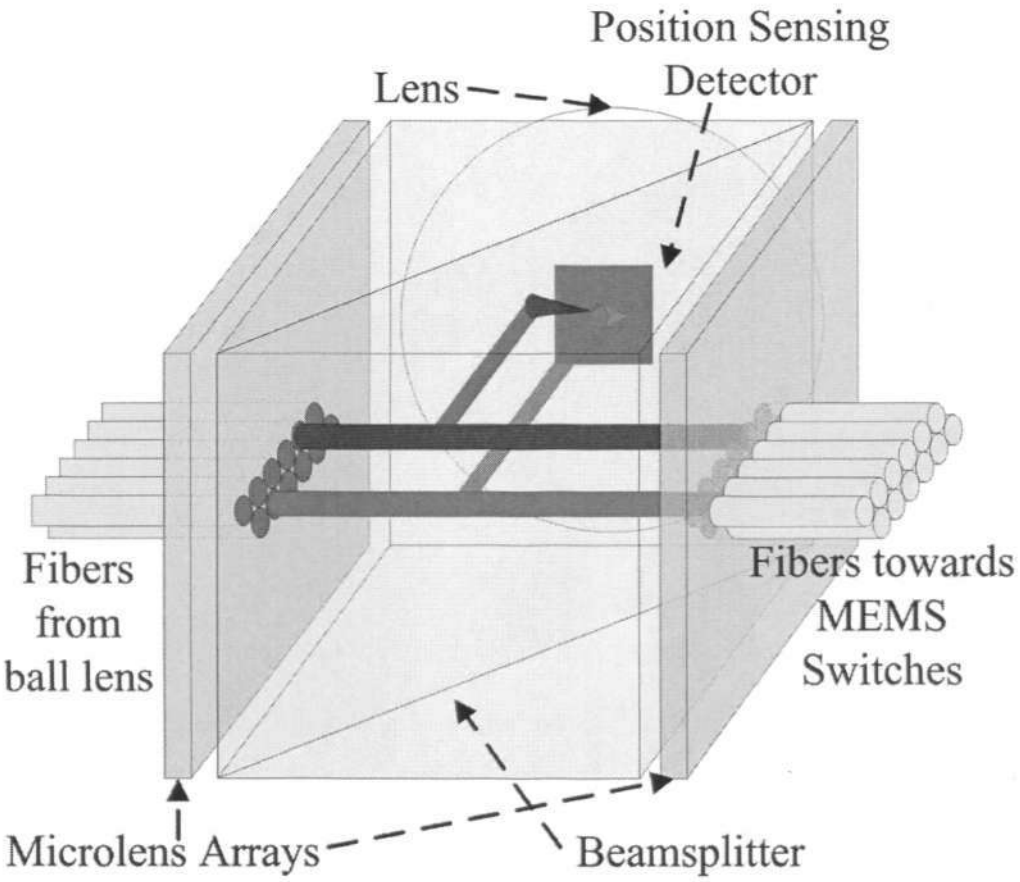

Figure 4-12: Detecting fibers with beams and direction of beams

Due to the large spot beam created by ball lens' spherical aberration, a single spot beam from a far platform will span across many fibers. However, the fiber, whose hexagonal FOV encompasses the center of the spot beam, will be carrying the highest beam power. The position of each fiber will be mapped onto unique pixel areas in the detector, allowing the detection of the spot beams to identify the fibers that are carrying the beam. As this fiber and its surrounding fibers will carry

varying amount of beam power, the use of the position sensing detector allows the identification of the fiber with the highest beam power.

In addition, the other function of the position sensing detector is to detect the direction of the light beam's source, which is the far platform. This information is required to steer the transmitter to align itself with the far platform. To improve the accuracy resolution of the directional information such that it is higher than the pixel resolution, the beam power distribution between the fiber and its surrounding fibers can be used since every unique location in the fiber's hexagonal FOV will produce a unique distribution of the beam power in its neighboring fibers. During multipoint FSOC links setup, multiple spot beams may be detected on the detector at the same time. To allow the identification of the spot beams with their corresponding flight platforms, unique pulse sequences for each platform can be carried by the light beams during the acquisition stage.

As the position sensing detector requires much lesser beam power compared to the communication detector, the beamsplitter's splitting amount can be made very low. The exact amount will depend on the choice of the positioning sensing detector and the communications detector. For flight platforms, their positions may change relatively to other each, thus the position sensing detector is required to have a suitable frame rate that can continue to detect the direction of the far platforms. For the microlens to microlens array coupling, excluding the splitting loss, the insertion loss between the arrays is expected to be lower than 3dB, due to the use of 1500μm fiber core, since the beam spread decreases with increasing

collimating beam diameter, and it is relatively easier to produce milli-meter range lenses compared to micro-meter lenses.

4.4.3 Optical MEMS Switching to Communications Detectors

As shown in Figure 4-13, the fibers after the beam splitter will be arranged into a single row and connected to another matching single row microlens array to be collimated and exited into the free-space. With respect to each communications detector, a single row of MEMS switches (denoted as a MEMS switch set) will be placed after the microlens array. Optical MEMS has been widely used in fiber optic communications in switches and their reliability, small size, light weight and ease of fabrication make them suitable for FSOC [99]. Details of MEMS can be found in [99]. The number of mirrors in one MEMS switch set is the same as the number of fibers. After identifying the fiber with the highest beam power from the position sensing detector, the corresponding mirror in the MEMS switch set will be activated to reflect the beam from the identified fiber into a corresponding communications detector, which can be based on p-type-intrinsic-n-type (PIN) or APD.

The remaining beams from other fibers will not be blocked by any MEMS switch meant for other beams and will continue to propagate until it hits the mirror activated for it. Narrowband filters are placed right before the communication detectors to filter away weak beams of other wavelengths to improve communications performance. A weakness in this design is that when a MEMS

switch is activated, the entire output of the corresponding fiber is reflected by the mirror. If there are 2 beams of different wavelengths within the same fiber, one of the beam will be filtered away to prevent interference. As such, it is essential for the flight platforms to be separated sufficiently to prevent their spot beams to fall onto the same fiber. Since the flight platforms in a cluster are expected to be positioned apart, it is unlikely that such situation will occur. In the event of occurrence, one of the two communication channels has to be dropped.

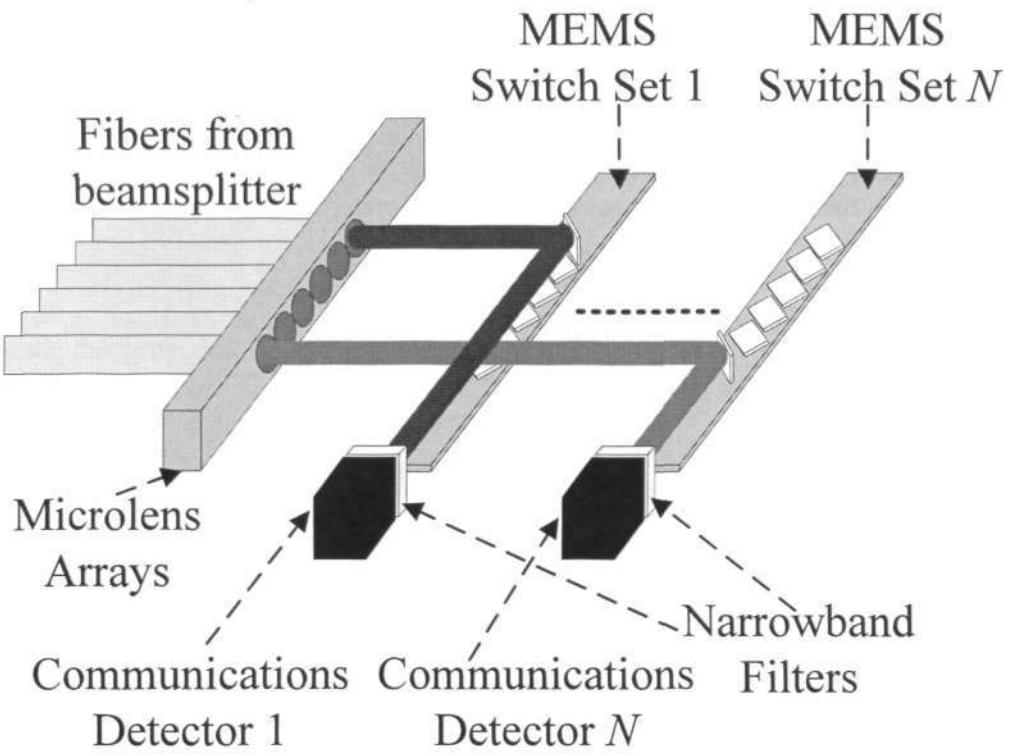

Figure 4-13: MEMS switching to communications detectors

The numbers of MEMS switch sets and communication detectors required will largely depend on the network design. If a specific flight platform is required to communicate with N platforms, then N MEMS switch sets and N communications detectors are required. It is noted that a small amount of loss is expected to occur at this stage.

4.5 Multipoint FSOC Transmitters

In a typical FSOC transceiver design, the transmit beam is usually collimated and transmitted through the same lens that is used for the receive beam collection. As the beam divergence is related inversely with the collimated beam waist, a big lens is essential to produce small beam divergence in micro-radians range that is required for long range communications. However, for short-range communications, the desired transmit beam divergence is typically in the range of milli-radians instead of micro-radians, and hence the collimated beam waist required is in the milli-meter range instead of centimeter range. Thus, the use of a big lens is not required for short-range communications.

Commercially available fiber pigtailed beam collimators, which are small and light, can sufficiently provide the desired milli-radian range beam divergences [100]. These beam collimators can be supported by 2-axis rotational motion motorized mounts to perform the pointing adjustment towards the far platform. The modulated optical beam from the laser source can be connected to the beam collimator by singlemode fiber, which will preserve the TEM_{00} mode and produce free-space Gaussian beam. While the number of pointing devices cannot be reduced as each transmitter has to be equipped with its individual pointing system, each pointing system is significantly scaled down due to the huge reduction of the weight from a FSOC transceiver to a lightweight beam collimator. The scaling down of both the transmitter and pointing system set is expected to greatly reduce the size, weight and power consumption, aiding to the multipoint communications

implementation on flight platforms. The transmitters, with beam divergences in milli-radians, will continue to provide high transmit gain to the far receivers, enabling FSOC distance in the range of kilometers.

4.6 Potential Applications of Multipoint FSOC System

Although the functionality of the proposed multipoint FSOC system design cannot be experimentally demonstrated due to the lack of actual hardware, a technical paper on the proposed design has been peer-reviewed and published in Applied Optics, showing that there is confidence in the workability of the proposed design.

With the proposed multipoint FSOC system, network communications can be implemented. The multipoint system can aid in the various types of basic topologies, such as mesh, star or hybrid. The employment of multipoint systems requires the justification that it is more advantageous in power, weight and size aspects compared to the use of the multiple transceiver design, thus it can be used in flight platforms that have numerous concurrent communications links.

The important mission data gathered by individual platforms are required to be sent back to a ground station eventually, which can be hundreds of kilometers away, but FSOC is not able to provide 100% availability to perform that due to its vulnerability under atmospheric conditions and its requirement for LOS. As such, within the cluster network, at least one platform must be fitted with RF communications to transport that data. Thus FSOC can provide the

communications within the cluster while RF communications can provide the communications outside the cluster with its all weather capability. In this situation, a star topology will be suitable where a certain flight platform will act as the central hub to link up all other flight platforms, each with a transceiver. It will receive the individual flight platform's data, process and compress the data, and transmit the processed data back to the ground station via RF communications. Thus the central platform can be sole platform to be equipped with the proposed multipoint system while the remaining flight platforms are each equipped with a transceiver. The central platform can be a bigger platform to have higher payload capacity to hold the multipoint system and RF communications components. However, due to the limited FOV of a multipoint system, the central platform may have to fly at higher altitude to have all other platforms contained within its FOV.

It is also worth noting that the full angular coverage around the central platform can be achieved with three units of multipoint receiver system, with each unit covering separate FOV of 120° each. Furthermore, the multipoint system can also be used in terrestrial FSOC networks to link up remote nodes (transceivers), especially if there are frequent network reconfigurations such as when remote nodes are added or taken out of the network or when their positions may be shifted.

The multipoint system is also envisioned to be able to perform the function of a free-space optical multipoint router/repeater for urban terrestrial network through some modifications without optical-electrical-optical (OEO) conversion. When

LOS cannot be achieved between two nodes due to obstacles or if the distance between the two nodes is beyond their capability, optical router/repeater can be used to establish the connection between them. Instead of using the MEMS switches in the multipoint receiver system to reflect beams from multimode fibers into detectors, the beams can be reflected into another multimode fiber, as shown in Figure 4-14.

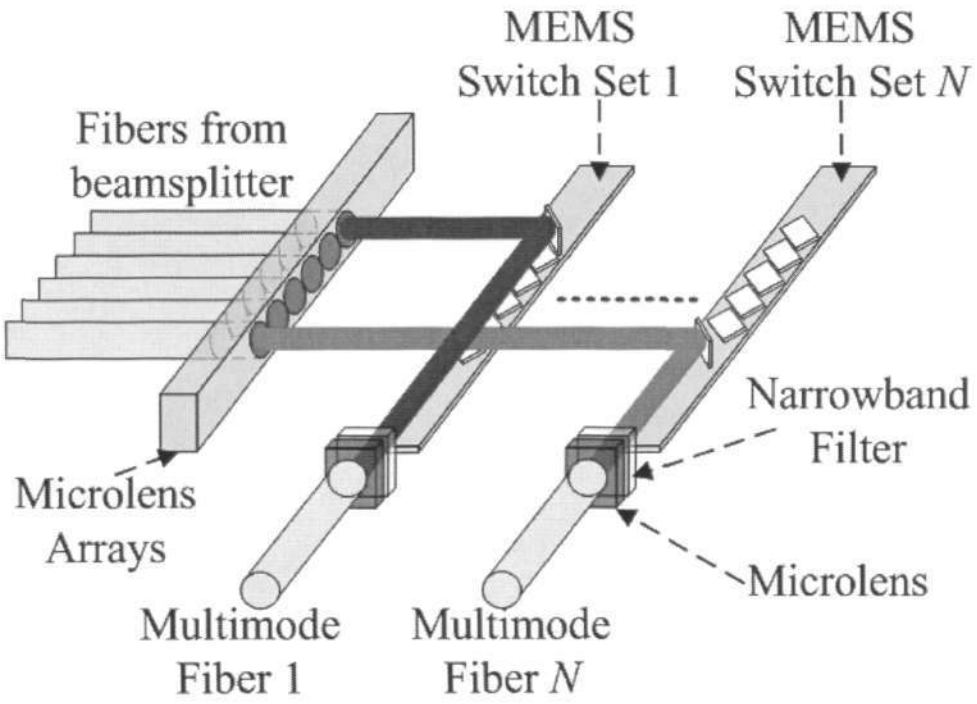

Figure 4-14: MEMS switching to multimode fibers

The beam in multimode fiber will then be transferred into a singlemode fiber through the use of a multimode-to-singlemode converter, which does the conversion through the use of optics. The beam in the singlemode fiber is amplified by an EDFA and sent to a beam collimator for free-space transmission to the destination. The layout is shown in Figure 4-15.

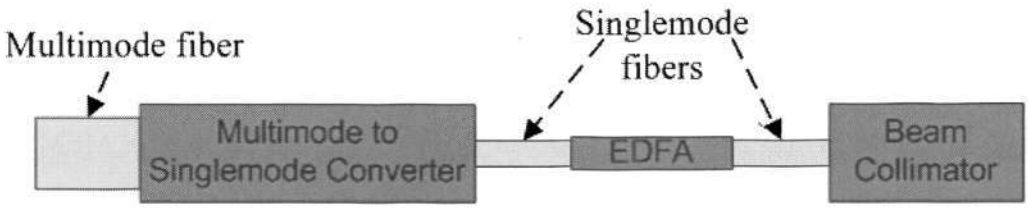

Figure 4-15: Multimode-to-singlemode conversion and amplification

4.7 Summary

For flight platforms in a cluster to have communications within a network, concurrent communications with multiple flight platforms are required. FSOC systems are typically designed with a transceiver configuration as the same receiving aperture can be used for collimating the transmit beam and a transceiver package requires only one pointing system. Although ideal for long range point-to-point communications, FSOC transceivers are not suitable for short-range FSOC multipoint communications on flight platforms.

The problems associated with using the FSOC transceivers for multipoint communications on flight platforms were discussed and examined. Having FOV to reduce background noise and having narrow transmit beam, FSOC transceivers are only suitable for point-to-point communications. If FSOC transceivers are to be used for multipoint communications, many FSOC transceivers are required for each FSOC link, resulting in increment in payloads' weight, size and power consumption. Furthermore, each FSOC transceivers requires its own active pointing system, adding more to the problem.

To address the problem, the author proposed a new multipoint system design that separates the transmitter and receiver. The proposed multipoint receiver design incorporates a ball lens to capture incoming beams from multiple directions and couple them into multimode fibers. The combination of the ball lens and multimode fibers allow light from many directions to be coupled into different fibers with small FOVs and the amount of receive gain from using different fiber core diameters and NAs are analyzed. The light beam's directional information is retained by the hexagonal arrangement of the fibers and through using microlens array, beam splitter and position sensing detector, the fibers carrying the beams can be identified and the incoming beam direction can be retrieved. Subsequently, the beams can be switched in free-space by the MEMS switches to respective communication detectors. As this receiver configuration allows light to be received from many directions, pointing capability is not required. The receiver design has a wide FOV and in the example, it is able to cover a third of a sphere.

Transmitters are separated from the receiver and their functions are performed through the use of beam collimators placed on motorized mounts. Beam collimators are sufficient to create the milli-radians beam required for short-range communications, despite their small sizes. Although a beam collimator is still required for each FSOC link with active pointing system, their light weight and size allows a much smaller pointing system to be used. The proposed design provides power, weight and size advantages over the conventional method of using more transceivers to provide multipoint communications, enables multipoint communications on flight platforms and aids in networks that have frequent reconfigurations.

Chapter 5. Dual Data Rate Schemes Using Single Photoreceiver for Inter-satellite FSOC

5.1 Introduction

The variation in distance between two communicating satellites in a cluster results in varying FSOC signal level. At longer distance, the received beam power is lower and to maintain communications, optical parameters can be enhanced such as higher transmit power, bigger transmit aperture and receive aperture etc. However, more power is required for more powerful laser source and bigger transmit or receive aperture requires better performance pointing system to support it structurally and to provide higher pointing resolution. Flight platforms' payload capacities are limited and this put a restriction on upgrading the optical components. If the optical components are already taxed to their limits, the optical parameters cannot be enhanced further, disallowing improvements to the design of the optical domain to boast transmission distance.

To extend FSOC distance when the optical components cannot be further enhanced due to payload limitations, modifications to the electrical domain can be made instead. By reducing the data rate as distance increases, inter-satellite FSOC can be maintained within the desired error rate of 10^{-9} despite the lower received power at a longer distance. Thus, the method is suitable for inter-satellite communications that requires a longer communication distance and can afford to have degradation in data transfer duration due to the data rate reduction.

Intuitively, one would think of using two sets of FSOC components to perform the data rate switching with each set designed for a certain data rate but that will increase the optical components. Thus instead of using two sets of photoreceivers for dual data rate switching, the author proposes two schemes that use only one photoreceiver. The proposed dual data rate schemes, which operate by switching to lower data rate as the distance increases, can be implemented through the addition of electrical components without increasing any optical components.

5.2 Proposed Dual Data Rate Schemes

The two levels of data rate considered in the proposed schemes are: 2.5Gbps and 1.25Gbps. Instinctively, one would think of using two photoreceivers with 2.5GHz and 1.25GHz frequency responses for each data rate. In this method, apart from using two photoreceivers, the switching of the optical signal to the respective photoreceiver is required to be made in the optical domain, thus an additional optical switch is required. Instead of performing the switching in the optical domain, the author proposes two dual data rate schemes that employ only one photoreceiver, with signal switching made in the electrical domain. In both schemes, there are two channels of 1.25Gbps digital data stream and the schemes will show how the channels can be combined into a 2.5Gbps data stream when they are operating in 2.5Gbps mode.

5.2.1 1st Scheme

Figure 5-1 shows the 1st proposed scheme using a 2.5GHz photoreceiver with built-in 2.5GHz PIN and 2.5GHz low pass filter (LPF). The 2.5GHz PIN is assumed to have typical receiver sensitivity of -23dBm. When operating in 2.5Gbps mode, the two 1.25Gbps channels of digital data are each fed into a return-to-zero (RZ) pulse generator to produce electrical RZ-OOK pulses of 0.5 duty cycle. They are subsequently combined by delaying one channel by half bit period and then added together to form a 2.5Gbps non-return-to-zero (NRZ) OOK pulse stream, as shown in Figure 5-2. Figure 5-3 shows the illustration through simulated waveforms from Optisystem, based on the digital data sequence from Figure 5-2 [101]. Therefore, for the 2.5Gbps mode in the 1st scheme, the resultant combined channel consists of only NRZ-OOK pulses. NRZ format is desired because it occupies smaller bandwidth than RZ format and with smaller bandwidth, there will be lower amount of noise.

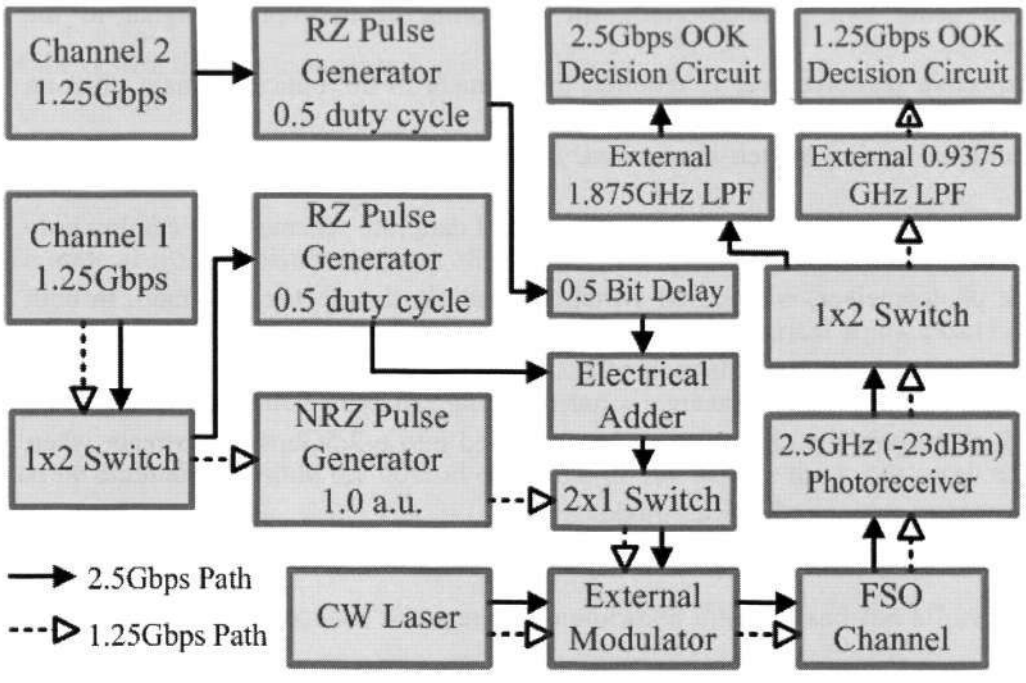

Figure 5-1: 1st Scheme: dual data rate using 2.5GHz photoreceiver

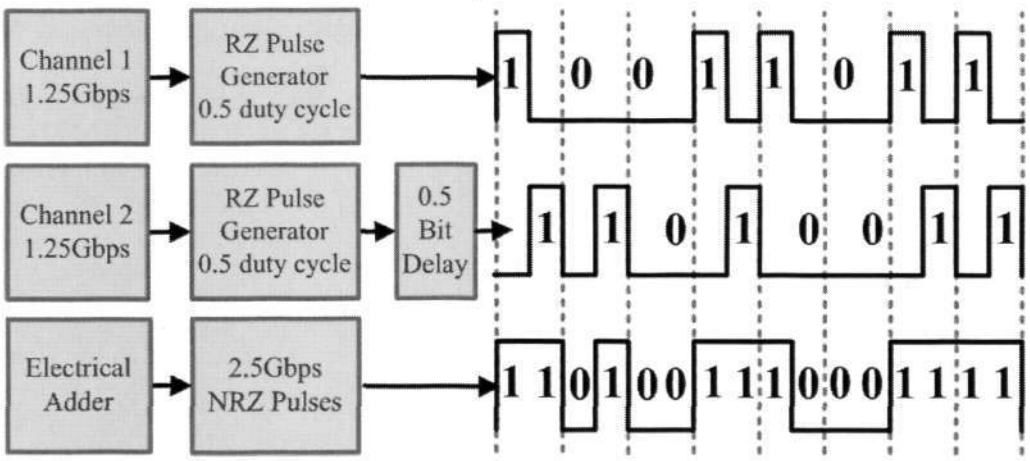

Figure 5-2: 1st Scheme: 2.5Gbps (NRZ) from two 1.25Gbps (RZ) channels.

In 1.25Gbps mode, only one channel will be used, which is Channel 1 in Figure 5-1. The data from that channel will be switched into an NRZ pulse generator to produce 1.25Gbps NRZ-OOK pulse stream. The pulse streams generated in both modes will be inputted into an external optical modulator which modulated a continuous wave (CW) signal into optical pulses.

After traveling through the FSOC medium, the optical signal is relayed to the 2.5GHz photoreceiver. Depending on which mode it is operating in, the photocurrent generated by the photoreceiver will be sent to external LPFs of 1.875GHz and 0.9375GHz for 2.5Gbps and 1.25Gbps mode respectively. The LPFs have a cut-off frequency at 0.75 of the bit rates as NRZ signals occupy lesser bandwidth. Due to the lower LPF rating in 1.25Gbps mode, more noise will be filtered away, giving rise to better communications performance in terms of error rate, compared to the 2.5Gbps mode for the same amount of received optical signal level. It also means that for the same amount of error rate, the FSOC distance can be longer for 1.25Gbps mode.

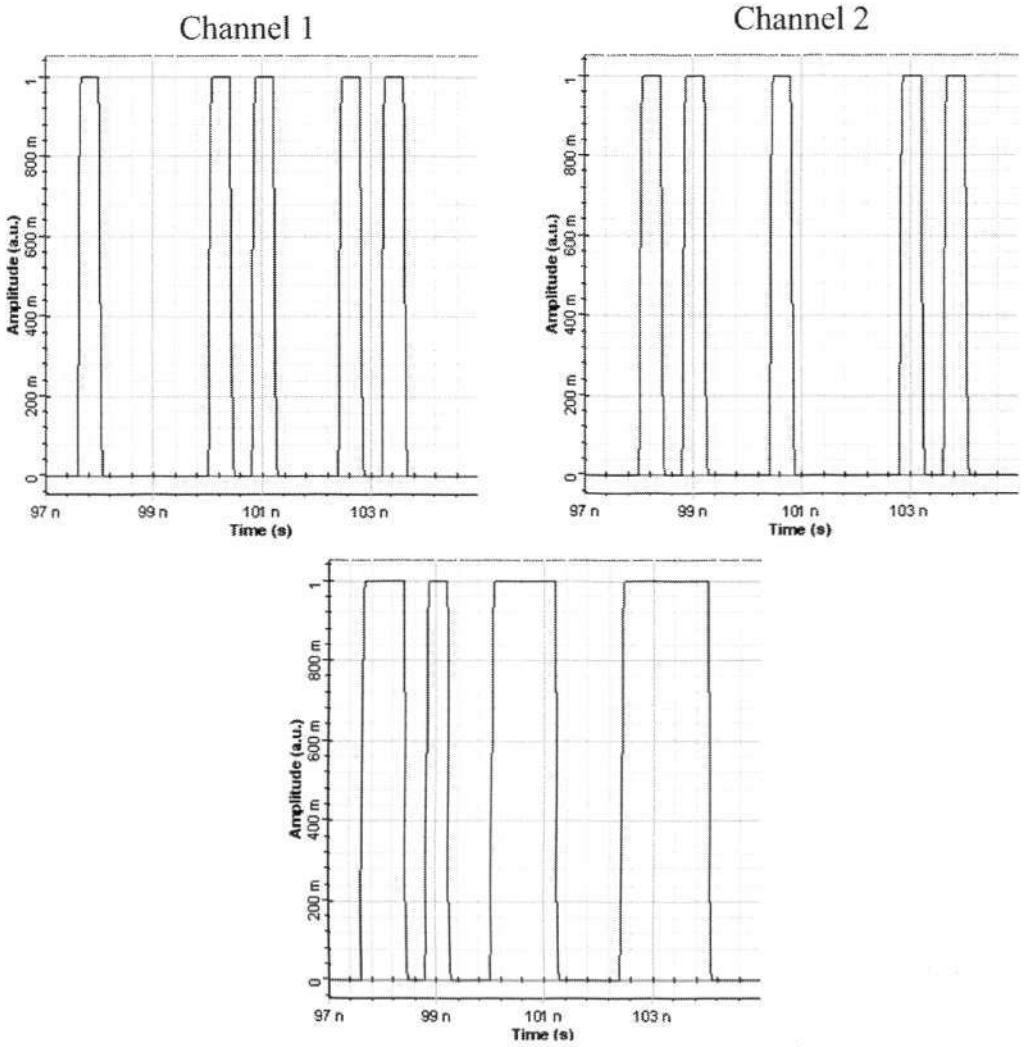

Figure 5-3: Simulation of channel combination in 1st Scheme

5.2.2 2nd Scheme

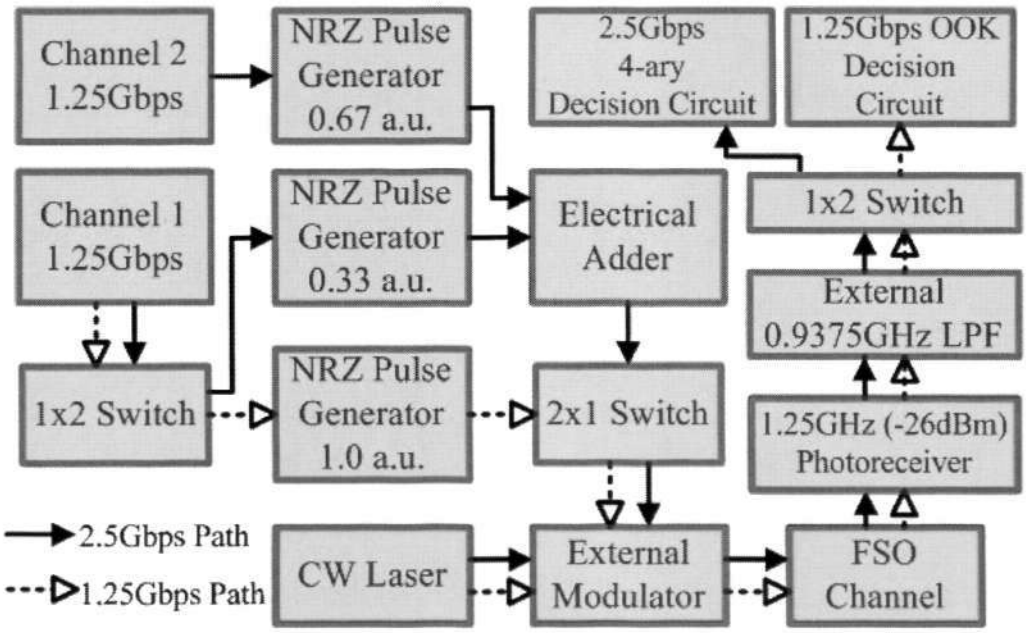

Figure 5-4: 2nd Scheme: dual data rate using 1.25GHz photoreceiver

Figure 5-4 shows the 2nd proposed scheme using a photoreceiver with built-in 1.25GHz PIN and 1.25GHz LPF. The 1.25GHz PIN is assumed to have receiver sensitivity of -26dBm. When operating in 2.5Gbps mode, the two 1.25Gbps channels of data are each sent into a NRZ pulse generator. For Channel 1, the NRZ pulse generator will generate NRZ-OOK pulses with amplitude at 0.67 of the external modulator's driving voltage. For Channel 2, the NRZ-OOK pulses generated have amplitude of 0.33 of the driving voltage. When the channels are combined together, a 4-ary-NRZ amplitude modulated pulse stream is generated with maximum amplitude equivalent to the modulator's driving voltage, as shown in Figure 5-5 [102]. Figure 5-6 shows the illustration through simulated waveforms from Optisystem, based on the digital data sequence from Figure 5-5 [101].

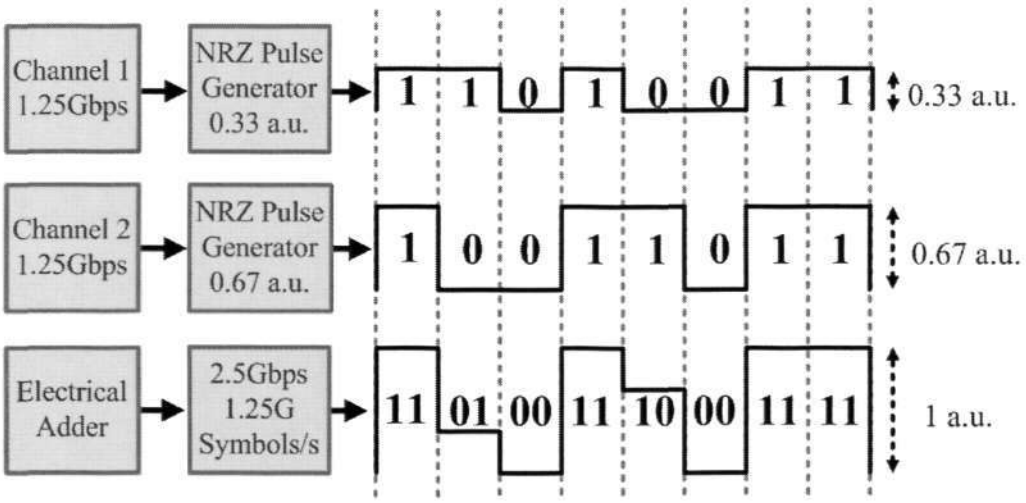

Figure 5-5: 2.5Gbps (4-ary-NRZ) from two 1.25Gbps (NRZ) channels.

In 1.25Gbps mode, only one channel, Channel 1 in Figure 5-4, will be used. The data from that channel will be switched into an NRZ pulse generator to produce 1.25Gbps NRZ-OOK pulse stream with amplitude equal to the modulator's driving voltage. The pulse streams generated in both modes will be inputted into an external optical modulator which modulated a CW signal into optical pulses.

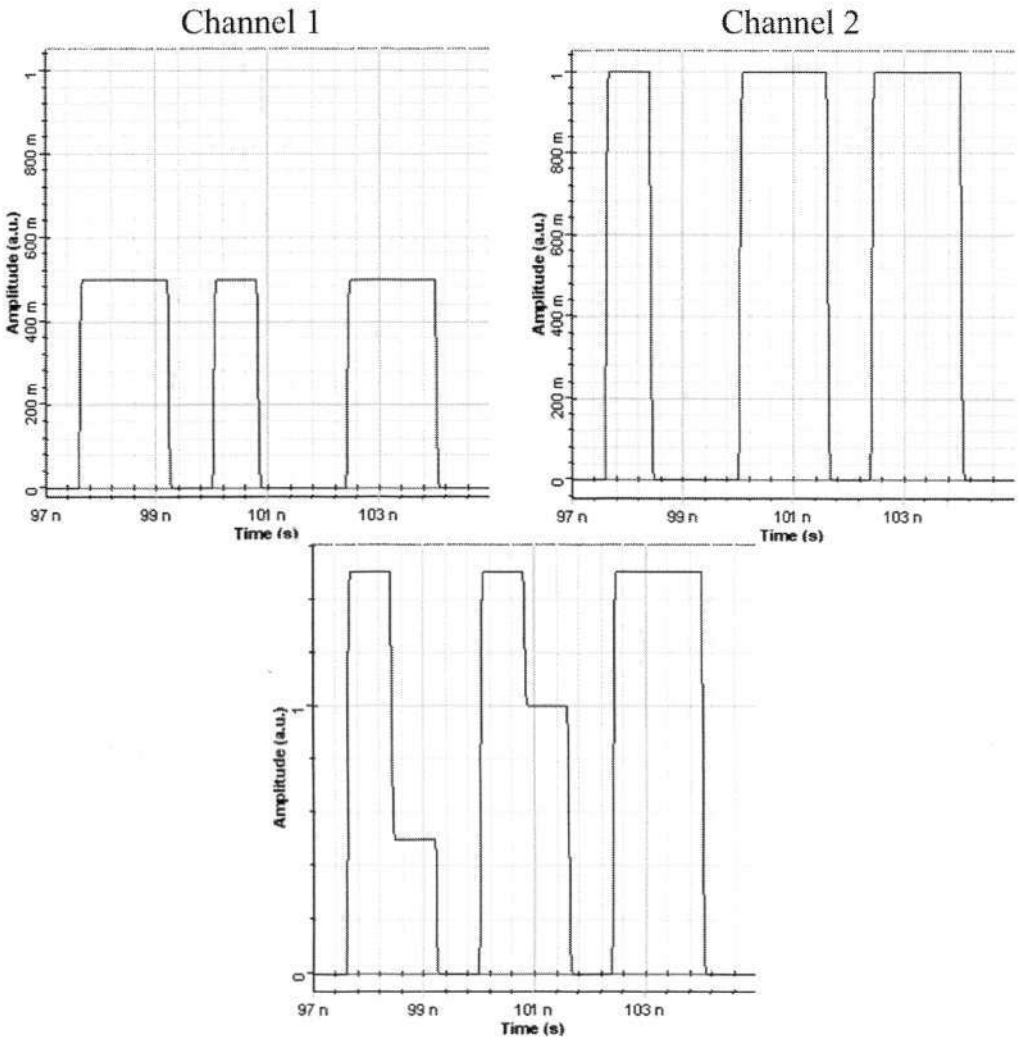

Figure 5-6: Simulation of channel combination in 2nd Scheme

The effective symbol rate of the pulse stream for both 2.5Gbps and 1.25Gbps modes is 1.25G symbols/s. The received optical signal is relayed to the 1.25GHz photoreceiver and the photocurrent generated by the photoreceiver will be sent to an external LPF of 0.9375GHz for 2.5Gbps and 1.25Gbps modes, followed by switching to their respective decision circuitry.

5.3 Factors Affecting Performance of Proposed Schemes

The performances of the two proposed schemes are affected by their photoreceivers with different frequency responses and their signal bandwidth. The error rate is a result of the signal current and signal noise at the receiver end. The received optical signal level is highly dependable on the FSOC channel parameters. For a PIN diode, a photocurrent, I_p, will be generated based on [103-104]:

$$I_p = \Re P_{rx} = \Re P_{tx} L_{tx} G_{tx} L_p L_R G_{rx} L_{rx} \tag{5.1}$$

where $\Re$ is responsivity of PIN diode. Assuming accurate beam pointing, values of these parameters are fixed except the range loss, which depends on the distance.

There are various sources of noise from the photoreceiver itself. They are signal shot noise, dark current shot noise and thermal noise, which is also known as Johnson noise. Considering the various noises in the detection process, noise current, i_{noise}, is given by [103-104]:

$$i_{noise} = \sqrt{\left[2q\left(i_p + i_{dark}\right)B\right] + \left[\frac{4kTB}{R_{eq}}\right]} \tag{5.2}$$

Where q is electron charge constant, i_{dark} is dark current, i_{shot} is shot noise current, $i_{thermal}$ is thermal noise current, B is signal bandwidth, k is Boltzmann constant, T is temperature and R_{eq} is the equivalent resistance.

$$\Delta f = \frac{1}{2\pi C_t R_{eq}} \tag{5.3}$$

Equation (5.3) gives the frequency response, Δf, of a PIN diode [105-106] and C_t is the platform capacitance of the PIN. The frequency response of the PIN diode is inversely related to the equivalent resistance, thus, for any wideband operating PIN, the required low R_{eq} will cause high thermal noise, resulting in thermal noise being the dominating noise source [103-104].

Assuming data bits 00, 01, 10 and 11 are defined as symbol 1, 2, 3 and 4 respectively, the symbol error, P_{error}, for the 4-ary amplitude modulation format is calculated according to [101]:

$$P_{error} = \sum_{k=1}^{4} P_m[k] \left[\sum_{l=1, l \neq k}^{4} \frac{1}{2} erfc\left(\frac{Q_{k,l}}{\sqrt{2}} \right) \right] \tag{5.4}$$

where $P_m[k]$ is the probability of occurrence of a symbol k and $Q_{k,l}$ is defined as:

$$Q_{k,l} = \frac{|i_k - i_l|}{\sigma_k + \sigma_l} \tag{5.5}$$

where i_k and i_l are the mean photocurrent levels for symbols k and l, σ_k and σ_l are the noise standard deviations for symbols k and l. Removing insignificant terms, Equation (5.4) and (5.5) can be expanded into:

$$P_{error} \approx \frac{1}{4} \left\{ erfc\left[\frac{|i_1 - i_2|}{\sqrt{2}(\sigma_1 + \sigma_2)} \right] + erfc\left[\frac{|i_2 - i_3|}{\sqrt{2}(\sigma_2 + \sigma_3)} \right] + erfc\left[\frac{|i_3 - i_4|}{\sqrt{2}(\sigma_4 + \sigma_4)} \right] \right\} \tag{5.6}$$

5.4 Evaluation and Results

The proposed schemes are evaluated using Optisystem [101]. The following parameters are used: 20dBm CW laser, 1550nm wavelength, 1mrad beam divergence, 10cm receive aperture, 0.95 transmit and receive optics efficiency, and 1.25GHz and 2.5GHz PIN diodes with responsivity of 0.8. Figure 5-7 shows the eye diagram of the 4-ary amplitude modulation in the 2nd scheme when operating in 2.5Gbps mode and Figure 5-8 shows the error rate against the transmission distance for the schemes. The transmission range achievable by the two schemes can be observed from Figure 5-8 at the point where the error rate is 10^{-9}.

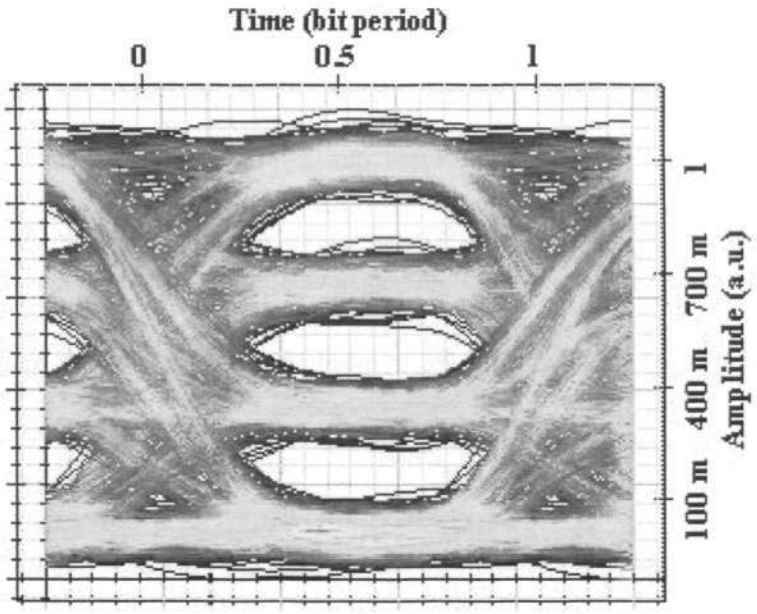

Figure 5-7: Eye diagram of 4-ary amplitude modulation in 2nd Scheme.

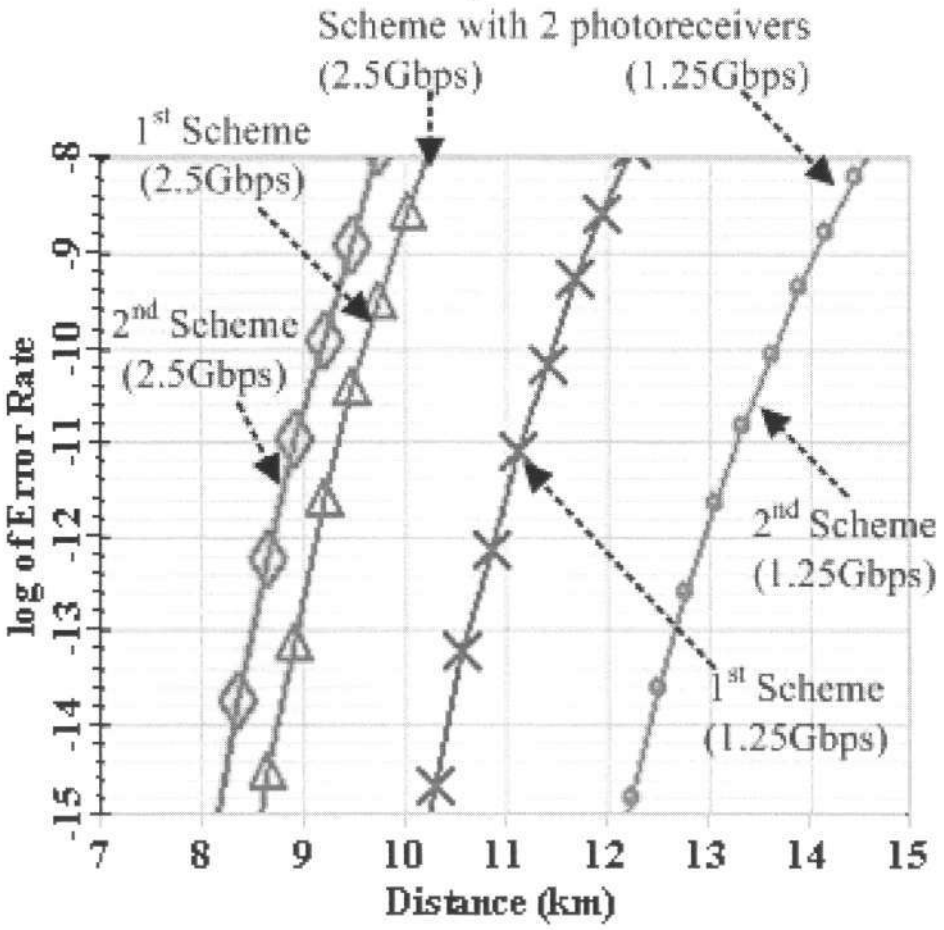

Figure 5-8: Error rate vs. transmission distance for the proposed schemes.

In Figure 5-8, the two schemes are compared against a two-photoreceiver scheme, assumed to have a photoreceiver for each data rate. The two-photoreceiver scheme is assumed to employ 2.5Gbps NRZ-OOK with a 2.5GHz photoreceiver and 1.25Gbps NRZ-OOK with a 1.25GHz photoreceiver. Figure 5-8 shows that for the 1st scheme, the maximum transmission distances for 2.5Gbps and 1.25Gbps are approximately 9.9km and 11.7km. Correspondingly, for the 2nd scheme, they are approximately 9.4km and 14km. Thus, both dual data rate schemes showed that transmission distance can be extended by lowering the data rates from 2.5Gbps to 1.25Gbps with a single photoreceiver.

Although the 1st scheme allows slightly longer transmission distance in 2.5Gbps mode than the 2nd scheme, the 2nd scheme performs significantly better than the 1st scheme in 1.25Gbps mode. In the 2nd scheme, because of lower frequency response from the 1.25GHz PIN, its R_{eq} is higher than that of the 2.5GHz PIN in the 1st scheme. As such, its thermal noise is lower due to the high R_{eq} and lower bandwidth, resulting in better communication performance when operating in 1.25Gbps mode than the 1st scheme. However, despite the lower thermal noise, in 2.5Gbps mode, the amplitude spacing between the four signal levels in 2nd scheme are reduced due to the 4-ary amplitude modulation format whereas 1st scheme has larger amplitude spacing although it has higher thermal noise. As such, the 1st scheme performs better in 2.5Gbps mode. Nevertheless, both schemes provide comparable performances with a two-photoreceiver scheme despite having only one photoreceiver with the 2nd scheme's performance closer to that of a two-photoreceiver scheme.

Having shown the performance of the proposed dual data rate switching schemes, there is a need to address whether a triple data rate scheme is beneficial. If triple data rate is used, there will be the introduction of a 3.75Gbps mode. For the triple data rate to work in the 1st scheme, at the transmitter end, complexity is increased by adding components to create the third channel and three decision circuits and a 3.75GHz photodetector has to be used at the receiver for the third data rate of 3.75Gbps. Due to the higher frequency response of the photodetector, the thermal noise will increase and result in the drop in performance when operating in 2.5Gbps or 1.25Gbps mode. This will result in significant reduction in the

communications distance when operating in 2.5Gbps or 1.25Gbps mode and therefore undesirable.

In the 2nd scheme, to have triple data rate scheme, an 8-ary amplitude pulse stream has to be created for the 3.75Gbps mode, which uses 8 amplitude levels to represent 3 bits. As a result of more amplitude levels, the eye openings between the levels will be much narrower, thus to maintain the same error rate, the communication distance will be greatly reduced. While the performance of 2.5Gbps and 1.25Gbps modes in the 2nd scheme will not be affected, the 3.75Gbps mode can be expected to operate over very short distance of a few kilometres but at the expense of added components and complexity into the payload, which is limited in the flight platforms.

On the other hand, a lower third data rate of 625Mbps is also possible in both schemes for triple data rate switching, resulting in the change in data rates into three modes of 625Mbps, 1.25Gbps and 1.875Gbps. While the transmission distance will increase when operating in the 625Mbps mode, it is not considered here since a key reason behind using FSOC is to have the high data rate on Gbps order. Moreover, the dual data rates in both schemes have already provided sufficient transmission distance for the flight platforms within a cluster considered in this thesis. Thus a lower third data rate is not considered here.

Therefore, if triple data rate is used, the introduction of a 3.75Gbps mode will be expected to either result in a drop in performance of the 2.5Gbps and 1.25Gbps modes in the 1st scheme or limited performance of the 3.75Gbps mode in the 2nd scheme. Moreover, to create the third data rate, additional components are required to be added to the FSOC system and these additions may be highly constrained due to the limited payload allowed by the flight platforms. Thus the introduction of a triple data rate scheme will largely result in a trade-off between performances of other data rate mode and added payload size. The introduction of a lower data rate of 625Mbps is not considered as the transmission distance provided by the dual data rate scheme is already sufficient for the flight platforms considered in this thesis. Unless necessarily required by the flight platform's mission requirements, the triple data rate is not recommended.

5.5 Summary

As the inter-satellite FSOC distance between two communicating satellite changes, the FSOC signal power level will changes. With increasing distance, the free-space range loss becomes larger, leading to a lower received FSOC signal power at the far platform. To increase the received power, parameters such as transmit power, bigger transmit and receive aperture can be enhanced but at some expenses such as more power consumption or requirement of more powerful pointing system to support the bigger apertures and narrower beams. With a limited payload on flight platforms, such enhancement methods may be highly restricted.

To extend the communications distance, data rate can be reduced as the distance increases. Although the data transfer duration will become longer, it allows data to be sent within the acceptable error rate and maintain data integrity. Instead of using two photoreceivers of different bandwidth and an optical switch to perform beam switching between the two photoreceivers, data rate reduction can be made through the electrical domain with only one photoreceiver.

The author proposed two dual data rate switching schemes that use only one photoreceiver. In the 1st scheme, a photoreceiver with 2.5GHz bandwidth is used. During 2.5Gbps mode, two channels of 1.25Gbps are combined to form a 2.5Gbps NRZ-OOK modulated channel while in 1.25Gbps mode, only one channel will be used. At the receiver end, the electrical signal generated from the photoreceiver will be switched between external filters of 1.875GHz and 0.9375GHz to reduce the noise generated by the photoreceiver in 2.5Gbps and 1.25Gbps modes respectively. For the 2nd scheme, a 1.25GHz photoreceiver is used. During 2.5Gbps mode, two channels of 1.25Gbps are added together with varying amplitude each to form a 4-ary amplitude modulated channel and only one channel of NRZ-OOK is used in 1.25Gbps mode. Because the electrical signal generated by the photoreceiver is 1.25GHz in both modes, only a 0.9375GHz filter is used.

The proposed schemes were evaluated using Optisystem and compared to a system which uses two photoreceivers scheme for the data rate switching. The results showed that in both proposed schemes, FSOC distance increases from

9.9km to 11.7km and 9.4km to 14km when data rate is switched from 2.5Gbps to 1.25Gbps in 1st and 2nd scheme respectively. The 1st scheme allows slightly longer transmission distance in 2.5Gbps mode than the 2nd scheme but the 2nd scheme performs significantly better than the 1st scheme in 1.25Gbps mode. Also, both schemes provide comparable performances with a two-photoreceiver scheme.

Chapter 6. Conclusions and Future Work

6.1 Conclusions

Due to their potential applications, there is increasing research in having multiple micro-satellites or nano-satellites and mini-UAVs in a cluster and FSOC is evaluated to be a suitable communication method between the individual flight platforms with advantages over RF such as higher data rate, lower power consumption, secure data transfer, low jamming and smaller size. However, due to the narrow laser beam, PAT is required to be performed by a pointing system to make the FSOC systems aligned before FSOC can begin.

Typically, research has been focused on long range or fixed point-to-point FSOC. With the rising interest in flight platforms within a cluster, research on FSOC for these flight platforms is emerging. Although satellites and UAVs are fundamentally different in terms of speed, flight altitude and flight dynamics, they share similarities from FSOC's perspective. They have payload limitations, their separation distances between individual platforms are limited to several kilometers, their separation distances will vary during their flight platform depending on their missions and they are required to have multipoint communications capability.

In Chapter 3, the problem of varying separation distance for short-range inter-satellite and inter-UAV FSOC is investigated. The varying distance leads to varying received signal power due to free-space range loss, which increases with increasing distance. It also changes the angular coverage required to cover the uncertainty area of the far platform. If a fixed beam divergence is used, the amount of angular coverage and transmit gain will not be sufficient to illuminate the uncertainty area or close the FSOC link. Thus typical FSOC system design which has a fixed beam divergence will fail in the presence of varying separation distance.

The author proposed the use of a beam divergence changing mechanism to solve the problem. Instead of a fixed beam divergence, methods are proposed to change the beam divergences according to the separation distance between the platforms. The entire range of separation distance is divided into regions, of which each will be used with a certain beam divergence, therefore creating beam footprints that will sufficiently cover the uncertainty area and produce suitable transmit gain to close the FSOC link. Four methods are proposed to implement the beam divergence changing mechanism and they are mainly based on creating varying amount of collimated Gaussian beam diameters, which dictate the beam divergence.

To show the ability of the beam divergence changing mechanism, inter-satellite and inter-UAV FSOC are analyzed for their ability to extend transmission distance by fulfilling the requirement of covering the uncertainty area and

providing the transmit gain. The results have showed that through the use of the mechanism, FSOC can occur over a range of separation distances. For inter-UAV FSOC, atmospheric effects such as atmospheric attenuation, scintillation and rain have been considered and compared to FSOC link that uses a fixed beam divergence system, the results have showed that inter-UAV FSOC links with the mechanism communicates further significantly in different levels of visibility, rainfall and atmospheric turbulence.

In Chapter 4, the author proposed a multipoint FSOC design that enables concurrent multipoint communications that is feasible for flight platforms. Typical FSOC system designs are of transceiver package design with the transmitter and receiver in a single housing, sharing the same aperture and pointing system. However, these FSOC transceivers usually have small FOV with narrow beam divergences, allowing them to have only point-to-point communications capability. If FSOC transceivers are used on flight platforms, to enable multipoint communications, many FSOC transceivers are required to establish each link and each transceiver requires an active pointing system for PAT. The number of transceivers increases with the number of concurrent links required and will not be possible with large number of links since the flight platforms have limited payload capacity. Thus transceiver design is not suitable for concurrent multipoint communications.

Instead of a transceiver design, the author proposed a multipoint receiver that uses a ball lens to receive lights from different directions and coupled them into

different multimode fibers that have separate FOVs. The amount of receive gain is analyzed against fibers of varying core diameters and NAs with the ball lens. Thus concurrent communications can take place since their light beams are coupled into different fibers. The beams from the fibers are partially split by a beamsplitter into a position sensing detector to determine which fibers are carrying beams and to identify the beams' incoming direction. The beams will subsequently be reflected by MEMS switches into communications detectors. This design allows the receiver to be positional-fixed and do not need a pointing system.

Instead of big apertures, the transmitters are small beam collimators, which are widely available, connected to the laser source by a singlemode fiber. Beam collimators are sufficient as short-range FSOC requires beam divergences in the milli-radians instead of micro-radians. Their small sizes allow themselves to be mounted on small pointing devices to be used instead of powerful gimbals for transceivers. Thus the combination of the multipoint receiver, the beam collimators and pointing devices can perform the duty of multipoint communications with power, weight and size advantages over the use of multiple transceivers and is more practical for flight platforms. It can also be applied in terrestrial network where multipoint communications is required.

Lastly, in Chapter 5, the author proposed two dual data rate schemes with one photoreceiver that aims at extending communications distance. Extensions in communication distances are usually based on increasing optical parameters like transmit power, transmit aperture and receive aperture etc. However, increasing

those parameters will require more power or better pointing system to support the improved FSOC systems. Assuming that the payload limitation prevents the improvement in these parameters, data rate can be reduced as the distances increase to reduce error rata at the expense of longer data transfer duration. Instead of two photoreceivers with different bandwidth for each data rate with switching in the optical domain, the proposed schemes use only one photoreceiver with modifications in the electrical domain.

In the 1st scheme with a photoreceiver with 2.5GHz bandwidth, two channels of 1.25Gbps are combined to form a 2.5Gbps NRZ-OOK modulated channel for 2.5Gbps mode and one channel of NRZ-OOK will be used for 1.25Gbps mode. The electrical signal generated from the photoreceiver will be switched between external filters of 1.875GHz and 0.9375GHz in 2.5Gbps and 1.25Gbps modes respectively. In the 2nd scheme with a 1.25GHz photoreceiver, the two channels of 1.25Gbps are added together with varying amplitude each to form a 4-ary amplitude modulated channel in 2.5Gbps mode and one channel of NRZ-OOK is used in 1.25Gbps mode. The electrical signal generated by the photoreceiver will be sent to a 0.9375GHz filter for both modes since their bandwidth is the same.

The proposed schemes have been evaluated using Optisystem and compared to a system which uses two photoreceivers scheme for the data rate switching. FSOC distance increases from 9.9km to 11.7km when data rate is reduced from 2.5Gbps to 1.25Gbps in the 1st scheme. For the 2nd scheme, the FSOC distance is increased

from 9.4km to 14km correspondingly. Moreover, both schemes provide comparable performances with a two-photoreceiver scheme.

6.2 Future Work

A FSOC experimental system has been built with limited functionality. Consisting of two terminals, one terminal is equipped with pointing system and the other terminal requires manual pointing. With the FSOC experimental system, FSOC performance in the atmosphere can be studied. A major adverse atmospheric effect is scintillation, which is the fluctuation of received power due to atmospheric turbulence along the transmission path.

Methods to mitigate the effects of scintillation can be investigated. When beams with wavelengths close to each other are transmitted together with the same beam parameters, they will be subjected to similar scintillation effects along their transmission paths since they travel across same segments of atmospheric turbulence. Therefore, it is possible for their received power to exhibit similar power fluctuations. The FSOC experimental system can be used to evaluate their correlation. It is possible that beams with close wavelengths will exhibit high correlation and that characteristic can be used to explore methods to suppress the effects of scintillation. Moreover, other modulations formats, such as differential phase shift keying (DPSK), can also be investigated for its ability to counter scintillation compared to OOK.

Apart from the FSOC itself, the PAT can be investigated. GPS-based PAT, without the use of position sensing detector and beacon laser, can be further studied using prediction tools to determine the trajectory of far flight platform. Alternatively, other PAT techniques can be explored for higher accuracy since higher PAT performance will lead to better FSOC performance through faster link connectivity between the flight platforms and the reduction of pointing loss. Laser ranging technique through the FSOC channel can also be investigated since flight platforms may require precise positioning within the cluster formation to perform their mission applications.

References

1. H.A. Willebrand and G.R. Clark, "Free space optics: a viable last mile alternative," Wireless and Mobile Communications, Proceedings of SPIE, Vol. 4586, p. 11-21, 2001.

2. D.L. Begley, "Laser cross-link systems and technology," IEEE Communications Magazine, Vol. 38, Issue 8, p.126-132, 2000.

3. S.G. Lambert and W.L. Casey, "Laser communications in space," Artech House, 1995.

4. A.K. Majumdar, "Free-space laser communication performance in the atmospheric channel," Journal of Optical and Fiber Communications Research, Vol. 2, p. 345-396, 2005.

5. J.E. Mulholland and S.A. Cadogan, "Intersatellite laser crosslinks," IEEE Transactions on Aerospace and Electronic Systems, Vol. 32, Issue 3, p. 1011-1020, 1996.

6. H. Hemmati, M. Wright, B. Sanii, N. Page, G.G. Ortiz, A. Biswas and K. Wilson, "Multi-gigabit data-rate optical communication depicting LEO-to-GEO and GEO-to-ground links," Proceedings of SPIE, Vol. 4635, p. 295-301,2002.

7. V.G. Sidorovich, "Optical countermeasures and security of free-space optical communication links," Proceeding of SPIE, Vol. 5614, p. 97-108, 2004.

8. T. Garlington, J. Babbitt and G. Long, "Analysis of free space optics as a transmission technology," U.S. Army Information Systems Engineering Command, 2005.

9. H.A. Willebrand and B.S. Ghuman, "Fiber optics without fiber," IEEE Spectrum, Vol. 38, Issue 8, p. 40-45, 2001.

10. E. Leitgeb, J. Bregenzer, M. Gebhart, P. Fasser and A. Merdonig, "Free-space optics: Broadband wireless supplement to fiber networks," Proceeding of SPIE, Vol. 4975, p. 57-68, 2003.

11. S.G. Lambert, G.W. Ulrich, A.J. Chenoweth, T.R. Morris and W.L. Casey, "Short-range multi-platform satellite crosslink communications," IEEE Military Communications Conference, Vol. 3, p. 1170-1174, 1992.

12. T.H. Ebben, C.C. Varner, K.A. Parrish, R.G. Marshalek and D.L. Begley, "Pointing, acquisition, and tracking demonstration system for laser communications," Proceeding of SPIE, Vol. 2699, p. 81-92, 1996.

13. S. Bloom, E. Korevaar, J. Schuster and H. Willebrand, "Understanding the performance of free-space optics," Journal of Optical Networking, Vol. 2, Issue 6, p.178-200, 2003.

14. V. Ragulsky and V.G. Sidorovich, "Availability of a free-space optical communication link operating under various atmospheric conditions," Proceeding of SPIE, Vol. 4530, p. 96-103, 2001.

15. H. Hemmati, "Deep space optical communications," Wiley-Interscience, 2006.

16. K.E. Wilson, J.R. Lesh and T.Y. Yan, "GOPEX: A laser uplink to the Galileo spacecraft on its way to Jupiter," Proceedings of SPIE, Vol. 1866, p. 138-146, 1993.

17. T.T. Nielsen and G. Oppenhaeuser, "In orbit test result of an operational optical intersatellite link between ARTEMIS and SPOT4, SILEX," Proceedings of SPIE, Vol. 4635, p. 1-15, 2002.

18. T. Jono, Y. Takayama, N. Kura, K. Ohinata, Y. Koyama, K. Shiratama, Z. Sodnik, B. Demelenne, A. Bird and K. Arai, "OICETS on-orbit laser communication experiments," Proceedings of SPIE, Vol. 6105, p. 610503, 2006.

19. K. Araki and Y. Suzuki, "Inter-satellite link by lightwave," International Topical Meeting on Microwave Photonics, p. 221-224, 1996.

20. M. Toyoshima, "Trends in satellite communications and the role of optical free-space communications," Journal of Optical Networking, Vol. 4, Issue 6, p. 300-311, 2005.

21. A.J. Mendez and R.M. Gagliardi, "Lasercom crosslinking for satellite clusters," Proceedings of SPIE, Vol. 4272, p. 50-59, 2001.

22. W. Leeb, A. Kalmar, K. Kudielka and P.J. Winzer, "Optical terminals for microsatellite swarms," Proceedings of SPIE, Vol. 4635, p. 202-214, 2002.

23. T. Eren, "Using angle information between directed links in coordinating satellite clusters," 3rd International Conference on Recent Advances in Space Technologies, p. 568-572, 2007

24. W. Leeb, A. Kalmar, K.H. Kudielka, P.J. Winzer and B. Furch, "Optical cross-Links for microsatellite fleets," 20th AIAA International Communication Satellite Systems Conference and Exhibit, p. 2002-2033, 2002.

25. "Unmanned aircraft systems roadmap, 2005-2030," Office of the Secretary of Defense, US Department of Defense, 2005.

26. P.J. Vincent and I. Rubin, "A swarm-assisted integrated communication and sensing network," Proceeding of SPIE, Vol. 5441, p. 48-60, 2004.

27. C. Chlestil, E. Leitgeb, N.P. Schmitt, S.S. Muhammad, K. Zettl and W. Rehm, "Reliable optical wireless links within UAV swarms," International Conference on Transparent Optical Networks, p. 39-42, 2006.

28. G.G. Ortiz, S. Lee, S. Monacos, M. Wright and A. Biswas, "Design and development of a robust ATP subsystem for the Altair UAV-to-Ground lasercomm 2.5 Gbps demonstration," Proceedings of SPIE, Vol. 4975, p. 103-114, 2003.

29. R.J. Feldmann and R.A. Gill, "Development of laser crosslink for airborne operations," IEEE Military Communications Conference, Vol. 2, p. 633-637, 1998.

30. W.L. Casey, G.R. Doughty, R.K. Marston and J. Muhonen, "Design considerations for air-to-air laser communications," Proceedings of SPIE, Vol. 1417, p. 89-98, 1991.

31. D.J. Petrovich, R.A. Gill and R.J. Feldmann, "U.S. Air Force development of a high-altitude laser crosslink," Proceeding of SPIE, Vol. 4214, p. 14-25, 2001.

32. V.W.S. Chan, "Optical space communications and networks," Proceeding of SPIE, Vol. 6304, p. 630401, 2006.

33. C. Chen, J.W. Alexander, H. Hemmati, S. Monacos, T. Yan, S. Lee, J.R. Lesh and S. Zingales, "System requirements for a deep space optical transceiver," Proceeding of SPIE, Vol. 3615, p. 142-152, 1999.

34. S. Lee, J.W. Alexander and M. Jeganathan, "Pointing and tracking subsystem design for optical communications link between the International Space Station and ground," Proceeding of SPIE, Vol. 3932, p. 150-157, 2000.

35. D. Kedar and S. Arnon, "Urban optical wireless communication networks: the main challenges and possible solutions," IEEE Communications Magazine, Vol. 42, Issue 5, p. S2-S7, 2004.

36. Y.Arimoto, K. Inagaki, M. Fujise, Y. Furuhama, M. Inoue and T. Kashiwase, "Simplified gimbal design for LEO satellites tracking to a GEO satellite," Proceeding of SPIE, Vol. 1866, p. 246-254, 1993.

37. A.S. Panahi and A.A. Kazemi, "Inter-satellite communications using laser based optical links," Proceeding of SPIE, Vol. 6758, p. 67580G, 2007.

38. S. Shimer and R. Gray, "High bandwidth optical intersatellite link technologies," International Topical Meeting on Microwave Photonics, Vol. 1, p. 101-104, 1999.

39. V.W.S. Chan, "Optical space communications," IEEE Journal on Selected Topics in Quantum Electronics, Vol. 6, Issue 6, p. 959-975, 2000.

40. H. Hemmati, "Optical systems for free-space laser communications," Proceeding of SPIE, Vol. 5173, p. 64-68, 2003.

41. L. Liu, X. Zhu, Y. Hu, Z. Luan, L. Wang, D. Liu, R. Gao, L. Xie and J. Yuan, "A prototype of intersatellite laser communications terminals," Proceeding of SPIE, Vol. 5892, p. 58920I, 2005.

42. J. A. Maynard and D. Begley, "Airborne laser communications: past, present, and future," Proceeding of SPIE, Vol. 5892, p. 58920A, 2005.

43. G. Baister, T. Dreischer and E. Fischer, "OPTEL family of optical terminals for space based & airborne platform communications links," Proceeding of SPIE, Vol. 5986, p. 59860Z, 2005.

44. MODTRAN, http://modtran.org/about/index.html.

45. O. Bouchet, H. Sizun, C. Boisrobert, F. Fornel and P. Favennec, "Free-space optics propagation and communication," ISTE, 2006.

46. R.W. Kaliski, S.M. Genco, D.A. Thompson, B. Breshears, T. O'Connor, K.M. Miller, E.W. Taylor, A.D. Sanchez, J.E. Winter and R.M. Ewart, "Laser communication intersatellite links realized with commercial off-the-shelf technology," Proceeding of SPIE, Vol. 3615, p. 170-178, 1999.

47. P. Krivak and O. Wilfert, "Long range free space optical link," 17th International Conference Radioelektronika, p. 1-5, 2007.

48. D.A. Rockwell and G.S. Mecherle, "Wavelength selection for optical wireless communications systems," Proceeding of SPIE, Vol. 4530, p. 27-35, 2001.

49. N.S. Kopeika and J. Bordogna, "Background noise in optical communication systems," Proceedings of the IEEE, Vol. 58, Issue 10, p. 1571-1577, 1970.

50. Z. Jia, Q. Zhu and F. Ao, "Atmospheric attenuation analysis in the FSO link," International Conference on Communication Technology, p. 1-4, 2006.

51. S.S. Muhammad, T. Kamalakis, E. Leitgeb, O. Koudelka, G. Kandus and T. Javornik, "Terrestrial free space optical links for high bandwidth connectivity," 9th International Multitopic Conference, p. 1-5, 2005.

52. D. Russell, H. Ansari and C.C. Chen, "Lasercom pointing, acquisition, and tracking control using a CCD-based tracker," Proceedings of SPIE, Vol. 2123, p. 294-303, 1994.

53. S.A. Self, "Focusing of spherical Gaussian beams," Applied Optics, Vol. 22, Issue 5, p. 658-661, 1983.

54. Melles Griot, "The Practical Application of Light," www.mellesgriot.com

55. E. Leitgeb, K. Zettl, S.S. Muhammad, N. Schmitt and W. Rehm, "Investigation in free space optical communication links between unmanned aerial vehicles (UAVs)," International Conference on Transparent Optical Networks, p. 152-155, 2007.

56. B. Epple, "Using a GPS-aided inertial system for coarse-pointing of free-space optical communication terminals," Proceedings of SPIE, Vol. 6304, p. 630418, 2006.

57. M. Scheinfeild, N.S. Kopeika and R. Melamed, "Acquisition system for microsatellites laser communication in space," Proceeding of SPIE, Vol. 3932, p. 166-175, 2000.

58. X. Zhi, Y. Ai and M. Lu, "Acquisition methods for microsatellite laser communication in space," Proceeding of SPIE, Vol. 4911, p. 372-379, 2002.

59. M. Guelman, A. Kogan, A. Kazarian, A. Livne, M. Orenstein, H. Michalik and S. Arnon, "Acquisition and pointing control for inter-satellite laser communications," IEEE Transactions on Aerospace and Electronic Systems, Vol. 40, Issue 4, p. 1239-1248, 2004.

60. B. Epple and H. Henniger, "Discussion on design aspects for free-space optical communication terminals," IEEE Communications Magazine, Vol. 45, Issue 10, p. 62-69, 2007.

61. R.J. Quaale, B. Hindman, B. Engberg and P. Collier, "Mitigating environmental effects on free-space laser communications," IEEE Aerospace Conference, p. 1-6, 2005.

62. B.L. Wilkerson, D. Giggenbach and B. Epple, "Concepts for fast acquisition in optical communication systems," Proceedings of SPIE, Vol. 6304, p. 63040A, 2006.

63. u-blox AG, "Essentials of satellite navigation," telecom.tlab.ch/~zogg/Dateien/GPS_Compendium(GPS-X-02007).pdf

64. Northrop Grumman, "LN-260 Advanced Embedded INS/GPS," http://www.es.northropgrumman.com/solutions/ln260/index.html

65. Surrey Satellite Technology Ltd, "SSTL SGR-10 Space GPS Receiver," http://www.sstl.co.uk/assets/Downloads/SGR-10%20v7_08.pdf

66. General Dynamics, "Monarch™ GPS Spaceborne Receiver," http://www.gd-space.com/documents/Monarch%20061006B%20(SS).pdf

67. D. Simon, "Kalman Filtering," Embedded Systems Programming, vol. 14, no. 6, pp. 72-79, June 2001.

68. B.K. Bhagavan and R.J. Polge, "Performance of the g-h Filter for Tracking Maneuvering Targets," IEEE Transactions on Aerospace and Electronic Systems, Vol. AES-10, Issue 6, p. 864-866, 1974.

69. D.G. Aviv, "Laser space communications," Artech House, 2006.

70. J. Wang, J.M. Kahn and K.Y. Lau, "Minimization of acquisition time in short-range free-space optical communication," Applied Optics, Vol. 41, Issue 36, p. 7592-7602, 2002.

71. J. Císar, O. Wilfert, F. Fanjul-Vélez, N. Ortega-Quijano and J. L. Arce-Diego, "New trends in laser satellite communications: design and limitations," Proceedings of SPIE, Vol. 7138, p. 71382I, 2008.

72. B.J. Klein and J.J. Degnan, "Optical antenna gain. 2: Receiving antennas," Applied Optics, Vol. 13, Issue 10, p. 2397-2401, 1974.

73. D.L. Panak and M.A. Doucet, "Fiber coupled transceivers in point-to-point and point-to-multipoint optical wireless systems," Proceeding of SPIE, Vol. 4530, p. 7-17, 2001.

74. S. Trisno, T. Ho, S.D. Milner and C.C. Davis, "Theoretical and experimental characterization of omnidirectional optical links for free space optical communications," Military Communications Conference, Vol. 3, p. 1151-1157, 2004.

75. M. Bilgi and M. Yuksel, "Multi-element free-space-optical spherical structures with intermittent connectivity patterns," IEEE INFOCOM Workshops, p. 1-4, 2008.

76. M. Yuksel, J. Akella, S. Kalyanaraman and P. Dutta, "Free-space-optical mobile ad hoc networks: auto-configurable building blocks," Wireless Networks, Vol. 15, p. 295-312, 2008.

77. J. Akella, C. Liu, D. Partyka, M. Yuksel, S. Kalyanaraman and P. Dutta, "Building blocks for mobile free-space-optical networks," IFIP/IEEE International Conference on Wireless and Optical Communications Networks (WOCN), p. 164–168, 2005.

78. N. Agrawal and C.C. Davis, "Design of free space optical omnidirectional transceivers for indoor applications using non-imaging optical devices," Proceedings of SPIE, Vol. 7091, p. 709107, 2008.

79. X. Song, L. Liu and J. Tang, "High-accuracy angle detection for ultra-wide-field-of-view acquisition in wireless optical links, " Optical Engineering, Vol. 47, p. 025010, 2008.

80. G. Lu, Y. Lu, T. Deng and Hui Liu, "Automatic alignment of optical beam based GPS for free-space laser communication system," Proceeding of SPIE, Vol. 5160, p. 432-438, 2004.

81. M.R. Garcia-Talavera, J.A. Rodriguez, T. Viera, H. Moreno-Arce, J.L. Rasilla, F. Gago, L.F. Rodriguez, P. Gomez and E.B. Ramirez, "Design and performance of the ESA optical ground station," Proceedings of SPIE, Vol. 4635, p. 248-261, 2002.

82. Special Optics, "Laser beam expander theory," http://www.specialoptics.com/56c.html

83. M. Achour, "Simulating atmospheric free-space optical propagation; Part II - Haze, fog, and low clouds attenuations," Proceeding of SPIE, Vol. 4873, p. 1-12, 2002.

84. I.I. Kim, B. McArthur and E.J. Korevaar, "Comparison of laser beam propagation at 785 nm and 1550 nm in fog and haze for optical wireless communications," Proceedings of SPIE, Vol. 4214, p. 26-37, 2001.

85. ITU-R: Prediction methods required for the design of terrestrial free-space optical links, Rec. ITU-R P.1814.

86. M. Chabane, M. Alnaboulsi, H. Sizun and O. Boucheta, "A new Quality of Service FSO software," Proceedings of SPIE, Vol. 5247, p. 362-372, 2003.

87. S.S. Muhammad, P. Kuhldorfer and E. Leitgeb, "Channel modeling for terrestrial free space optical links," 7th International Conference on Transparent Optical Networks, Vol. 1, p. 407-410, 2005.

88. Y. Ai, Q. Geng, J. Yang, H. Yang, Y. Zhou, X. Lu and K. Li, "5Gps 2.1km WDM free-space optical communication experiments," Proceeding of SPIE, Vol. 6025, p. 602513, 2006.

89. T.H. Carbonneau and D.R. Wisely, "Opportunities and challenges for optical wireless; the competitive advantage of free space telecommunications links in today's crowded market place," Proceeding of SPIE, Vol. 3232, p. 119-128, 1998.

90. S. Bloom, "The physics of free space optics," AirFiber, Inc, 2002.

91. A.K. Majumdar and J.C. Ricklin, "Effects of the atmospheric channel on free-space laser communications," Proceeding of SPIE, Vol. 5892, p. 58920K, 2005.

92. C. Chen and J.R. Lesh, "Overview of the optical communications demonstrator," Proceeding of. SPIE, Vol. 2123, p. 85-95, 1994.

93. R.G. Zenick and K. Kohlhepp, "GPS micro navigation and communication system," for clusters of micro and nanosatellites," in Aerospace Conference (2001).

94. M. Jeganathan, A. Portillo, C. Racho, S. Lee, D. Erickson, J. DePew, S. Monacos and A. Biswas, "Lessons learnt from the optical communications demonstrator (OCD)," Proceeding of SPIE, Vol. 3615, p. 23-30, 1999).

95. A. Azzawi, "Photonics: Principles and practices," CRC Press, 2006.

96. M.J. Riedl, "Optical design fundamentals for infrared systems," SPIE, 2001.

97. ZEMAX development corporation, "ZEMAX: Software for optical system design," http://www.zemax.com/.

98. Thorlabs, "Bare optical fibers and patch cables," http://www.thorlabs.com/navigation.cfm?Guide_ID=26.

99. C. Wen, W. Deng and Y. Li, "Technology of optical MEMS in optical communication," Proceeding of SPIE, Vol. 5281, p. 122-128, 2004.

100. Thorlabs, "Pigtailed Aspheric Fiber Collimators," http://www.thorlabs.com/NewGroupPage9.cfm?ObjectGroup_ID=3212.

101. OptiSystem 7, http://www.optiwave.com/site/products/system.html.

102. S. Lanka, M.B. Tayashi, J. Cartsens and L. Hofmann, "4-ary PAM signaling for increasing the capacity of metro light-wave systems," Proceedings of SPIE, Vol. 6105, p. 610509, 2006.

103. W. B. Leigh, "Devices for Optoelectronics," Marcel Dekker, 1996.

104. P. Bhattacharya , "Semiconductor Optoelectronic Devices," Prentice Hall, 1996.

105. Hamamatsu, "Photodiode Technical Information," http://sales.hamamatsu.com/assets/applications/SSD/photodiode_technical_information.pdf

106. A. Ramli, S.M. Idrus and A.S.M. Supa'at, "Optical Wireless Front-End Receiver Design," International RF and Microwave Conference, p. 331-334, 2008.

Author's Publications

Publications: Journal papers

1. K.H. Heng, W.D. Zhong, T.H. Cheng, N. Liu and Y. He, "Beam divergence changing mechanism for short-range inter-unmanned aerial vehicle optical communications," Applied Optics, Vol. 48, Issue 8, p. 1565-1572, 2009.

2. K.H. Heng, W.D. Zhong and T.H. Cheng "Multipoint FSO System for Short-Range Communications between Flight Platforms," Applied Optics, Vol. 49, Issue 2, p. 258-266, 2010.

Conference papers

1. K.H. Heng, Y. He, N. Liu, W.D. Zhong and T.H. Cheng, "Beam divergence shaping mechanism in laser intersatellite crosslink system," 6th International Conference on Information, Communications & Signal Processing, paper no. P843, Singapore, Dec 2007.

2. K.H. Heng, N. Liu, Y. He, W.D. Zhong and T.H. Cheng, "Adaptive Beam Divergence for Inter-UAV Free Space Optical Communications," International Conference on Optical Communications and Networks, paper no. conf195a124, Singapore, Dec 2008.

3. K.H. Heng, W.D. Zhong and T.H. Cheng, "Dual Data Rate Schemes Using Single Photoreceiver for Intersatellite FSO Communications," 14th Optoelectronics and Communications Conference, paper no. ThLP72, Hong Kong, China, July 2009.